GALAXIES

INFRARED EMISSION SPECTRUM OF THE GALAXY AND EXTERNAL GALAXIES BASED ON THE IRTS AND ISO ARCHIVAL DATA

Takashi Onaka[1], Haruko Mochizuki[1,4], Toshinobu Takagi[2], and Hiroshi Shibai[3]

[1]Department of Astronomy, Graduate School of Science, University of Tokyo, Tokyo 113-0033, Japan
[2]Astrophysics Group, Imperial College of Science, Technology and Medicine, London, SW7 2BW, U.K.
[3]Graduate School of Science, Nagoya University, Nagoya 464-8602, Japan
[4]Present address: Hopes Co., Tokyo 111-0042, Japan

ABSTRACT

The infrared spectral energy distribution (IR SED; 12–155 μm) of nearby galaxies has been investigated in terms of the IR SED of our Galaxy by using the IRTS/FILM and ISO/LWS 155 μm data in addition to the IRAS data. The 12 μm emission is shown to be well correlated with the far-infrared emission both in the Galaxy and galaxies. The 12 μm emission in galaxies can be accounted for fairly well by the superposition of the empirical emissivity derived from the observations of the Galactic plane or the dust model that includes PAHs and thermally fluctuating very small grains. However, the current dust model does not account for the characteristics of the 25–60 μm emission relative to the far-infrared in the Galaxy and galaxies consistently. The empirically derived IR SED from the observations of the Galaxy does not account for the IR SED of the sample galaxies either and the 25–60 μm emission is suggested to constitute a different component from the far-infrared emission.

Key words: ISO – Galactic plane: SED – galaxies: SED – dust model

1. INTRODUCTION

The diffuse infrared emission from our Galaxy is known to have an excess component in 6–60 μm over the thermal emission from submicron-sized grains (e.g. Dwek et al. 1997; Onaka 2000). The excess component in 6–14 μm has been shown to consist of several emission bands, which are attributed to very small grains or large molecules containing aromatic structures in them (Onaka et al. 1996; Mattila et al. 1996). The exact form of the carriers of these bands, however, remains unidentified. The excess emission in 25–60 μm has been attributed to thermally fluctuating very small grains. Several dust models including these ingredients have so far been constructed to understand the spectral energy distribution (SED) of the diffuse emission (Draine & Anderson 1985; Désert et al. 1990; Siebenmorgen & Krügel 1992; Dwek et al. 1997; Li & Draine 2001).

The SED of external galaxies has also been shown to have similar characteristics (Helou 1986). Recently Dale et al. (2001) have developed a galaxy SED model for 3 to 100 μm based on the dust model calculations to account for the latest ISO observations. Dale & Helou (2002) have extended their model to 20 cm, while Nagata et al. (2002) have examined the 60–200 μm SED of galaxies empirically based on the observations of the Galactic plane. Takagi (2001) has investigated the SEDs of external galaxies from ultraviolet to far-infrared by using the chemical evolution and dust model.

Observations by the IRTS (Murakami et al. 1996; Yamamura et al. 2002) and the COBE/DIRBE (Boggess et al. 1992) have shown that the 25–60 μm emission of the Galactic plane shows a steep dependence on the temperature of submicron grains, which contradicts the model prediction (Okumura et al. 1999; Shibai et al. 1999). In this report we investigate the 12–155 μm SED of external galaxies in terms of the observations of the Galactic plane. The data longer than 100 μm, which IRAS did not cover, are crucial to correctly estimate the thermal emission component.

2. DATA

The IRTS/FILM 155 μm continuum data of the W51 and the Galactic center regions were used for the data longer than 100 μm of the Galactic plane (Okumura et al. 1996). In addition we used the far-infrared spectra of the Carina region obtained by ISO/LWS (Mizutani et al. 2002) and estimated the 155 μm continuum intensity. For external galaxies the ISO/LWS spectra extracted from the ISO Data Archive were employed. We used the spectra of the LWS01 sample (Negishi et al. 2001) and the LWS02 data of the U.S. Key project (Malhotra et al. 2001), and estimated the continuum intensity at 155 μm. We have excluded the galaxies whose data have large uncertainties and are largely different from the IRAS data. The present sample contains 24 galaxies for the LWS01 sample and 54 galaxies for the LWS02 sample and consists mostly of starburst and normal galaxies. The LWS02 sample may have slightly larger uncertainties than the LWS01 sample, but no systematic difference is seen in between the two data sets. The LWS data reduction was made with the ISO Spectral Analysis Package (ISAP[1]). Recently Brauher (2002) has derived the far-infrared continuum intensities of more than 200 galaxies from the LWS data after careful data processing.

In addition to the 155 μm data sets we used the IRAS 12, 25, 60, and 100 μm intensities. The present analysis uses the same 5 band data both for the Galactic plane and the exter-

[1] The ISO Spectral Analysis Package (ISAP) is a joint development by the LWS and SWS Instrument Teams and Data Centers. Contributing institutes are CESR, IAS, IPAC, MPE, RAL, and SRON.

Proceedings of the Symposium *"Exploiting the ISO Data Archive - Infrared Astronomy in the Internet Age"*, 24–27 June 2002, Sigüenza, Spain (C. Gry, S. B. Peschke, J. Matagne et al. eds., ESA SP-511)

nal galaxies and thus enables a direct comparison between our Galaxy and external galaxy SEDs.

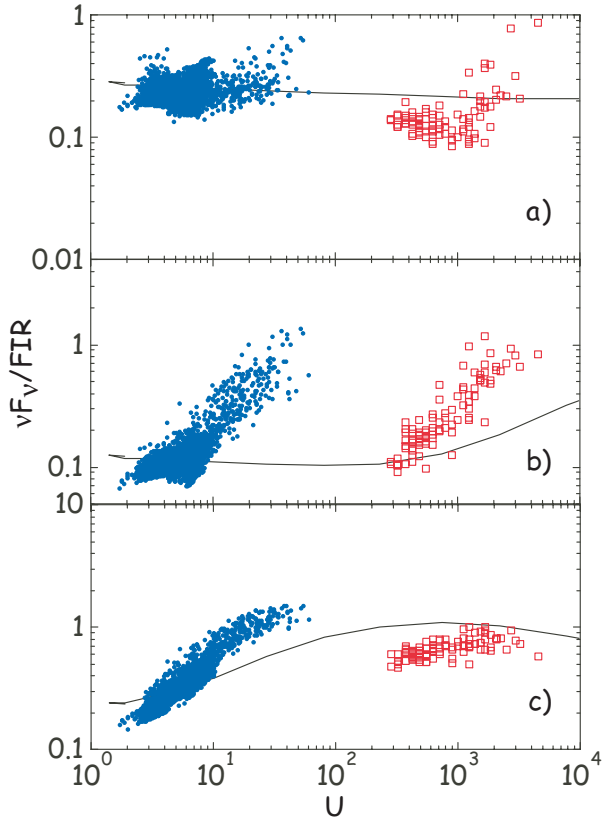

Figure 1. Infrared intensity (νF_ν) divided by the far-infrared intensity (FIR) against the radiation field strength in units of the solar neighborhood value (see text). a) 12 μm, b) 25 μm, and c) 60 μm. The dots indicate the Galactic plane data obtained by IRTS, while the open circles show the data of the Carina region by ISO. The solid lines indicate the model predictions.

3. GALACTIC PLANE EMISSION

For the Galactic plane data we estimate the total intensity of the thermal emission FIR as

$$FIR = \tau_{100} \int (100\mu\mathrm{m}/\lambda)^\beta B_\lambda(T_d) d\lambda, \quad (1)$$

where τ_{100} is the optical depth at 100 μm, β is the power law index of the dust emissivity, and $B_\lambda(T_d)$ is the Planck function of the temperature T_d. We assume that $\beta = 2$ for the IRTS data and $\beta = 1$ for the Carina spectrum (Chan et al. 2001). The thermal emission should be equal to the absorbed energy and thus we have

$$FIR = \bar{\tau}_{abs} U / 4\pi, \quad (2)$$

where U is the radiation field strength and $\bar{\tau}_{abs}$ is the absorption optical depth averaged over the incident radiation spectrum. In the following we use U in units of the solar neighborhood value $1.6 \times 10^{-6}\,\mathrm{Wm}^{-2}$. According to the thermally fluctuating dust model, the excess intensity is supposed to be proportional to U, but the spectral shape should not change.

Fig. 1 shows the Galactic plane emission data. The 12 μm intensity divided by FIR seems to be constant for the IRTS data points. The ISO data of the Carina region are smoothly connected to the IRTS data and start decreasing with U. The decrease may be attributed to the destruction of the carriers or the inefficient emission mechanism at high U (Onaka et al. 2000). The observed trend is well described by the thermally fluctuating dust model except for the possible upturn for $U > 10^3$ if the decrease of the emission is taken into account. The upturn seems to be related to a tail of the 25 μm emission, which increases with U (see below). The 25 μm intensity divided by FIR, on the other hand, shows a quite different trend and indicates that the ratio is proportional to U (Fig. 1b). In addition the Carina data are located in the region just shifted from the Galactic plane data. As indicated by the solid lines, these trends cannot be interpreted in terms of the thermally fluctuating dust model. Thus the 25 μm emission is suggested to have a component uncorrelated with the far-infrared emission. The 60 μm intensity also shows a similar behavior (Fig. 1c).

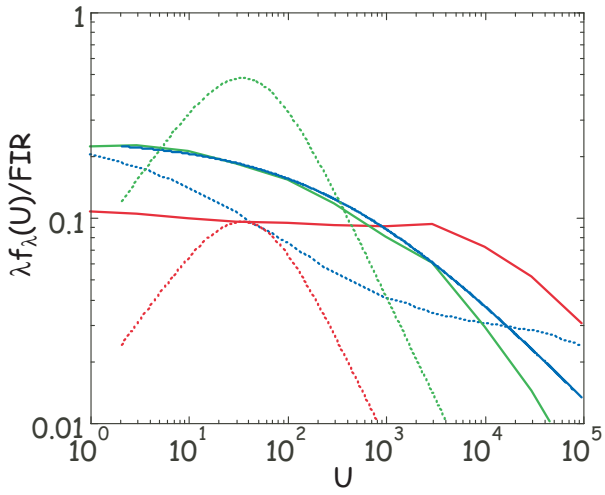

Figure 2. Local emissivity functions for the thermally fluctuating component divided by FIR. The solid lines indicate those calculated from the dust model, while the dotted lines show those estimated from the Galactic plane data. Blue, red, and green indicate those for 12 μm, 25 μm, and 60 μm, respectively.

4. GALAXIES

The infrared emission from external galaxies consists of contributions from various components. According to Dale et al. (2001), we assume that the IR emission of galaxies F_λ can be described by

$$F_\nu(\lambda) = \int_{U_{min}}^{U_{max}} f_\nu(U, \lambda)\, U^{-\alpha} dU, \quad (3)$$

where $f_\nu(U,\lambda)$ is the local emissivity of a function of U, α is the power law index to describe the activity of the galaxy, and U_{max} and U_{min} indicate the range of the radiation field strength in the galaxy.

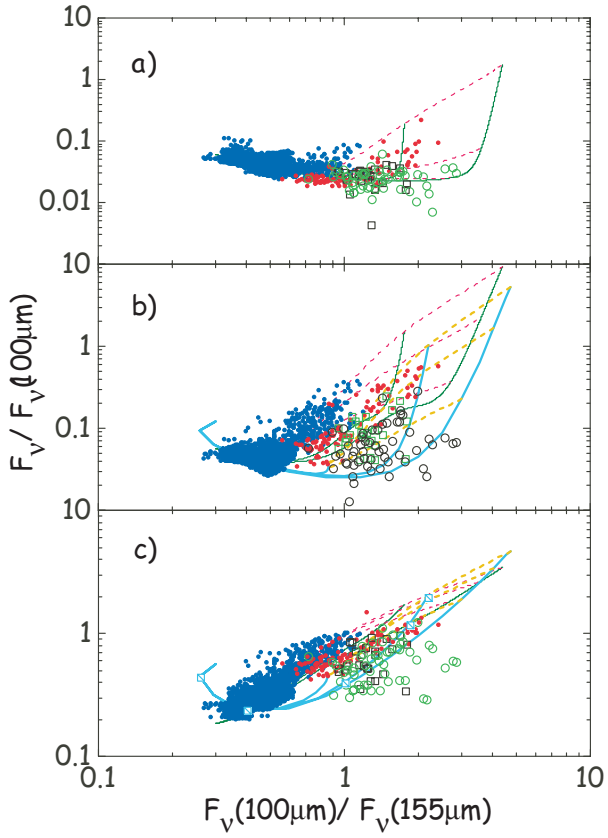

Figure 3. Two-color diagrams of the Galactic plane emission and external galaxy data. a) $F_\nu(12\,\mu m)/F_\nu(100\,\mu m)$, b) $F_\nu(25\,\mu m)/F_\nu(100\,\mu m)$, and c) $F_\nu(60\,\mu m)/F_\nu(100\,\mu m)$ against the far-infrared color $F_\nu(100\,\mu m)/F_\nu(155\,\mu m)$. The dots indicate the the Galactic plane data, while the open squares (LWS01 sample) and circles (LWS02 sample) show the external galaxies. The thin lines (green and red) indicate the results of the empirical emissivity and the thick lines (blue and yellow) depict those of the dust model. The solid lines indicate those with constant α (α = 1, 1.7, and 2.5), while the dashed lines show those with constant U_{max} (U_{max} = 10^3, 10^4, and 10^5).

The local emissivity function $f_\nu(U,\lambda)$ is further divided into a component of the thermal emission from sub-micron-sized grains and that from thermally fluctuating very small grains. For the latter we use the one calculated by the standard dust model (Takagi 2001) and the one empirically estimated from the observations of the Galactic plane. The adopted local emissivity functions are shown in Fig. 2. The empirical emissivity functions for 25 μm and 60 μm are set to vary linearly with U at low U as the observations suggest, and approximately take into account the decrease at high U. In the following we investigate whether the local emissivities empirically estimated from the Galactic plane data or those calculated by the dust model can account for the observed galaxy SEDs.

Fig. 3 shows the two-color diagrams of the Galactic plane emission and external galaxies. The diagram of 12–100–155 μm (Fig. 3a) indicates that the galaxy data are located on the same trend as the Galactic plane data and both data points are well described by the empirical emissivity and thus by the thermally fluctuating dust model. On the other hand, as expected from the Galactic data, the 25–100–155 μm diagram (Fig. 3b) shows a quite large scatter and neither the empirical emissivity (thin lines) nor the dust model (thick lines) can describe the Galactic and galaxy data consistently. Because the galaxy data show blue colors in 100/155 μm but similar colors in 25/100 μm compared to the Galactic plane emission, it is almost impossible to account for the both data sets by the same emissivity function. The 60–100–155 μm diagram shows a similar scatter and trend (Fig. 3c), which cannot be accounted for either by the empirical emissivity or model emissivity.

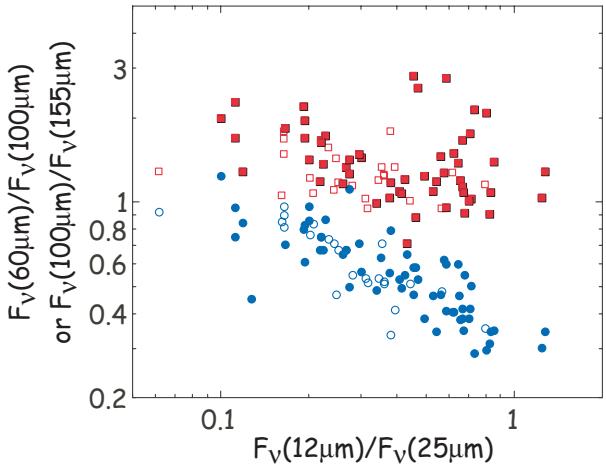

Figure 4. Far-infrared colors plotted against the mid-infrared colors for the sample galaxies. The circles indicate the color of 60 to 100 μm, while the squares show the 100 to 155 μm color. The open symbols indicate the LWS01 sample and the filled symbols show the LWS02 sample.

To further examine the nature of the 25–60 μm emission, Fig. 4 plots the far-infrared colors of 60 μm to 100 μm and 100 μm to 155 μm of the sample galaxies against the mid--infrared color of 12 μm to 25 μm. The clear correlation seen between the 12 to 25 and 60 to 100 μm colors has already been pointed out by Helou (1986), while the color of 100 to 155 μm seems to be poorly correlated with the mid-infrared color. The latter uncorrelation suggests that the 25 μm emission behaves rather independently of the far-infrared emission longer than 100 μm since the 12 μm emission is well correlated with the far-infrared. This is in agreement with the trends seen in Figs. 1 and 3. The former correlation can then be interpreted if the 60 μm emission is better correlated with the 25 μm emission rather than with the far-infrared. Thus the trends seen in Figs. 3 and 4 can be understood if the 12 μm emission is well corre-

lated with the far-infrared emission for $\lambda > 100\,\mu$m, while the 25–60 μm emission constitutes an independent component.

5. SUMMARY

The present analysis indicates that the 12 μm intensity in the Galactic plane and external galaxies is well correlated with the far-infrared intensity longer than 100 μm and can be described by the thermally fluctuating dust model fairly well. Since a large fraction of the IRAS 12 μm intensity comes from the aromatic bands (Onaka et al. 1996), the good correlation suggests the presence of some mechanism to keep the abundance of the band carriers relative to the submicron-sized grains. On the other hand, the emission of 25–60 μm seems to constitute a different component from the far-infrared emission. Its trend cannot be accounted for by the dust model and the external galaxy data cannot be described in terms of the Galactic plane data. The nature of the 25–60 μm emission has not been well investigated. The dust model assumes that it originates from very small grains, which are slightly larger than the band carriers. Therefore it may not be surprising that this component behaves independently of the other components. Particularly the size distribution of the very small grains is not well constrained by the observations and the variation in the size distribution may result in the shift observed in Figs. 1b and c. Further investigations are definitely needed to elucidate the nature of the 25–60 μm emission.

ACKNOWLEDGEMENTS

This work was based on observations with IRTS and ISO. IRTS is a joint project between ISAS and NASA, managed and operated by ISAS. ISO is an ESA project with instruments funded by ESA Member States (especially the PI countries: France, Germany, the Netherlands and the United Kingdom) and with the participation of ISAS and NASA. We thank all the members of the IRTS project and the members of the Japanese ISO team for their continuous support. This work was supported in part by a Grant-in-Aids for Scientific Research from the JSPS.

REFERENCES

Boggess, N. W., Mather, J. C., Weiss, R., et al., 1992, ApJ, 397, 420
Brauher, J. R., 2002, this volume
Chan, K.-W., Roellig, T. L., Onaka, T., et al., 2001, ApJ, 546, 273
Dale, D. A., Helou, G., 2002, ApJ, in press
Dale, D. A., Helou, G., Contursi, A., et al., 2001, ApJ, 549, 215
Desert, F.-X., Boulanger, F., Puget, J. P., 1990, A&A, 237, 215
Draine, B. T., Anderson, N., 1985, ApJ, 292, 494
Dwek, E., Arendt, R. G., Fixsen, D., et al., 1997, ApJ, 475, 565
Helou, G. 1986, ApJL, 311, L33
Li, A., Draine, B. T., 2001, ApJ, 554, 778
Malhotra, S., Kaufman, M. J., Hollenbach, D., et al., 2001, ApJ, 561, 766
Mattila, K., Lemke, D., Haikala, L. K., et al., 1996, A&A, 351, L353
Mizutani, M., Onaka, T., Shibai, H., 2002, A&A, 382, 610
Murakami, H., Freund, M. M., Ganga, K., et al. 1996, PASJ, 48, L41
Nagata, H. Shibai, H., Takeuchi, T. T., Onaka, T., 2002, PASJ, in press
Negishi, T., Onaka, T., Chan, K.-W., Roellig, T. L., 2001, A&A, 375, 566
Okumura, K., Hiromoto, N., Okuda, H., et al., 1999, in: Star Formation 1999, ed. T. Nakamoto (Nobeyama Radio Observatory, Nobeyama), 97
Onaka, T., 2000, Adv. Sp. Res., 25, 2167
Onaka, T., Mizutani, M., Chan, K.-W., et al., 2000, ESA SP-456, 55
Onaka, T., Yamamura, I., Tanabè, T., et al., 1996, PASJ, 48, L59
Okumura, K., Hiromoto, N., Okuda, H., et al. 1996, PASJ, 48, L123
Shibai, H., Okumura, K., Onaka, T., 1999, in: Star Formation 1999, ed. T. Nakamoto (Nobeyama Radio Observatory, Nobeyama), 67
Siebenmorgen, R., Kruegel, E., 1992, A&A, 259, 614
Takagi, T., 2001, PhD Thesis, Rikkyo University
Yamamura, I., Tanaka, M., Takahashi, H., et al., 2002, this volume

THE SMALL MAGELLANIC CLOUD IN THE FAR INFRARED: NEW ISO RESULTS

Karsten Wilke, Manfred Stickel, Martin Haas, Uwe Herbstmeier, Ulrich Klaas, and Dietrich Lemke

Max-Planck-Institut für Astronomie, Königstuhl, D-69117 Heidelberg, Germany

ABSTRACT

For the first time, ISOPHOT generated a complete view of the Small Magellanic Cloud (SMC) at 170μm with 1.5 arc-min resolution. The map is analysed using an automated photometry program enabling accurate photometric characterization of the far infrared (FIR) emitting regions. In order to compare the detected sources with those obtainable from the IRAS satellite data, the 12μm, 25μm, 60μm, and 100μm IRAS high resolution maps of the SMC are re-examined using the same method. In contrast to former studies, this provides an all-band ISO/IRAS source catalog which is no longer based on eyeball classification, but relies on an algorithm which is capable of automated, repeatable photometry, even of irregular sources. The color temperature obtained from a 170μm/100μm map suggests an average dust temperature of $T_D = 20.5K$. All three FIR bands at 170μm, 100μm, and 60μm reproduce the overall morphological structure of the SMC similarly well, in contrast to the 12μm and 25μm maps which only contain a limited number of extended sources, but do not trace the main body of the SMC. 243 sources are detected in the in the ISO 170μm map, 155 of them with $F_\nu \geq 2.0Jy$. Comparable numbers are found for the two FIR IRAS maps at 60μm (384) and 100μm (338) with flux densities up to $450Jy$. 70 of the 243 170μm sources are assigned a general SED type ("cold", "warm", i.e., $< 30K$, $> 30K$) for the first time. Remarkably, many sources with flux densities up to 40Jy listed in former catalogs cannot be identified in our data.

Key words: Galaxies: Magellanic Clouds – ISO: ISM – ISM: general – ISM: dust, extinction

1. OBSERVATIONS

Exposures were obtained in raster scanning mode with the C200 detector, a 2 × 2 pixel array of stressed Ge:Ga with a pixel size of 89″, in conjunction with the C_160 broad band filter (reference wavelength 170 μm, equivalent width 89μm). Due to the rather large area of the SMC on the sky ($6^\circ \times 8^\circ$), the ISOPHOT (Lemke et al. 1996) observations had to be split into a mosaic of nine separate fields. Adjacent parts of the whole map were designed to be slightly overlapping, while the raster step size of each part was a full detector size without any overlap. The total exposure time for all maps was $\approx 70000sec$. The final map (Fig. 1) was produced and restored with a 40" pixel size and a FWHM of 2'.

The image is morphologically dominated by the main body of the SMC (the bar), to the east the so-called "wing" with numerous bright and extended sources is visible. Note that in contrast to former IRAS maps, the effective resolution of the restored ISO map is perfectly symmetric. The FIR emission shows a wealth of filamentary structure in addition to several bright star forming regions in the SMC main body (dark blue/white), which are obviously coupled to bright HII regions and surrounded by regions of moderate intensity (green). Extended emission also covers the NE part of the SMC, the bridge to the LMC. The observations did not cover the SW region (the wing) towards the Magellanic Stream to full extent.

2. COLOR TEMPERATURE MAP

The 100μm IRAS image and the 175μm ISO map were used to derive the color temperature distribution for the SMC. Due to large IRAS flux fluctuations outside the SMC main body we decided to consider the IRAS 100μm fluxes down to a lower limit of 5MJy/sr only. To adjust the IRAS pixel size to that of our ISO map, the 100μm image was rebinned to a 30" linear resolution. After the division of the 175μm ISO map by the modified IRAS 100μm image and the conversion of the resulting flux ratios to temperatures we obtained the maps shown in Fig. 2.

In general, this map shows a fairly smooth temperature distribution with values ranging from $\approx 18K$ to $\approx 22K$ over the SMC main body. No distinct or large scale structures are visible. Higher temperatures are found for some star forming regions which were discovered by Davies, Elliott, and Meaburn (1976) already. Three different temperature regimes can be identified:

- $T_d < 20.0K$ are generated by diffuse emission from dust heated by the interstellar radiation field (ISRF), moderately far away from the big HII regions in the SMC. This temperature range covers $\approx 45\%$ of the whole SMC area above the IRAS threshold limit of 5MJy/sr (38% in the interval $18.0K < T_d < 20.0K$ and 7% below).
- $20.0K < T_d < 22.0K$ corresponds to warmer diffuse emission in the close environment of the majority of HII regions, contributing $\approx 42\%$ to the total emitting area.

Proceedings of the Symposium *"Exploiting the ISO Data Archive - Infrared Astronomy in the Internet Age"*, 24–27 June 2002, Sigüenza, Spain (C. Gry, S. B. Peschke, J. Matagne et al. eds., ESA SP-511)

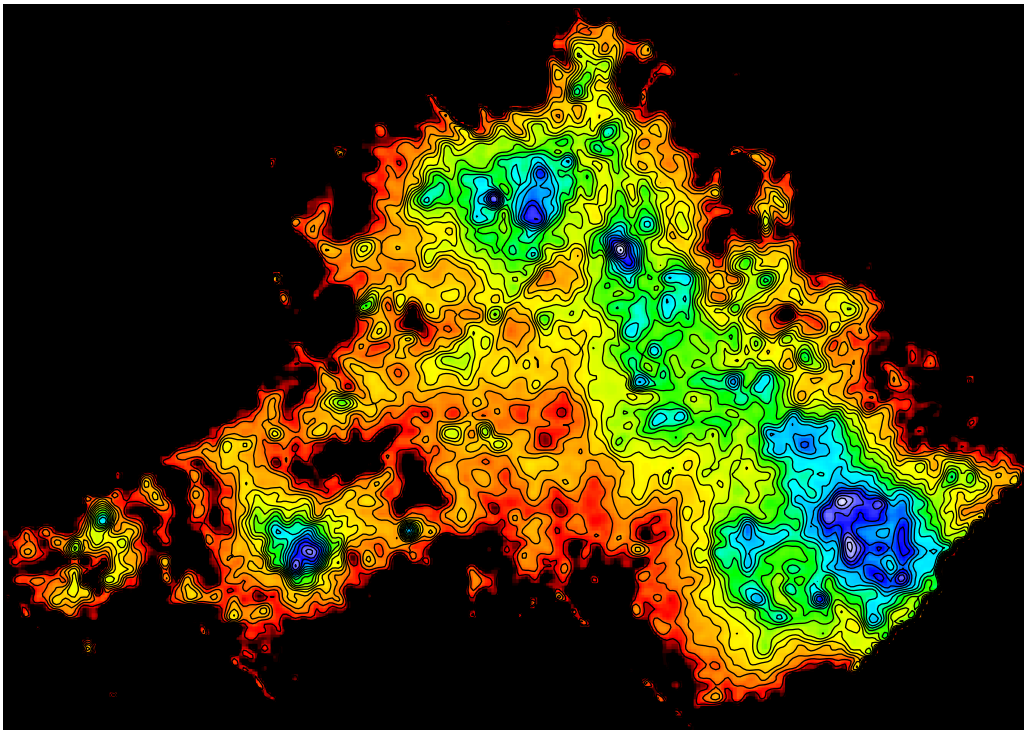

Figure 1. False color representation 170μm ISO map of the SMC. Logarithmic contours are overplotted to the original image at intensities 0.04, 0.06, 0.08, 0.13, 0.20, 0.30, 0.47, 0.72, 1.11, 1.70, 2.63, 4.04, 6.22, 9.58, 14.76, 22.73, and 35.00Jy/pix. Note that not only the main body of the SMC (the bar) is well traced, but also the "wing" connecting the SMC to the LMC in south-eastern direction.

– Temperatures above $22.0K$ are found for discrete hot HII regions, however with $\approx 12\%$, their contribution is comparably small.

These temperature values are in good agreement with the results of Schlegel, Finkbeiner and Davies (1998) who found the dust temperature of the Galaxy to vary between 17K and 21K. Our dominant temperature interval $18.0K \ldots 22.0K$ with peak values up to $\approx 41K$ suggests only slightly higher values, thereby hinting at a stronger ISRF due to lower metallicity and higher star-formation rates. Some global results are listed in Tab. 1.

Table 1. Global properties of the SMC, derived from the 170μm ISO and the 100μm IRAS map.

F_{40-220}	$5.6 \times 10^{-10} W/m^2$
F_{1-1000}	$7.6 \times 10^{-10} W/m^2$
L_{1-1000}	$8.5 \times 10^7 L_\odot$
SFR	$0.0148 M_\odot/yr$
$T_{dust,\,170/100,\,averaged}$	$20.5K$
M_{dust}	$3.7 \times 10^5 M_\odot$
M_{gas}/M_{dust}	≈ 1140

3. SOURCE EXTRACTION

For the source determination, the HIIphot package, a robust and fully automated method, was used (Thilker, Braun, and Walterbros 2000). This program surpasses many other existing algorithms (e.g., DAOPHOT or ALLFRAME) in many aspects: i) no assumptions on the intrinsic source structure are required ii) the program provides adaptivity to the actual source morphology by making use of an iterative approach for growing sources from an initial guess at the shape and orientation, and iii) overlapping sources are accurately detected even in crowded fields and in the presence of a substantially inhomogeneous background.

Results of the source extraction are shown in Fig. 3. Obviously, most of the bright sources are found in large regions covering the NE and SW part of the SMC with some single bright sources in between. The most prominent region lies in the SW part of the SMC, with a ring-like structure consisting of very bright individual HII regions. The overall SMC morphology is very similar to that found in the FIR (60μm and 100μm) IRAS data, which (together with the two MIR IRAS bands at 12μm and 25μm) were examined using exactly the same method. We obtained the following statistics (for detailed results see Wilke et al. 2002):

– total number of detections at 170μm: 243
– 155 sources with $F_\nu > 2.0Jy$:
  – 8 sources with a warm spectrum ($T > 30.0K$ for a BB with $\beta = 2$), most of them HII regions

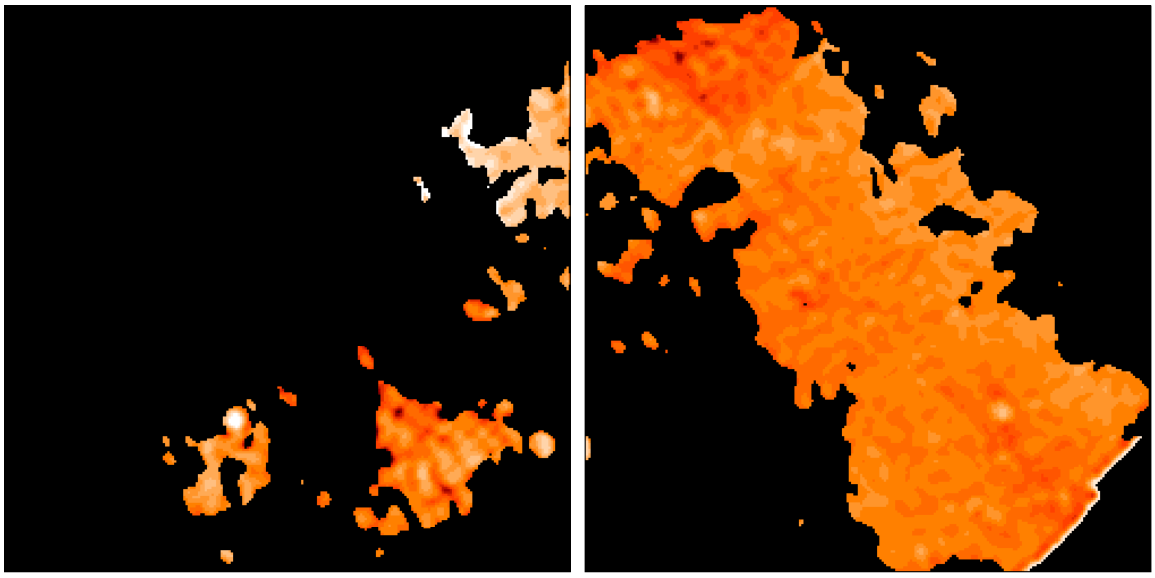

Figure 2. Color temperature map of the ISO-to-IRAS flux ratio (175μm to 100μm). The IRAS image was smoothed to the ISO pixel size of 30". Regions of low IRAS signal values ($\leq$ 5MJy/sr) have been filtered out and are displayed in white. Darker spots correspond to higher temperatures. The resulting map shows no distinct large scale structures, only small wiggles over an otherwise smooth plateau. This means that the SMC temperature distribution is very flat over its whole extension. The main body of the SMC has average temperatures of $T_c = 20.0K \ldots 22.5K$, dropping to $T_c = 18.5K$ in some regions. Higher temperatures are found, e.g., for some star forming regions.

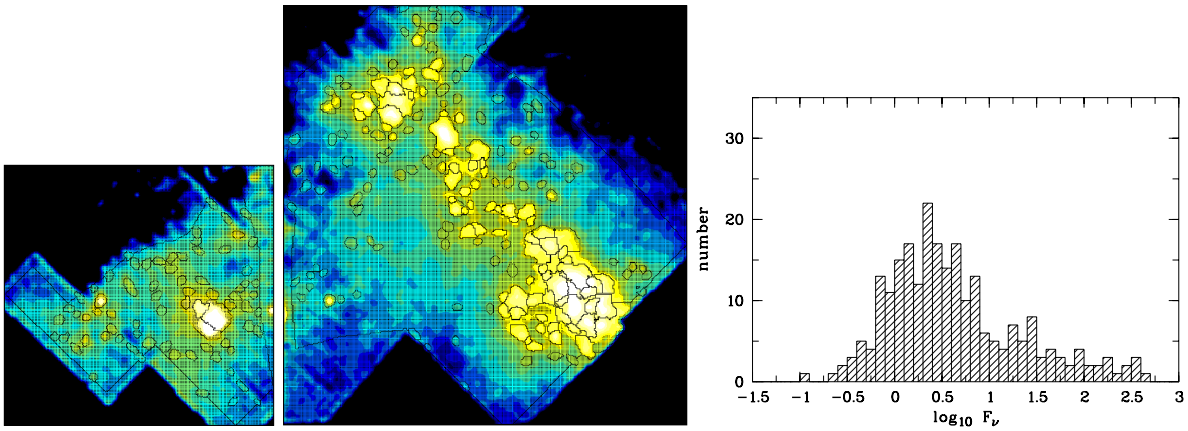

Figure 3. Left and center: SMC growth maps. Source borderlines and data field boundaries are given. The lower growth limit for the sources was 1.4MJy/sr, only potential detections with $S/N \geq 1.5$ were accepted. Maximum source growth radius: 50pc. Right panel: Source flux distribution histogram for the 170μm catalog. All sources are included. A large number of sources in the lowest flux bins ($0.0Jy \ldots 5.0Jy$) dominates the histogram distribution. On the other hand, single sources are detected at very high flux densities, ranging up to the 450Jy level.

  - 98 sources with a cold spectrum ($T < 30.0K$), most of them molecular clouds:
    - 73 sources with $F_{170}/F_{100} > 1.0$
    - 17 sources with $F_{170}/F_{100} < 1.0$
  - 49 unclassified detections due to source confusion and/or missing wavelengths bands, most probably HII regions.
- 70 of the 243 170μm sources are assigned a general SED type for the very first time.
- it is found that the average FIR flux densities of the brightest 175μm sources can be generated by only one O5V or B0V star already if its bolometric flux density is re-radiated in the FIR, i.e.,
  $L_{1-1000,\,single\ source} \approx 1 \cdot L_{O5\,V} \ldots 1 \cdot L_{B0\,V}$.

Although source catalogs for this wavelength range were published in the past already (for an extensive comparison of IRAS SMC source catalogs with other wavelength bands see, e.g., Schwering & Israel (1989), hereafter SI89), we decided to re-analyse the IRAS high resolution (HiRes hereafter) data in order to treat ISO results and IRAS data in an identical and reproducible way. The quantitative results of the source extraction process for all five wavelength bands are given in Tab. 2.

4. DISCUSSION

- The FIR IRAS and the ISO map of the SMC were found to be closely correlated by tracing the overall morphology of

source extraction/flux density distribution: ISO compared to IRAS

data set	**ISO 170μm**	**IRAS 12μm**	**IRAS 25μm**	**IRAS 60μm**	**IRAS 100μm**
$n_{source\,total}$	243	73	135	384	338
	155 with $F_\nu > 2.0\,Jy$			124 with $F_\nu > 1.0\,Jy$	167 with $F_\nu > 1.0\,Jy$
F_ν **range [Jy]**	0.3…450	0.1…1.0	0.06…3.0	0.06…25	0.08…160
n_C	99 (64%)	18 (25%)	41 (30%)	95 (77%)	90 (54%)
n_W	7 (5%)	3 (4%)	6 (4%)	6 (5%)	7 (4%)
n_Q	19 (12%)	—	9 (7%)	9 (7%)	18 (11%)
$n_{IRAS\,sources}$	51 (33%)	25 (34%)	60 (44%)	71 (57%)	63 (38%)
$n_{HII\,regions}$	18 (12%)	14 (19%)	31 (23%)	33 (27%)	22 (13%)
$n_{ELS/EMO}$	61 (40%)	38 (52%)	79 (59%)	84 (68%)	70 (42%)
$N_{SI89,\,NOT\,id.}$	—	69%	41%	35%	31%

Table 2. Comparison between the ISO and the IRAS statistical results from our analysis. Columns are labelled as follows:

$n_{source\,total}$: total number of detected sources in each band
cross-id. xxx μm: number of sources cross-identified in the xxx μm catalog
F_ν range [Jy]: flux density range covered by most of the sources
$F_{\nu,\,landmarks}\ [Jy]$: flux densities of the five sources serving as landmark points in all five wavelength bands
n_C: number of sources classified as cold ("C", meaning $T_{BB} < 30K$ for $\beta = 2$)*
n_W: number of sources classified as warm ("W", meaning $T_{BB} > 30K$ for $\beta = 2$)*
n_Q: number of sources which could not be classified "W" or "C" due to source confusion between different wavelength bands*
$n_{IRAS\,sources}$: number of sources identified as IRAS Point Source Catalog (PSC) or Faint Source Catalog (FSC) objects in Simbad*
$n_{ELS/EMO}$: number of sources classified as emission line star or emission object in Simbad*
$N_{SI89,\,NOT\,id.}$: number of sources found by SI89 which could NOT be recovered in our analysis*

*: if flux limitations apply (e.g., sources with flux densities $> 1.0\,Jy$ or $2.0\,Jy$, as given in the fourth line from top), numbers refer to selected flux range only.

the SMC main body, the bridge and the wing in a similar manner and producing similar source counts with hundreds of sources (243 to 384, depending on the FIR band) with comparable flux density distributions.

– The percentage of cold sources contributing to the total number of detections is nearly identical for all three FIR bands.
– Most compact sources with reliably determined fluxes are already detected in the MIR wavelength range (73 at 12μm and 135 at 25μm), although the MIR IRAS data is not capable of shedding much light on the complex morphological structure of the SMC main body. MIR source flux densities predominantly lie below 1.0Jy.
– It is evident from the flux density distributions that the HIIphot algorithm confirms the general results for the 12μm and 25μm bands obtained in the SI89 study and produces comparable source numbers and flux distributions for both, luminous and fainter sources.
– Our 60μm and 100μm results strongly differ in number counts and flux density distributions from those found in previous studies. Compared to the SI89 results, the HIIphot algorithm on average assigns lower fluxes for faint sources and higher or similar fluxes to bright ones, depending on the environment of the source.
– Adjacent sources are disentangled unambiguously by our source extraction algorithm. A remarkable result is that numerous sources listed in the SI89 data set were NOT found by our method. This does not only refer to faint sources with flux densities slightly above the detection limit, but even occurs for sources with SI89 flux densities up to $45\,Jy$. In detail, 69% (12μm), 41% (25μm), 35% (60μm), and 31% (100μm) of the sources identified by SI89 were not found by our study. The exact reason for that remains unknown, however, discrepancies have been reported several times already, e.g., by Filipovic et al. (1998). Since the SI89 catalog was generated using eyeball fitting methods, we believe that the results presented here are a more reliable base for cross-correlation with other spectral regions.

ACKNOWLEDGEMENTS

The authors would like to thank D.Thilker for publishing his code in the internet and thereby making it accessible for an interested public. This work was supported by the DLR fund 50QI0201, the MPG , and ESA funds supporting the scientific data reduction.

REFERENCES

Davies, R.D., Elliot, K.H., Meaburn J., 1976, MNRAS, 81, 89D
Filipović M.D., Jones P.A., White G.I., Haynes R.F., 1998 A&AS, 130, 441
Lemke, D., Klaas, U., Abolins, J., et al., 1996, A&A, 315, L64
Schwering P.B.W., Israel F.P., 1989, A&AS, 79, 79 (SI89)
Schlegel, D.J., Finkenbeiner, D.P., Davis, M., 1998, AJ, 500, 525
Thilker, D.A., Braun, R., Walterbros, R.A.M., 2000, AJ, 120, 3070
Wilke, K., Stickel, M., Haas, M., et al., 2002, A&A, submitted

FAR-INFRARED EMISSION FROM DUST IN NORMAL GALAXIES

Richard J. Tuffs[1] **and Cristina C. Popescu**[2,3,4]

[1]Astrophysics Division, Max-Planck-Institut für Kernphysik, Saupfercheckweg 1, 69117 Heidelberg, Germany
[2]The Observatories of the Carnegie Institution of Washington, 813 Santa Barbara Str., Pasadena, 91101 California, USA
[3]IPAC(Caltech/JPL), 770 S. Wilson Avenue, Pasadena, California 91125, USA
[4]Research Associate, The Astronomical Institute of the Romanian Academy, Str. Cuţitul de Argint 5, Bucharest, Romania

ABSTRACT

We review the morphological and spectral energy distribution characteristics of the dust continuum emission (emitted in the 40 - $200\,\mu$m spectral range) from normal galaxies, as revealed by detailed ISOPHOT mapping observations of nearby spirals and by ISOPHOT observations of the integrated emissions from representative statistical samples in the local universe.

Key words: ISO

1. INTRODUCTION

The sensitivity of ISO and its spectral grasp extending to $200\,\mu$m made it the first observatory capable of routinely measuring the infrared emission corresponding to the bulk of starlight absorbed by interstellar dust in "normal"[1] galaxies. Here we review ISO's view of the morphological and spectral energy distribution (SED) characteristics of the dust continuum emission (emitted in the 40 - $200\,\mu$m spectral range) from normal galaxies, and its interpretation. In this review we only discuss the results from the ISOPHOT instrument (Lemke et al. 1996) on board ISO.

Although technically more demanding than observations in the Mid-Infrared (MIR) regime, only observations in the Far-Infrared (FIR) directly probe the role played by dust in the energy budget of star-forming galaxies. All star-forming galaxies are at least in part optically thick in the ultraviolet (UV)-optical regime, and the absorbed energy is predominantly re-radiated in the FIR. But the real investigative power of FIR astronomy lies in the fact that even for optically thin components of the interstellar medium, the large grains which dominate the FIR emission are in (or near to) equilibrium with the ambient interstellar radiation field (ISRF). Therefore, the grains act as test particles with FIR colours characteristic of the intensity and colour of the ISRF. This is illustrated in Fig. 1, which shows the predicted variation of infrared colours with radiation field intensities, for standard filter combinations of the ISOPHOT and ISOCAM instruments (on board ISO), and of the IRAS survey.

[1] We use the term "normal" to denote star-forming systems not undergoing a starburst, and not dominated by AGN activity.

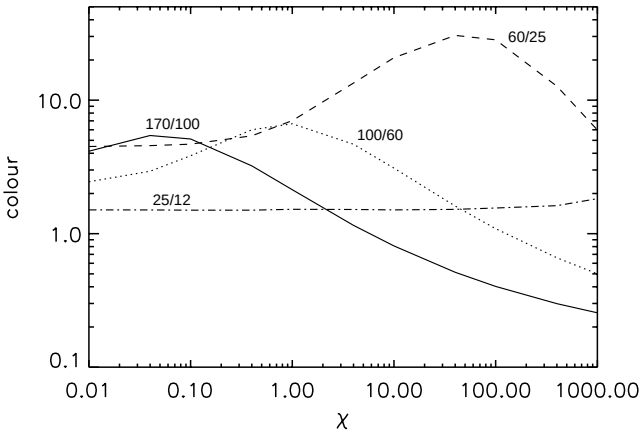

Figure 1. Predicted colour ratios for standard filter combinations 170/100 μm (solid line); 100/60 μm (dotted line); 60/25 μm (dashed line) and 25/12 μm (dot-dashed line) as a function of the strength of the local ISRF χ, where $\chi = 1$ near the sun. The calculations were made for spherical grains of astrophysical silicate, with the optical properties given by Laor & Draine (1993). A grain size distribution $n(a)\,da \propto a^{-3.5}$ was assumed, where a is the grain radius ($0.001 \leq a \leq 0.25\,\mu$m). The colour of the radiation field illuminating the grains is fixed to that determined for the solar neighbourhood by Mezger, Mathis & Panagia (1982).

In particular, a filter set covering the range 60 to 170 μm probes intensities in the ISRF ranging from those expected for HII regions to those expected in the outskirts of disks of normal galaxies. By contrast, the MIR colour ratios are almost independent of the intensity of the ISRF, since they are determined by the relative abundance of small, impulsively heated grains.

2. ISOPHOT MAPPING OBSERVATIONS OF NEARBY SPIRALS

ISO represented a big improvement compared with IRAS in angular resolution, spectral grasp and sensitivity. Thus, in terms of imaging, the ISOPHOT instrument was able to make a better distinction between diffuse and discrete sources and their colours. Another point was the extension in wavelength coverage to $200\,\mu$m. In fact observations of nearby galaxies displayed a wide range of FIR colours between various morphological components, implying UV/optical/ near-infrared (NIR) interstellar radiation fields with a wide range of intensities and/-or colours:

Proceedings of the Symposium *"Exploiting the ISO Data Archive - Infrared Astronomy in the Internet Age"*, 24–27 June 2002, Sigüenza, Spain (C. Gry, S. B. Peschke, J. Matagne et al. eds., ESA SP-511)

– **Star formation regions**: HII regions ($40 \leq T_{\rm D} \leq 60$ K) and Parent Clouds ($15 \leq T_{\rm D} \leq 20$ K)
– **Nuclear emission** ($T_{\rm D} \sim 30$ K)
– **Diffuse Emission**: spiral arms and disk ($12 \leq T_{\rm D} \leq 20$ K)

These features appear to be general to nearby spirals mapped by ISOPHOT. They are perhaps best illustrated by the ISOPHOT map of M 31 (Haas et al. 1998), reproduced in Fig. 2. A ring of 10 kpc radius and a diffuse disk component are clearly seen on this image at 170 μm. The diffuse emission can be traced out to a radius of 22 kpc, so the galaxy has a similar overall size in the FIR as seen in the optical bands. In addition, there is a faint nuclear source, which is seen more prominently in HIRES IRAS 60 μm maps at similar resolution and in H_α. The overall SED, which is also constrained by a 240 μm COBE/DIRBE point, can be well described as a a superposition of two modified (m=2) Planck curves, with 16 and 45 K. The cold dust component at 16 K arises from both the ring structure (30%) and the diffuse disk (70%), illustrating the importance of the diffuse emission at least for this example. The 45 K component matches up well with HII region complexes in the ring structure. Associated with each HII region complex are also compact, cold emission sources (see Fig. 3 of Schmidtobreick, Haas & Lemke 2000) with dust temperatures in the 15 to 20 K range. These could well represent the parent molecular clouds in the star formation complexes which gave rise to the HII regions. Detailed examination of the morphology of the ring shows a smooth component of cold dust emission as well as the discrete cold dust sources.

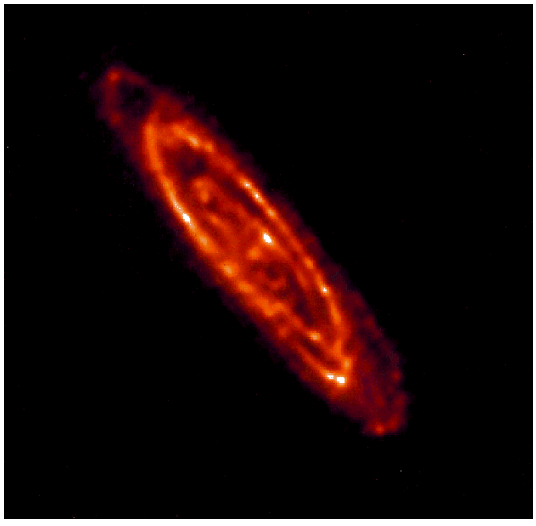

Figure 2. ISOPHOT 170 μm map of M 31 (Haas et al. 1998), with an angular resolution of 1.3 arcmin. North is towards the top, and East is towards the left. The field size is 2.9×2.9 degrees.

There are also beautiful datasets on normal galaxies which are more active in star formation than M 31, notably the Small Magellanic Cloud (type Sm), which was described by Bot et al. (2002) and by Wilke et al. (2002), and M 33 (type Scd; Hippelein et al. 2002). These galaxies also show a prominent diffuse cold dust component, upon which a warm dust component associated with HII region complexes is superimposed. The statistics of the HII region complexes are superior to those in M 31, and, in the case of M 33, the HII region complexes exhibit a trend for the 60:100 μm colour temperature to become colder with increasing galactocentric distance, as observed in our galaxy.

Preliminary results from ISOPHOT maps of nearby spiral galaxies were obtained by Tuffs et al. (1996) for NGC 6946, by Hippelein et al. (1996a,b) for M 51 and M 101 and for a sample of nearby galaxies by Alton et al. (1998b) and Davies et al. (1999). Claims by the latter two references that the FIR disks are more extended than the optical disks are not supported by the higher linear resolution maps of M 31 and M 33 nor by the deep map of NGC 891 (Popescu et al. 2001). However, the maps presented by Alton et al. (1998b) and Davies et al. (1999) were not corrected for transient effects of the detector, and therefore both the calibration and the derived scale lengths are uncertain.

In general there is a wealth of imaging data in the ISO archive still to be exploited, particularly from observations using the dedicated mapping "P32" astronomical observation template. Excellent photometric images are now becoming available for this mode, reduced using new software techniques (see for example the map of M 101 in Tuffs & Gabriel 2002a,b).

3. INTERPRETATION OF FIR EMISSION FROM NEARBY SPIRALS

The ISOPHOT imaging studies have directly demonstrated that spiral galaxies are inhomogeneous. Variations in FIR colours between the observed structures indicate ISRFs which vary by orders of magnitude in intensity. In general, this can be attributed to an inhomogeneous distribution of both emitters and absorbers. Large variations in the colour of the ambient UV-optical radiation field are also expected, especially if structures are optically thick to all or part of the stellar light. Since the absorption probability of stellar photons by grains is a strong function of wavelength, this will also give rise to strong variations in the intensity and colour of the FIR emission. A quantitative interpretation of the FIR emission therefore requires realistic models for the propagation of stellar photons in galaxian disks, to calculate both the colour and intensity of radiation fields illuminating grains.

George Helou described the semi-empirical model of Dale & Helou (2002), which assumes a power law distribution of dust masses over UV-optical radiation energy densities (all of a common intrinsic colour). This model can reproduce observed trends in the MIR-FIR-submm colours of statistical samples, and has also been used to extract bolometric IR emission and dust masses from the ISO data. However, a quantitative interpretation of dust emission in terms of star formation rates and star formation histories requires a combined analysis of the UV-optical/FIR-submm SEDs, embracing a self-consistent model for the propagation of the photons.

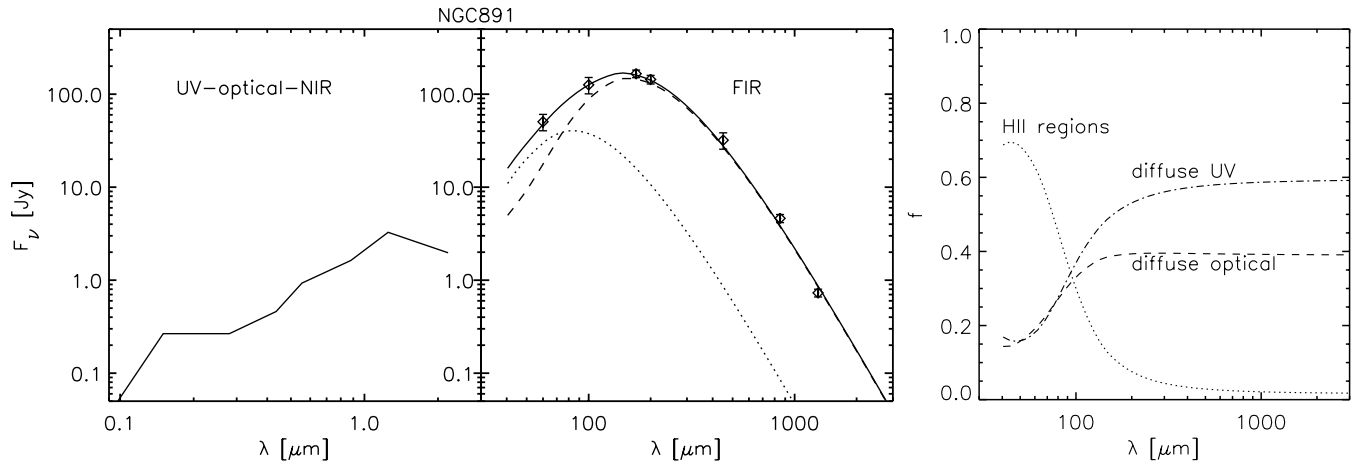

Figure 3. a) The predicted SED of NGC 891 from Popescu & Tuffs (2002a), for a model with $SFR = 3.8\,\mathrm{M}_\odot$*/yr,* $F = 0.22$ *and* $M_{\rm dust} = 7 \times 10^7\,\mathrm{M}_\odot$ *LH panel: the intrinsic emitted stellar radiation (as would have been observed in the absence of dust). RH panel: the re-radiated dust emission, with diffuse and HII components plotted as dashed and dotted lines, respectively. The data (integrated over* $\pm 225'$ *in longitude), are from Alton et. al 1998a (at 60, 100, 450 & 850* μ*m), Guélin et al. 1993 (at* $1300\,\mu$*m) and from Popescu & Tuffs (2002a) (at 170 & 200* μ*m). b) The fractional contribution of the three stellar components to the FIR emission, calculated for the case of NGC 891.*

There are several such models in use which incorporate various geometries for the stellar populations and dust. We will concentrate here on the model of Popescu et al. (2000a), since this is the only model where the geometry of the dust and stellar populations is directly constrained by the optical images. It is furthermore the only model which has been used to make direct predictions for the spatial distribution of the FIR emission for comparison with the ISO images. Full details of the model are given by Popescu et al. (2000a), Misiriotis et al. (2001) and Popescu & Tuffs (2002a). In brief, the model includes solving the radiative-transfer problem for a realistic distribution of absorbers and emitters, considering realistic models for dust, taking into account the grain-size distribution and stochastic heating of small grains and the contribution of HII regions. The FIR-submm SED is fully determined by just three parameters: the star-formation rate SFR, the dust mass $M_{\rm dust}$ associated with the young stellar population, and a factor F, defined as the fraction of non-ionising UV photons which are locally absorbed in HII regions around the massive stars.

Here we illustrate this model with the example of the edge-on galaxy NGC 891. The model can however be applied to galaxies of any inclination. The best fit obtained for the FIR-submm SED of NGC 891 is shown in the right hand panel of Fig. 3a.

If L_0 is the intrinsic UV luminosity corresponding to unity SFR, the relation between the FIR luminosity $L_{\rm FIR}^{\rm tot}$ and SFR can be described by:

$$L_{\rm FIR}^{\rm tot} = L_{\rm FIR}^{\rm HII} + L_{\rm FIR}^{\rm UV} + L_{\rm FIR}^{\rm opt}$$

$$L_{\rm FIR}^{\rm tot} = SFR \times L_0 \times F + SFR \times L_0 \times (1-F) \times G_{uv} + \\ + L_{\rm FIR}^{\rm opt}$$

where G_{uv}, which also depends on $M_{\rm dust}$, is the probability that a non-ionising UV photon released into the diffuse dust will be absorbed there.

It can be seen that a natural outcome of this modelling technique is the prediction of a diffuse cold component of dust emission powered by a combination of non-ionising UV and optical-NIR photons, and a warm component of dust emission corresponding to the ensemble of discrete HII regions. This corresponds to what we have seen in the ISOPHOT maps of nearby galaxies.

The model also predicts the relative contributions of the young and old stellar populations to the dust emission as a function of FIR wavelength (Fig. 3b). An increase in the relative importance of UV heating in the diffuse dust emission component towards longer wavelengths is apparent. This arises because the coldest grains are those which are in weaker radiation fields, either in the outer optically thin regions of the disk or because they are shielded from radiation by optical depth effects. In the first situation the absorption probabilities of photons are controlled by the optical properties of the grains, so the UV photons will dominate the heating. The second situation arises for dust associated with the young stellar population, where the UV emissivity far exceeds the optical emissivity.

This analysis, together with the observational evidence from the maps produced by ISOPHOT, throws new light on the physical interpretation of the 60:100 μm ratio, which is commonly used as a gauge of star formation activity (Helou & Lonsdale 1987). This ratio has to be understood in terms of the inhomogeneous nature of disks in the FIR. Thus, the emission at 60 μm mainly traces locally heated warm grains in and around HII regions, whereas the emission at 100 μm mainly traces the

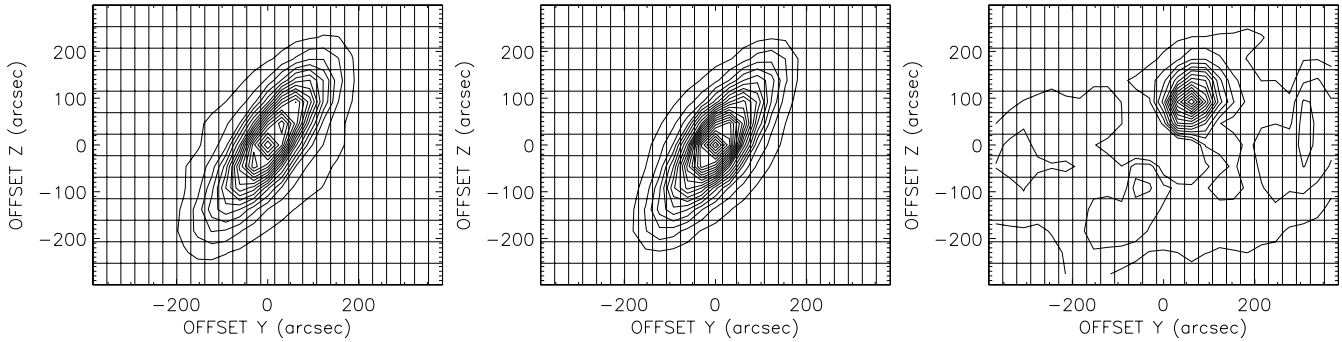

Figure 4. a) Contour plot of the observed brightness distribution of NGC 891 at 170 μm (Popescu & Tuffs 2002a). The contours are plotted from 10.7 to 230.0 MJy/sr in steps of 12.2 MJy/sr. The grid indicates the actual measured sky positions sampled at $31 \times 46''$ in the spacecraft coordinates Y and Z. b) Contour plot of the simulated diffuse brightness distribution of NGC 891 at 170 μm. The contours are plotted from 10.4 to 239.7 MJy/sr in steps of 10.4 MJy/sr. c) Contour plot of the observed minus simulated diffuse brightness distribution of NGC 891 at 170 μm. The contours are plotted from 2.2 to 46.1 MJy/sr in steps of 3.1 MJy/sr. The unresolved source from the Northern side of the galaxy and the faint extended source from the Southern side account for 8% of the integrated flux density, in agreement with the model prediction for FIR localised sources at this wavelength.

emission from the diffuse dust, powered by optical photons as well as by (non-ionising) UV photons.

A particularly stringent test of the model is to compare its predictions for the morphology of the diffuse dust emission component near the peak in the FIR SED with spatially resolved maps. This comparison is shown in Fig. 4a,b, again for the case of NGC 891. A remarkable agreement between the maps is apparent. The residual map between the observed and the simulated maps of the diffuse component (Fig. 4c) reveals a compact source on the Northern side of the galaxy (and a faint extended source seen in the Southern side), with integrated fluxes in agreement with the model predictions for localised sources. The excess emission in the northern side may be a giant molecular cloud complex associated with one of the spiral arms. The remaining diffuse emission is at a level of 1% of the peak brightness and is probably attributable to residual detector artifacts.

4. ISOPHOT OBSERVATIONS OF STATISTICAL SAMPLES

A total of 31 hours of the ISO mission was dedicated to ISOPHOT pointed observations of statistical samples of local universe galaxies. All these projects were complementary in terms of selection and observational goals. In descending order of depth, the published surveys are: the ISOPHOT Virgo Cluster Deep Survey (63 galaxies), the Coma/A1367 Survey (18 galaxies) and the ISO Bright Spiral Galaxies Survey (77 galaxies). In addition, 115 galaxies have been catalogued from the Serendipity Survey. Furthermore, the statistical sample of 60 bright galaxies studied spectroscopically by LWS by Malhotra et al. (2001) was also observed by ISOPHOT at 170 μm with short stares, but the photometry is not yet published.

The ISOPHOT Virgo Cluster Deep Survey (Tuffs et al. 2002; Popescu et al. 2002) represents the *deepest survey* (both in luminosity and surface brightness terms) of normal galaxies yet measured in the FIR. A complete volume- and luminosity sample of 63 gas-rich Virgo Cluster galaxies selected from the Virgo Cluster Catalog (Binggeli, Sandage & Tammann 1985; see also Binggeli, Popescu & Tammann 1993) with Hubble types later than S0 and brighter than $B_{\rm T} \leq 16.8$ were measured with ISOPHOT at 60, 100 and 170 μm. Deep oversampled P32 strip maps covered the entire optical extent of each target (down to the 25.5 mag arcsec^{-2} B-band isophote) as well as adjacent background directions. The faintest detected emissions from the survey are 50, 40 and 80 mJy at 60, 100 and 170 μm, respectively. The total on target time (ISOPHOT) for the survey was 20 hours. The sample was also mapped by ISOCAM (Boselli et al. 1997) and was (in part) observed by LWS (Leech et al. 1999).

The ISOPHOT Virgo Cluster Deep Survey is providing the basis for statistical investigations of the FIR spectral energy distributions of gas rich galaxies in the local universe spanning a broad range in star-formation activity and morphological types, including dwarf systems and galaxies with rather quiescent star formation activity.

The Coma/A1367 Survey (Contursi et al. 2001) consists of 6 spiral and 12 irregular galaxies having IRAS detections at 60 μm. The galaxies were selected to be located within 2 or 1 degrees of the X-ray centres of Coma and A1367 clusters, respectively, with emphasis on peculiar optical morphologies. Each galaxy was observed in a single pointing, by chopping between the galaxy and a background direction. The data were taken at 60, 80, 100, 120, 170 and 200 μm (but only reduced for 120, 170 and 200 μm) for a total on target time (ISOPHOT) of 2 hr. The sample, also observed with ISOCAM, provided a

database of integrated flux densities for a pure cluster sample of high luminosity spiral and irregular galaxies.

The ISO Bright Spiral Galaxies Survey (Bendo et al. 2002a) consists of 77 spiral and S0 galaxies chosen from the Revised Shapley-Ames Catalog (RSA), with $B_{\rm T} \leq 12.0$. Almost all are IRAS sources. Mainly an ISOCAM survey, the project also used 7 hr of on target ISOPHOT time to take 60, 100 and 170 μm short stares towards the nucleus of the galaxies and towards background fields. The sample provides a database of FIR surface brightnesses of the central regions of bright spiral galaxies, including S0s.

The ISO Bright Spiral Galaxies Survey and the ISOPHOT Virgo Cluster Deep Survey represent the principle investigations of optical selected samples of normal galaxies. It should be emphasised that the main difference between them is primarily one of shallow versus deep, rather than field versus cluster, since by design the Virgo Sample predominantly consists of infalling galaxies from the field, and no cluster specific effects could be found.

The Serendipity Survey (Stickel et al. 2000) has so far catalogued 115 galaxies with $S_\nu \geq 2$ Jy at 170 μm and with morphological types predominantly S0/a - Scd. This sample provides a database of integrated 170 μm flux densities for relatively high luminosity spiral galaxies, all detected by IRAS at 60 & 100 μm. A more detailed description of this survey was given in the presentation of Stickel (Stickel et al. 2002a).

5. INTERPRETATION OF FIR EMISSION FROM STATISTICAL SAMPLES

The emerging result of all ISOPHOT statistical studies was that the SEDs of normal galaxies in the 40 - 200 μm spectral range require both warm and cold dust emission components to be fitted. First indications of this result were given by the multi-filter ISOPHOT photometry obtained for 8 inactive spiral galaxies (Krügel et al. 1998; Siebenmorgen, Krügel & Chini 1999). Stickel et al. (2000) and Contursi et al. (2001) found a cold dust component for most of the galaxies in their samples (The Serendipity and the Coma/A1367 samples, respectively), for which upper limits for the cold dust temperatures were inferred. The cold dust component is most prominent in the most "quiescent" galaxies, like those contained in the ISOPHOT Virgo Cluster Deep sample, where the cold dust temperatures were found to be broadly distributed, with a median of 18 K (Popescu et al. 2002), some 8 - 10 K lower than would have been predicted by IRAS. The corresponding dust masses were correspondingly found to be increased by factors of typically 2 - 10 (Stickel et al. 2000) for the Serendipity Sample and by factors 6 - 13 (Popescu et al. 2002) for the Virgo Sample, with respect with previous IRAS determinations. As a consequence, the derived gas-to-dust ratios are much closer to the canonical value of ~ 160 for the Milky Way (Stickel et al. 2000, Contursi et al. 2001), but with a broad distribution of values (Popescu et al. 2002). The FIR properties of the analysed galaxies do not seem to be affected by the environment (Contursi et al. 2001).

Of particular interest are the results concerning the trends with Hubble type found by Popescu et al. (2002) for the ISOPHOT Virgo Cluster Deep sample. A tendency was found for the temperatures of the cold dust component to become colder, and for the cold dust surface densities (normalised to optical area) to increase with increasing lateness in the Hubble type (Figs. 5a,b). A particularly surprising result was the low dust temperatures (ranging down to less than 10 K) and large dust masses associated with the Virgo Im and Blue Compact Dwarf (BCD) galaxies. Another important trend is the increase of the normalised (to K$'$ band magnitude) FIR luminosity as we progress from the early to the later Hubble types (Fig. 5c). This result was later confirmed by Bendo et al. (2002b) for the RSA sample. A related result was also obtained by Pierini et al. (1999) for the LWS data on Virgo galaxies, where a strong correlation of normalised [CII] emission with Hα equivalent widths was interpreted as a trend of increasing star-formation rate along the Hubble sequence.

Finally, Popescu & Tuffs (2002b) also found an increase of the ratio of the dust emission to the total stellar emitted output along the Hubble sequence. This correlation is quite strong, ranging from typical values of $\sim 15\%$ for early spirals to up to $\sim 50\%$ for some late spirals (Popescu & Tuffs 2002b). This, together with the trend for a decrease in the temperature of the cold dust, would suggest a trend of increasing opacities with increasing star-formation activity. The extreme BCDs can have even higher percentages of their bolometric output re-radiated in the thermal infrared. This correlation can be also interpreted as a sequence from normal to dwarf gas rich galaxies, with the dwarfs having an increased contribution of the FIR output to the total bolometric output. These findings could be important for our perception of the distant Universe, where, according to the hierarchical galaxy formation scenarios, gas rich dwarf galaxies should prevail. We would then expect these galaxies to make a higher contribution to the total FIR output in the early Universe than previously expected.

6. DUST OUTSIDE GALAXIES

In some systems dominated by cold dust emission there is evidence that the cold dust emission is external to any optically emitting region and/or that dust is supplied from an external dust reservoir.

Thus, the unexpected result that large amounts of cold dust exist in some Virgo BCDs (Popescu et al. 2002) was interpreted as being indicative of dust surrounding the optical galaxy, originating in an external dust reservoir. In fact, in two cases direct evidence was found of resolved emission at 170 micron on scales of up to 10 kpc. The BCD galaxies were found to have the highest dust mass surface densities (normalised to optical area) and the coldest dust temperatures of the galaxies in the sample. This is a particularly unexpected result, since the IRAS observations of BCDs could be accounted for in terms of dust heated locally in HII regions, with temperatures of 30 K or more. To qualitatively account for the FIR and optical extinction characteristics of BCDs, Popescu et al. (2002) pro-

Figure 5. Trends with Hubble type for the ISOPHOT Virgo Cluster Deep sample (Popescu et al. 2002). The distribution of a) cold dust temperatures $T_{\rm D}^{\rm cold}$; b) cold dust mass surface densities $M_{\rm D}^{\rm cold}/D^2$; c) normalised FIR luminosity (to the K' band magnitude) for different Hubble types. The hatched histograms represent the distributions for the galaxies with SEDs fitted by only one dust component. The filled histograms represent the distributions for the galaxies with detections only at 100 and 170 μm.

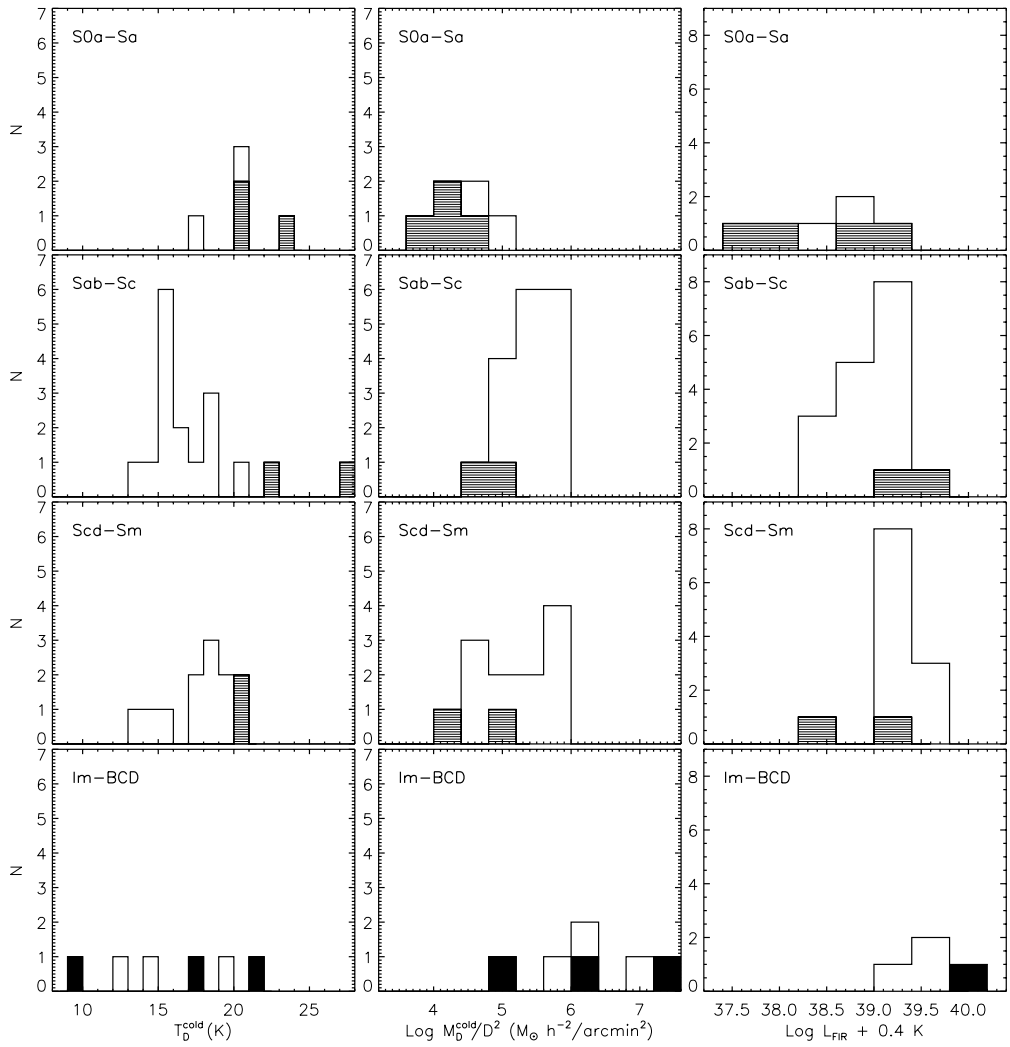

posed two scenarios invoking collisionally or photon-heated emission from grains originating in the surrounding intergalactic medium. In the one scenario, grains are swept up from a surrounding protogalactic cloud and heated collisionally in an optically thin wind bubble blown from the BCD. In the other, the grains are taken to be photon-heated in an optically thick disk surrounding the optical galaxy. The disk is indicative of a massive gas/dust accreting phase which makes dwarf galaxies sporadically bright optical-UV sources when viewed out of the equatorial plane of the disk. In both scenarios the dust does not have a galactic origin, but needs to exist in the immediate vicinity of the galaxies, where it can either be heated by winds or can accrete into the dwarfs.

Dust outside galaxies has also been discovered in a deep ISOPHOT survey of a field centred on the giant elliptical galaxy M86 in the Virgo cluster by Stickel et al. (2002b). One of the sources of FIR emission seen in the periphery of the field is extremely cold and has no obvious optical counterpart. It could trace a dust-rich "relic" of the interstellar media of two spiral galaxies removed in an interaction as postulated by Völk & Xu (1994). Such objects could themselves undergo localised

episodes of star formation and could conceivably account for the large dust masses associated with the Virgo BCDs.

Moving more in the direction of the intragroup medium, the classical example is Stephan's Quintet (SQ), mapped by ISOPHOT using its oversampling mapping mode P32. The 60 μm map (Sulentic et al. 2001) and the 100 μm map (Xu & Tuffs 2002) show the probable detection of FIR diffuse emission from the intragroup medium. In particular the 100 μm map shows clear evidence for extended FIR emission in the periphery of SQ, its morphology having a striking resemblance to the morphology of the diffuse synchrotron radio emission. Since the diffuse radio emission very probably traces a large scale shock in the intragroup medium, the diffuse FIR emission is likely to be also associated with the passage of the shock front. Such an association was predicted by Popescu et al. (2000b) for the case of large-scale accretion shocks in clusters.

ACKNOWLEDGEMENTS

We thank Dr. Jörg Fischera for providing us with Fig. 1, and Prof. Heinrich Völk, for informative discussions.

REFERENCES

Alton P.B., Bianchi S., Rand R.J., et al., 1998a, ApJ, 507, L125
Alton, P.B., Trewhella, M., Davies, J.I., et al. 1998b, A&A, 335, 807
Bendo, G.J., Joseph, R.D., Wells, M. et al. 2002a, AJ 123, 3067
Bendo, G.J., Joseph, R.D., Wells, M. et al. 2002b, AJ in press
Binggeli, B., Popescu, C.C. & Tammann, G.A. 1993, A&AS, 98, 275
Binggeli, B., Sandage, A. & Tammann, G.A. 1985, AJ, 90, 1681
Bruzual, G. & Charlot, S. 1993, ApJ, 405, 538
Boselli, A., Lequeux, J., Contursi, A. et al. 1997, A&A, 324, L13
Bot, C. et al. 2002, this volume
Contursi, A., Boselli, A., Gavazzi, G. et al. 2001, A&A 365, 11
Dale, D. & Helou, G. 2002, ApJ in press
Davies, J.I., Alton, P., Trewhella, M., Evans, R., & Bianchi, S. 1999, MNRAS, 304, 495
Guélin, M., Zylka, R., Mezger, P.G., et al., 1993, A&A, 279, L37
Haas, M., Lemke, D., Stickel, M., et al. 1998, A&A, 338, L33
Helou, G. 2002, this volume
Helou, G. & Lonsdale, C. 1987, ApJ 314. 513
Hippelein, H., Lemke, D., Tuffs, R.J., et al. 1996a, A&A, 315, L79
Hippelein, H., Lemke, D., Haas, M., et al. A&A, 315, L82
Hippelein, H. et al. 2002, in preparation
Kylafis, N.D., & Bahcall, J.N. 1987, ApJ, 317, 637
Krügel, E., Siebenmorgen, R., Zota, V., & Chini, R. 1998, A&A, 331, L9
Laor A., & Draine B. T. 1993, ApJ 402, 441
Leech, K.J., Völk, H.J., Heinrichsen, I., et al. 1999, MNRAS, 310, 317
Lemke, D., Klaas, U., Abolins, J. et al. 1996, A&A, 315, L64
Malhotra, S., Kaufman, M.J., Hollenbach, D., et al. 2001, ApJ 561, 766
Mezger P.G., Mathis J.S., Panagia N., 1982, A&A 105, 372
Misiriotis A., Popescu, C.C., Tuffs, R.J., & Kylafis, N.D. 2001, A&A, 372, 775
Pierini, D., Leech, K.J., Tuffs, R.J., & Völk, H.J. 1999, MNRAS 303, L29
Popescu, C.C., Misiriotis A., Kylafis, N.D., Tuffs, R.J., & Fischera, J., 2000a, A&A, 362, 138
Popescu, C.C., Tuffs, R.J., Fischera, J. & Völk, H.J. 2000b, A&A, 354, 480
Popescu, C.C., Madore, B.F., Tuffs, R.J., & Kylafis, N.D. 2001, AAS198, 76.01
Popescu, C.C. & Tuffs, R.J. 2002a, Reviews in Modern Astronomy, vol 15.
Popescu, C.C. & Tuffs, R.J. 2002b, MNRAS Letters, in press
Popescu, C.C., Tuffs, R.J., Völk, H.J., Pierini, D. & Madore, B.F., 2002, ApJ 567, 221
Schmidtobreick, L., Haas, M., & Lemke, D. 2000, A&A 363, 917
Siebenmorgen, R., Krügel, E., & Chini, R. 1999, A&A, 351, 495
Stickel, M., Lemke, D., Klaas, U. et al. 2000, A&A 359, 865
Stickel, M. et al. 2002a, this volume
Stickel, M. et al. 2002b, in preparation
Sulentic, J.W., Rosaldo, M., Dultzin-Hacyan, D., et al. AJ 122, 2993, 2001
Tuffs, R.J. & Gabriel, C., 2002a, in Proc. "ISOPHOT Workshop on P32 Oversampled Mapping", ESA SP-482
Tuffs, R.J. & Gabriel, C., 2002b, this volume
Tuffs, R.J., Popescu, C.C., Pierini, D., et al. 2002, ApJS 139, 37
Tuffs, R.J., Lemke, D., Xu, C., et al. 1996, A&A, 315, L149
Völk, H.J. & Xu, C. 1994 Infrared Phys. Technol., 35, 527
Wilke, K. et al. 2002, this volume
Xu, C. & Tuffs, R.J. 2002, in: "Proc. ISOPHOT Workshop on P32 Oversampled Mapping", ESA SP-482

EXTRAGALACTIC RESEARCH WITH ISOPHOT PIPELINE PRODUCTS

Ulrich Klaas[1], Martin Haas[1], Philip J. Richards[2], Helen J. Walker[2], and Karsten Wilke[1]

[1]ISOPHOT Data Centre, Max-Planck-Institut für Astronomie, Königstuhl 17, 69117 Heidelberg, Germany
[2]UK ISO Data Centre, CLRC, Rutherford Appleton Laboratory, Chilton, Didcot, OX11 0QX, United Kingdom

ABSTRACT

Several extragalactic research projects on ULIRGs, Seyferts, quasars and normal galaxies are presented, which made direct use of ISOPHOT pipeline (OLP) products from the Legacy ISO Data Archive. The OLP products of several observing modes, like spectrophotometry and FIR raster mode photometry, have now sufficient photometric accuracy and are well characterized. During the ISO Active Archive Phase the UK ISO Data Centre and the ISOPHOT Data Centre will produce updated user-friendly data products of even higher quality for several observing modes.

Key words: radiation mechanisms: thermal – astronomical data bases: ISO Data Archive – infrared: galaxies, galaxies: active, photometry, starbursts

1. INTRODUCTION

One feature of the ISO Data Archive (IDA, Salama 2002) is the graphical representation of different types of data products via the Browse products. These are based on the Auto Analysis Results (AAR) produced by the automatic data reduction pipeline OLP. It has been very often stated that the AAR products should not be used for scientifc research. In the case of ISOPHOT (Lemke et al. 1996) we want to promote here the fact that research can be done well for some observing modes starting from the AAR products and we demonstrate this by the presentation of some recently published extragalactic research results.

2. SCIENTIFIC VALIDATION OF OLP PRODUCTS

One major effort of our data centres during the past ISO Post Mission Phase was to fill the ISO Legacy Archive with well characterized ISOPHOT products. For this purpose comprehensive scientific validation programmes for the individual observing modes were performed. The pure Auto Analysis Result products were accessed and, if appropriate, background subtraction and color correction were applied. The results were compared with reference photometry provided by models and ground-based or other satellite measurements.

3. STATUS OF SCIENTIFIC VALIDATION

In this way practically all of ISOPHOT's 11 main and 28 submodes were characterized and most of them have been declared scientifically validated with the release of the ISO Legacy Archive, which was established with the pipeline OLP10. A status overview is presented in Klaas & Richards (2002). The validation process itself is not the subject here. The consolidated modes with the most reliable products are as follows:

1. Multi-filter photometry with the aperture photometer ISOPHOT-P in telescope staring mode for bright sources (AOT PHT03).
   The achieved accuracies are $< 10\,\%$ absolute and $< 20\,\%$ relative in multi-filter mode for the standard apertures.
2. Multi-filter photometry with the aperture photometer ISOPHOT-P in telescope nodding mode (AOT PHT03).
3. Multi-filter photometry with the array photometer ISOPHOT-C in telescope staring mode for bright sources (AOT PHT22).
   The achieved accuracies are $< 15\,\%$ absolute and $< 20\,\%$ relative in multi-filter mode.
4. Photometry with the array photometer ISOPHOT-C in telescope raster map mode (AOT PHT22).
   The achieved accuracies are $< 25\,\%$ for sources as faint as 50 mJy in the 60 – 100 μm range and 200 mJy in the 120 – 200 μm range. However, these sensitivity limits depend on the local cirrus confusion noise level (see Kiss et al. (2001) for an estimate depending on the sky background level).
5. Spectroscopy with ISOPHOT-S in telescope staring mode (AOT PHT40).
   The achieved accuracies are $< 10\,\%$ absolute and $< 15\,\%$ relative with regard to the spectral shape.
6. Spectroscopy with ISOPHOT-S in chopped mode (AOT PHT40).
   The achieved accuracies are $< 10\,\%$ absolute and $< 10\,\%$ relative with regard to the spectral shape.

The scientific examples in the sections 4 & 5 are covered by these observing modes. The general accuracies of these pipeline AAR products reflect the calibration accuracies and they would not be improved significantly by interactive processing.

Proceedings of the Symposium *"Exploiting the ISO Data Archive - Infrared Astronomy in the Internet Age"*, 24–27 June 2002, Sigüenza, Spain (C. Gry, S. B. Peschke, J. Matagne et al. eds., ESA SP-511)

4. PAH SPECTRA OF GALAXIES

4.1. DUST COMPONENTS IN ULIRGS

Spectroscopy of dust features has helped to constrain the characteristics of the dust components of ultra-luminous infrared galaxies. In Fig. 1 two OLP10 example spectra, one of a normal galaxy and one of a ULIRG, are presented. The peak flux of the most prominent PAH feature at 7.7 μm is indicated.

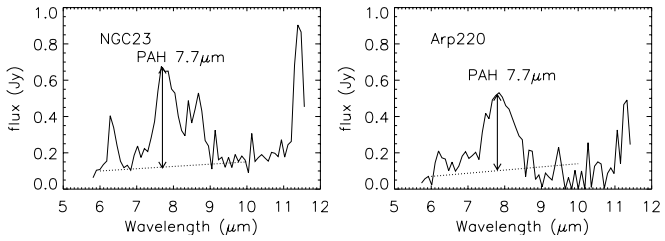

Figure 1. ISOPHOT-S spectra from the archived OLP10 AAR for the normal galaxy NGC 23 and the ULIRG Arp 220. The most prominent feature in both spectra is the PAH 7.7 μm emission. The assumed continuum level is indicated by a dotted line and the peak flux of the 7.7 μm feature by an arrow.

Assuming thermodynamical equilibrium the FIR SED of dust emission can be formally described by

$$S_\lambda = B_\lambda(T)(1 - e^{-\tau_\lambda})$$

with the wavelength dependence of the optical depth parametrized as

$$\tau_\lambda = \tau_{100}(100/\lambda)^\beta$$

The FIR SEDs of ULIRGs can well be fitted by this single component function (Klaas et al. 2001), but these fits yield in most cases $\tau_{100} > 1$. We would therefore expect a significant impact on the shape of the MIR range and hence the strength of the PAH feature. In Fig. 2 we plot the PAH 7.7 μm peak flux normalized by the 850 μm submm continuum flux versus these optical depths at 100 μm derived from the fits. The 850 μm flux is a measure of the total amount of dust mass, since it is from a wavelength regime with optically thin emission.
From Fig. 2 we take the following two conclusions:

1. There is no decrease of the relative PAH strength with τ_{100} indicating that there is not such a severe MIR extinction effect as expected from its value.
2. Most of the ULIRGs show the same $F_{PAH7.7\,\mu m}/F_{850\,\mu m}$ ratio as a comparison sample of normal galaxies (for which we could not perform the FIR SED fits). An exception is Arp 220, see section 4.2.

This leads us to conclude that the FIR SEDs are composed of the emission by several dust components and the PAH feature is coupled to the less IR active one. In fact, the PAH 7.7 μm to 100 μm ratio is systematically decreased for ULIRGs compared to normal galaxies.

More details of this discussion are given in Klaas et al. (2001). For the general relation of PAH strength with cold dust we refer to Haas et al. (2002) in this volume.

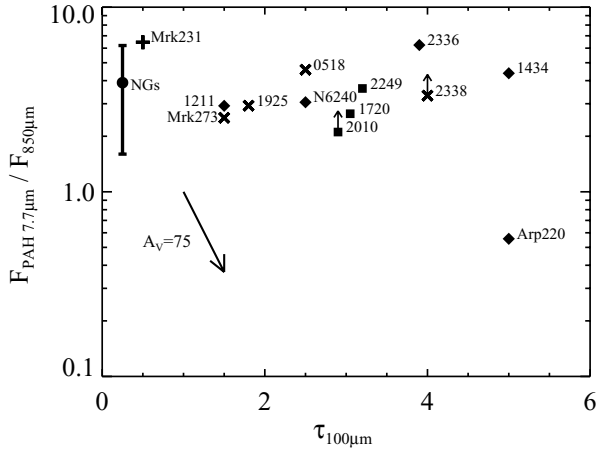

Figure 2. Ratio of the PAH 7.7 μm peak flux to the 850 μm continuum flux versus the optical depth at 100 μm for ULIRGs. $F_{PAH7.7\,\mu m}$ was derived as shown in Fig. 1, $F_{850\,\mu m}$ are SCUBA fluxes and τ_{100} was derived from fits to the FIR/submm SEDs measured with ISOPHOT using the fit function as described in the text. The range of $F_{PAH7.7\,\mu m}/F_{850\,\mu m}$ covered by normal galaxies is indicated by a bar labelled NGs.

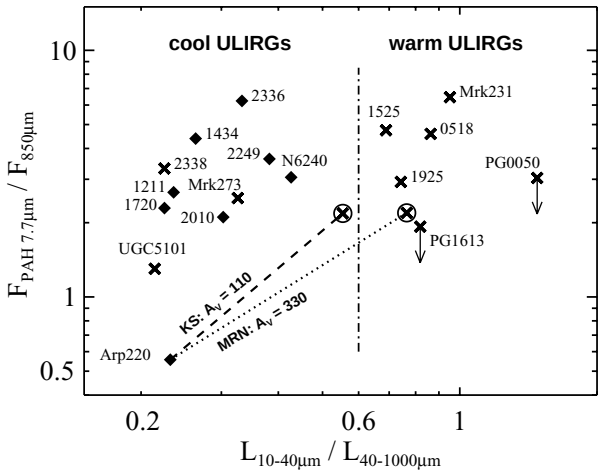

Figure 3. Ratio of the PAH 7.7 μm peak flux to the 850 μm continuum flux versus ratio of the MIR luminosity to FIR/submm luminosity. The vertical dash-dotted line indicates the separation between cool ULIRGs (dominated by starbursts) and warm ULIRGs (dominated by AGN). Dereddening with two different extinction laws is indicated; MRN = Mathis, Rumpl & Nordsieck extinction law (Mathis et al. 1983), KS = Krügel & Siebenmorgen (1994) extinction law.

4.2. EXTINCTION IN ARP 220

In the case of Arp 220 strong MIR extinction seems to be the only explanation for its extreme locus in Fig. 2. A minimum optical absorption of A_V(mixed) = 110 seems to be implied.

Dereddening of Arp 220 by this amount increases the MIR luminosity so much that Arp 220 is no longer a quite cool ULIRG, but rather a warm one which are dominated by AGNs (Fig. 3). This gives some evidence that Arp 220 houses a very

deeply embedded quasar. For more details we refer to Haas et al. (2001).

5. FIR PHOTOMETRY OF NGC 3079

NGC 3079 is a highly inclined edge-on spiral with a LINER nucleus which had been observed with ISOPHOT as a source of the CfA Seyfert sample to determine the relative AGN and starburst energy contributions. A quite spectacular view of this galaxy is given on the HST WFPC2 images published by Cecil et al. (2001).

The FIR photometry consists of single pointing multi-filter staring observations (PHT22) with the C100 and C200 cameras (Fig. 4), which were placed somewhat off-centre. Not covering the whole galaxy disk does not lead to a significant underestimate of the total flux and there is a fair coverage of the spatially resolved 850 μm emission measured by Stevens & Gear (2000).

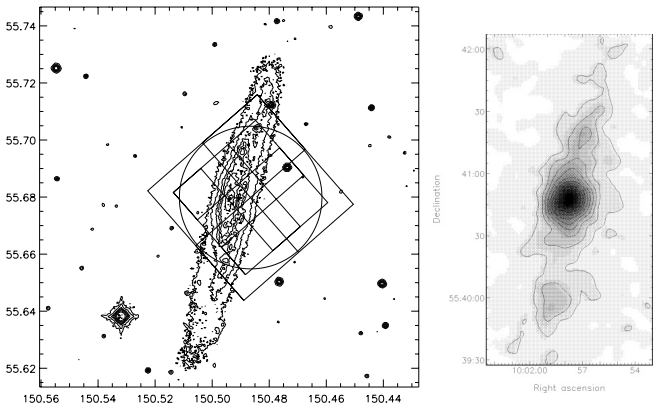

Figure 4. Overlay of the ISOPHOT apertures on a contour plot of the DSS2 red image of NGC 3079. The C200 array (2 × 2 pixels) gives the outer bound, a PHT-P circular aperture used for MIR photometry is located inside it, circumscribing the C100 array (3 × 3 pixels). The 850 μm SCUBA map by Stevens & Gear (2000) is presented in approx. double scale to the right.

The spatial intensity distribution at 60 μm on the C100 camera pixels as contained in the OLP product (Fig. 5 left) shows that the source is resolved. The intensity distribution F(i) traces the location of the pixels on the disk; pixel 3, being far off, has a minimum intensity. Applying the appropriate footprint values $\mathrm{f_{psf}}(i)$ of the central point source allows the core $\mathrm{F_c}$ and disk component $\mathrm{F_d}$(i) to be disentangled for each pixel i as follows:

$$F(i) = F_{\mathrm{d}}(i) + f_{\mathrm{psf}}(i) \times F_{\mathrm{c}}$$

Assuming a flat disk emission in the centre, the disk component in the central pixel 5 can be described by the contributions in the two adjacent pixels 4 and 9 (cf. Fig. 5):

$$F_{\mathrm{d}}(5) = (F_{\mathrm{d}}(4) + F_{\mathrm{d}}(9))/2$$

yielding for the core component:

$$F_{\mathrm{c}} = \frac{2 \times F(5) - F(4) - F(9)}{2 \times f_{\mathrm{psf}}(5) - f_{\mathrm{psf}}(4) - f_{\mathrm{psf}}(9)}$$

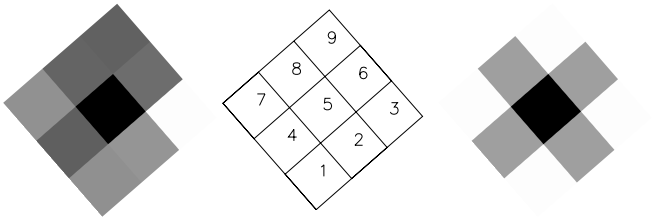

Figure 5. Left: Intensity (low: white, high: black) distribution for NGC 3079 on the C100 array at 60 μm. Middle: C100 pixel numbering scheme for the orientation of the array during the NGC 3079 observation. Right: Intensity distribution for a pure point source centered in pixel 5.

Due to the pointing offset the intensity in C200 pixel 2, whose centre coincides with the one of C100 pixel 3, allows us to do some decomposition also for the C200. The end result is that the disk component amounts to 25 % of the unresolved core component and its contribution rises to 40 % at 200 μm.

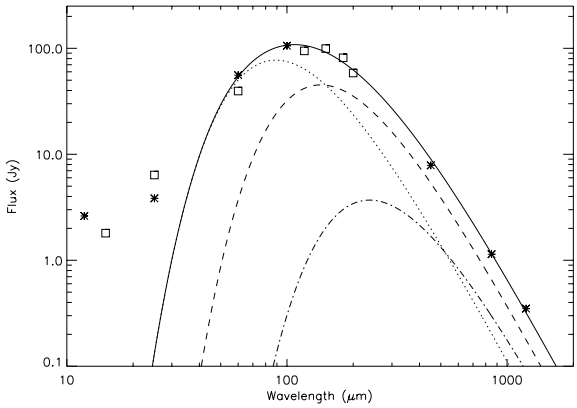

Figure 6. Measured SED of NGC 3079 (total fluxes) from IRAS, ISOPHOT, SCUBA and IRAM. The meaning of the symbols is the following: asterisks: IRAS (12 - 100 μm), SCUBA (450 & 850 μm) and IRAM (1220 μm), squares: ISOPHOT photometry: sum of fluxes from an unresolved core and an extended disk component. The solid line is the superposition of three modified blackbodies ($\varepsilon \propto \lambda^{-2}$) with T_1 = 32 K (dotted curve), T_2 = 20 K (dashed curve) and T_3 = 12 K (dash-dotted curve).

The total fluxes composed of the contribution by the core and disk components are plotted in Fig. 6. The FIR and submm SED can be fitted by multiple modified blackbodies. The short wavelength part needs a 32 K dust component with a mass of 2.7×10^6 $\mathrm{M_\odot}$, the wavelength regime beyond 150 μm is dominated by a 20 K component, and, to get the right slope in the submm a 12 K component of approximately equal dust mass has been introduced. This yields a total dust mass of 4×10^7 $\mathrm{M_\odot}$ and a gas-to-dust mass ratio of about 200, close to that for the Milky Way.

The full description of this analysis can be found in Klaas & Walker (2002).

6. SUMMARY AND OUTLOOK

– We have shown results of several extragalactic scientific publications which utilized ISOPHOT OLP products from the ISO Data Archive.
– The automatic pipeline processing (OLP) of the following ISOPHOT observing modes has reached high stability and accuracy:
  - staring and chopped spectroscopy (AOT PHT40)
  - staring mode photometry of bright sources (PHT03, PHT22)
  - nodding (PHT03 linear raster, standard apertures only) and mini-map (PHT22 raster) photometry of faint sources. As a guideline for reliability, the source should be recognizable in the centre of the map on the IDA browse product displays.

For more detailed information on the status of each observing mode, please refer to:

1) Report on the Scientific Validation of PHT OLP Version 10.0 (Klaas & Richards 2002)
2) ISOPHOT Calibration Accuracies, Version 5.0
   http://www.iso.vilspa.esa.es/users/exp_lib/PHT_top.html

During the ISO Active Archive Phase further improvements will be implemented into the ISOPHOT pipeline running at UKIDC (Richards & Klaas 2002). Among them there will be better deglitching of chopped PHT-S spectra (Fig. 7) and an easy to access presentation of point source fluxes in the file headers of mini-raster maps allowing the SEDs like in Fig. 8 to be established directly from the OLP products.

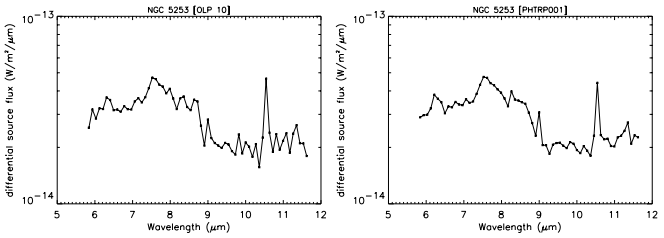

Figure 7. ISOPHOT-S spectrum of NGC 5253. Left: OLP10 product. Right: Pipeline product with improved deglitching produced by a bulk re-processing of chopped ISOPHOT-S measurements during the Active Archive Phase. The continuum has become smoother and PAH and ionic line features at 9 and 10.5 μm stick out more clearly.

A bulk re-processing of all suitable data sets will be performed, selected test cases will undergo a validation and the new full AAR equivalents (in FITS format) will be imported into the IDA.

ACKNOWLEDGEMENTS

The ISOPHOT Data Centre is supported by the Max-Planck-Gesellschaft and Deutsches Zentrum für Luft- und Raumfahrt e.V. (DLR) with funds from Bundesministerium für Bildung und Forschung, grant No. 50 QI 0201.

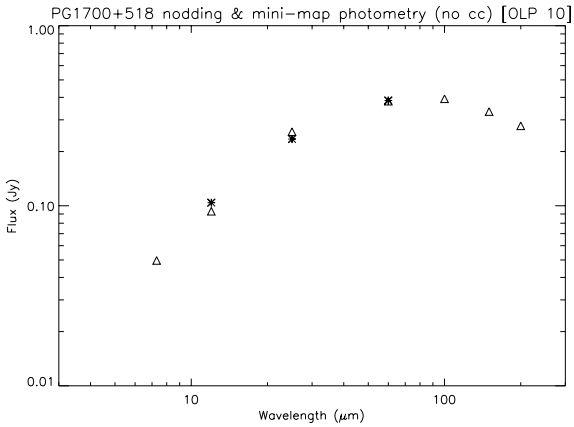

Figure 8. Combined nodding (PHT03, $\lambda < 50\,\mu m$) and mini-map (PHT22, $\lambda > 50\,\mu m$) photometry of the quasar PG 1700+518. The meaning of the symbols is the following: asterisks: IRAS (12 - 60 μm), triangles: ISOPHOT.

REFERENCES

Cecil, G., Bland-Hawthorn, J., Veilleux, S., & Filippenko, A.V. 2001, ApJ, 555, 338
Haas, M., Klaas, U., Müller, S.A.H., et al. 2001, A&A, 367, L9
Haas, M., Klaas, U., Bianchi, S. 2002, ESA SP-511, this volume
Kiss, Cs., Ábrahám, P., Klaas, U., Juvela, M., Lemke, D. 2001, A&A 379, 1161
Klaas, U., Haas, M., Müller, S.A.H., et al. 2001, A&A, 379, 823
Klaas, U., & Richards, P.J. 2002, Report on the Scientific Validation of PHT OLP version 10.0, version 1.0, 09-April-2002, http://www.iso.vilspa.esa.es/users/expl_lib/PHT_list.html
Klaas, U., & Walker, H.J. 2002, A&A, 391, 911
Krügel, E., & Siebenmorgen, R. 1994, A&A, 288, 929
Lemke, D., Klaas, U., Abolins, J., et al. 1996, A&A, 315, L64
Mathis, J.S., Mezger, P.G., & Panagia, N. 1983, A&A, 128, 212
Richards, P.J., & Klaas, U. 2002, ESA SP-511, this volume
Salama, A. 2002, ESA SP-511, this volume
Stevens, J.A., & Gear, W.K., 2000, MNRAS, 312, L5

ISO SPECTROSCOPY OF BRIGHT GALACTIC NUCLEI

Dieter Lutz

Max-Planck-Institut für extraterrestrische Physik, Postfach 1312, 85741 Garching, Germany

ABSTRACT

Mid- and far-infrared spectroscopy of galactic nuclei has made a significant step forward with the large set of observations that is now publicly available in the ISO archive. This paper discusses some of the infrared diagnostics tools that have been developed on the basis of the lines and features detected over this wavelength range, and presents selected results on the physical conditions and power sources of the nuclear regions of star forming, active, and ultraluminous galaxies.

Key words: ISO – galaxies: starburst – galaxies: active – infrared: galaxies

1. INTRODUCTION

With the exception of the brightest lines in the very brightest sources, mid- and far-infrared spectroscopy of galaxies has been impossible to obtain from ground-based telescopes or the Kuiper Airborne Observatory. Complete wavelength coverage and high sensitivity of the ISO cryogenic space telescope have changed this situation, providing spectra of unprecedented detail. The combined SWS and LWS spectrum of the Circinus galaxy, which hosts both a type 2 AGN and star formation, collects most of the elements of infrared spectra of galaxies that can be used as spectroscopic or photometric diagnostics (Fig. 1). A rich spectrum of ionic fine structure lines, hydrogen recombination lines and molecular hydrogen rotational lines is superposed on the far-infrared dust emission, a mid-infrared AGN continuum, and the mid-infrared emission and absorption features.

2. CONTINUUM AND FEATURES

The 6-13 μm spectra of star forming galaxies are dominated by strong emission features from transiently heated aromatic carriers, called PAH features in the following according to one of their most popular identifications. These PAH spectra are very similar among different star forming galaxies covering a wide range of luminosities (Rigopoulou et al. 1999, Helou et al. 2000). An exception to be noted is the weakness or absence of the PAHs in the spectra of low metallicity starbursting dwarfs, e.g., SBS 0355-052 (Thuan et al. 1999), 30 Dor in the LMC (Sturm et al. 2000), NGC 5253 (Rigopoulou et al. 1999). While this is of little relevance for studies of nearby dusty starbursts, it may have implications on future mid-infrared observations of lower metallicity galaxies at higher redshift, both for determining their redshifts and for studying their nature. The minimum near 10μm between the two major PAH complexes is difficult to disentangle from silicate absorption. At longer wavelengths, a rising continuum likely due to very small grains sets in. Close comparison of the SWS spectra of M 82 and NGC 253 (Sturm et al. 2000) as well as CAM-CVF spectroscopy of several, partly spatially resolved, starbursts (Laurent et al. 2000) confirms that the PAH feature emission is fairly similar from source to source and likely originates in photodissociation regions (PDRs). Conversely, the rising continuum at longer wavelengths varies with physical conditions in the H II regions of the starburst and is most intense in compact regions like the one in the interaction zone of the Antenna galaxies (Mirabel et al. 1998).

In accordance with previous ground-based results, the aromatic emission features are found to be weaker or absent in many Seyfert spectra. Spatially resolved ISO spectra of NGC 1068, Cen A, and Circinus demonstrate even more convincingly that the PAH features observed in Seyferts are not related to the AGN proper (Alexander et al. 1999, Mirabel et al. 1999, Moorwood 1999, Le Floc'h et al. 2001). PAH emission is undetected in the nuclei but seen on larger scales, where it excited in a starburst or cirrus type situation. The case for PAH weakness or destruction close to an AGN, based on the morphology of PAH emission and continuum, is further supported by a comparison of PAH emission and warm molecular hydrogen emission in the rotational lines (Rigopoulou et al. 2002). These two tracers correlate well in starburst galaxies. This is plausible if in starbursts both mostly originate in a dense, warm component representing a few per cent of the total gas mass, that mostly resides in PDRs. However, some AGN have a very low PAH/H_2 ratio, as expected for a significant contribution of X-ray dominated regions where molecular hydrogen emission is strong but the PAH carriers destroyed (Voit 1992a). Finally, in the context of unified scenarios for Seyferts, the PAH equivalent widths of Seyfert 2's are found to be larger than those of Seyfert 1's while the PAH fluxes of both categories are similar (Clavel et al. 2000). Such behaviour can be explained if the PAH emission originates on larger scales and is emitted isotropically, while the AGN continuum is emitted anisotropically changing significantly with angle between line of sight and axis of the putative dust torus.

Proceedings of the Symposium *"Exploiting the ISO Data Archive - Infrared Astronomy in the Internet Age"*, 24–27 June 2002, Sigüenza, Spain (C. Gry, S. B. Peschke, J. Matagne et al. eds., ESA SP-511)

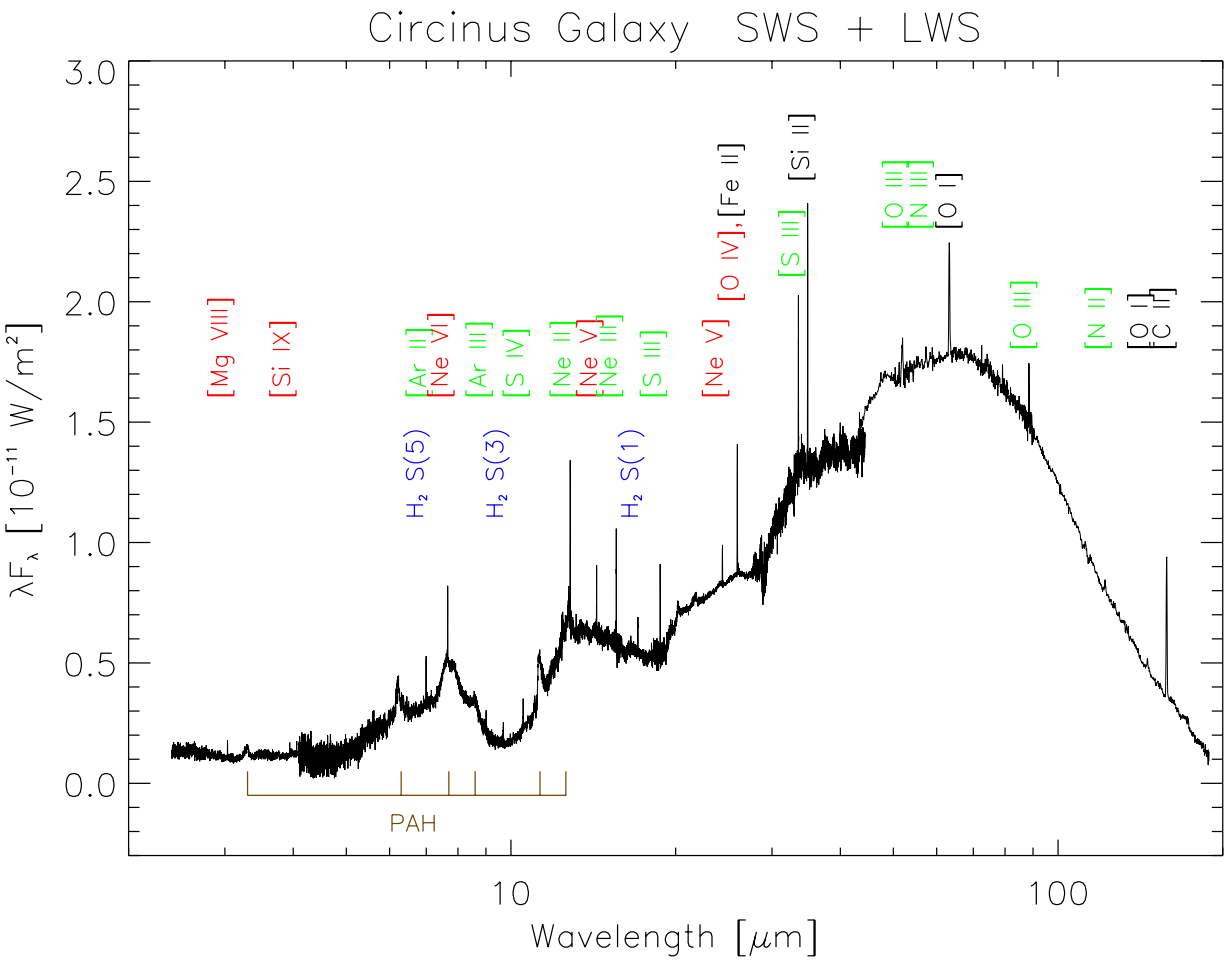

Figure 1. The ISO 2.4-195μm spectrum of the Circinus galaxy collects most elements of infrared spectra of galaxies.

As noted above, the shapes of the PAH spectra change relatively little over a wide range of normal and starbursting galaxies. The relation between PAH luminosity and far-infrared luminosity does show a trend with activity, however (Helou et al. 2001), as does the [C II] 158μm luminosity (see also below). At the high star formation activity end of this sequence, different interpretations have been given. An increasing radiation field may modify or destroy some of the PAH carriers, reducing their role in the photoelectric heating compared to the larger grains, thus naturally linking reduced heating (photoelectric effect on PAHs and grains) and cooling ([C II] emission) (Helou et al. 2001, see also Contursi et al. 2002). Alternatively, two component models have been postulated in which one component is 'normal' in the relation of PAH, [C II] and FIR emission, and the second component is a pure FIR continuum (Fischer 2001). Another issue can additionally arise in such decompositions. Is such a PAH component (in overall actively star forming galaxies) due to PDRs in star forming regions, or due to cold dust and molecular clouds excited by the general interstellar radiation field (Haas et al. 2002)? In galaxy disks, PAHs correlate better with extinction corrected Hα (the youngest stars) than with the blue light representing a somewhat older population (Roussel et al. 2001). This, and the similarity of PAH maps with maps of star formation tracers (e.g. Brγ or radio emission in the Antennae starburst) suggest most of the PAH emission in these objects is from PDRs associated with active star forming regions. Finally, while the PAH luminosities for the most active starbursts do not directly scale with the FIR luminosity, they are well above that of a quiescent low L_{FIR} spiral in absolute terms. Then, the above issue may be mainly a semantic one of directly calling these regions 'PDRs associated with active star forming regions' vs. '... regions dominated by cold dust and molecular clouds ... excited by the interstellar radiation field which in star forming galaxies is sufficiently strong' (Haas et al. 2002).

In this context of quantification of the PAH emission in star forming galaxies, systematic mining of the archive of *Galactic* PAH and [C II] observations may be crucial to better quantify the relation of these tracers to local conditions like hardness and intensity of the UV radiation field, the ratio of UV field intensity and gas density, or metallicity. Some promising steps in quantifying, e.g., the relation between PAH emission and UV field intensity have already been shown at this conference, but the wide spread of assumptions in the community

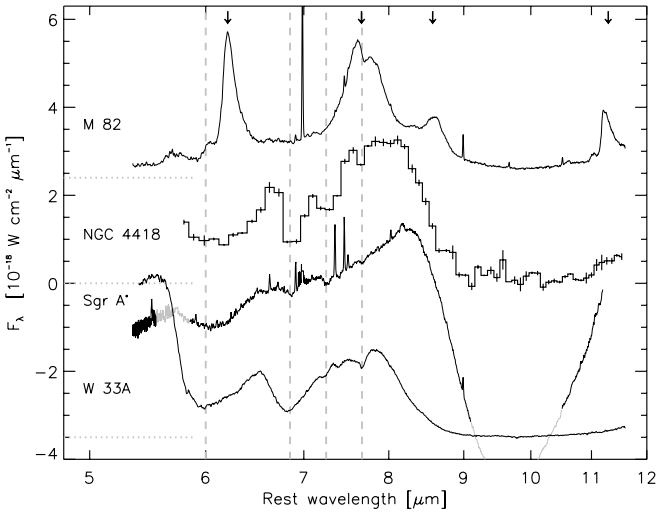

Figure 2. The spectrum of the obscured infrared galaxy NGC 4418 shows strong ice absorptions (Spoon et al. 2001). For comparison, the absorbed Galactic spectra of Sgr A and W33A are shown. In a heavily obscured spectrum like that of NGC 4418, regions of reduced extinction at 6.5-6.7μm and the maximum in the 8μm region may look like emission features at first glance. However, such spectra can be distinguished from a true PAH spectrum like that of M82 on the basis of the feature wavelengths.*

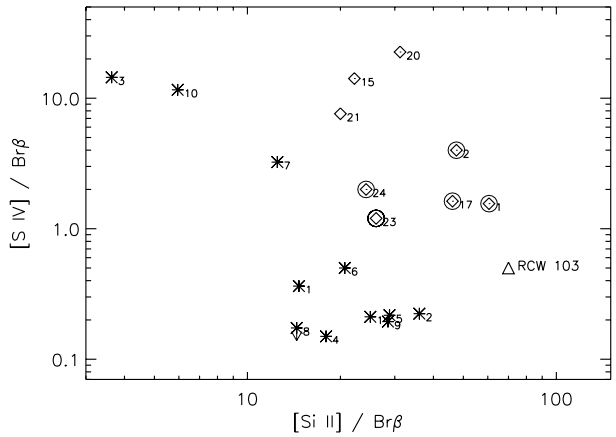

Figure 3. A mid-IR diagnostic diagram to distinguish starbursts and AGNs in dusty environments. AGNs are shown as diamonds, starburst galaxies as stars. The supernova remnant shock source RCW 103 is shown as a triangle (Sturm et al. 2002).

on if and under exactly which conditions PAHs are 'destroyed' (i.e. their observed emission weakened compared to the mid- to far-infrared continuum) warrants systematic efforts.

3. ICES

Detailed mid-infrared spectroscopy with ISO has considerably widened the observational database of ice features in spectra of Galactic objects. Careful inspection of the ISO database shows them to be present in external galaxies as well. Detections range from moderate 3μm water ice absorption in M82 and NGC 253 (Sturm et al. 2000) to strong water and CO_2 ice absorption in NGC 4945 (Spoon et al. 2000), and to the extreme absorption dominated spectrum of NGC 4418 (Fig. 2, Spoon et al. 2001) that has similarities with absorption-dominated spectra of strongly embedded young stellar objects. At first glance, one might expect the cold environment of molecular clouds in starbursts to be more beneficial to the presence of ices than the warm or hot dusty medium close to an AGN, a point of view that is supported by the absence of ices in the spectrum of NGC 1068 (Sturm et al. 2000). The ices in the spectrum of the most likely AGN-dominated NGC 4418, however, caution that more investigations will be needed to elucidate the contributions of starburst molecular clouds, cold regions of circum-AGN molecular material, and the larger scale hosts to the observed extragalactic ice absorptions.

Spoon et al. (2002) have recently searched all ISOPHOT-S and ISOCAM-CVF spectra of galaxies for indications of ice features. At the detection limits of the ISO data, ices are detected in a moderate fraction (∼20%) of objects in this heterogeneous sample. Systems with extreme ice absorption like NGC 4418 must be the exception. The highest detection rate is in ULIRGs, consistent with the presence of large quantities of molecular material in these objects. Ice absorptions will also modify the observed emission features, by weakening the 6.2μm one which is inside a main water ice feature. The striking differences in relative strength of absorption features due to ice and due to carbonaceous material when comparing M 82 and NGC 1068, and even for several lines of sight close to the Galactic center (Chiar et al. 2000) are a further warning that the mid-infrared absorption features in galaxies may vary considerably - observations are clearly inconsistent with being due to a unique absorption curve that is just applied at different absolute levels of absorption.

Ice absorptions add another complication to the interpretation of mid-IR low resolution spectra. The ISO experience clearly demonstrates that good S/N and wavelength coverage are needed to reliably disentangle the various components. The incomplete wavelength coverage of ground-based N band spectra and of ISOPHOT-S spectra in both cases leads to degeneracies, ISOCAM-CVF with its larger wavelength coverage does better. Successful models for future low resolution spectroscopy with e.g. SIRTF-IRS will have to extend the three component models of PAHs, H II region continuum and an AGN continuum (Laurent et al. 2000) with a more sophisticated treatment of absorption for each of these components.

4. FINE STRUCTURE LINES AND DIAGNOSTIC DIAGRAMS

Diagnostic diagrams to discriminate starburst and AGN activity in heavily obscured regions have been developed on the basis of ISO data using a combination of broad emission features and fine structure lines (Genzel et al. 1998), a more complete use of the continuum and PAH features (Laurent et al. 2000, Tran et al. 2001, see also previous sections) and 2-dimensional

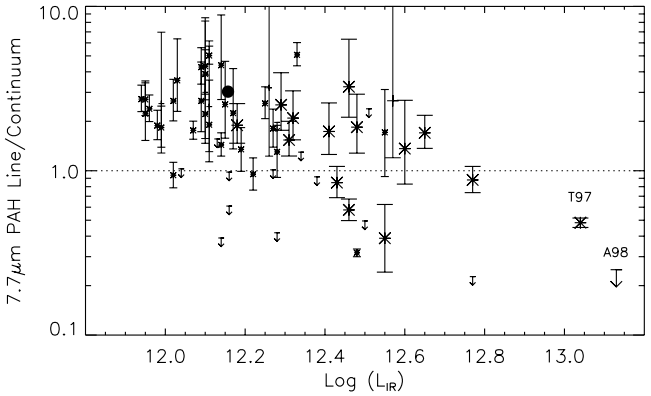

Figure 4. Line-to-continuum ratio for the 7.7μm PAH feature as a function of infrared luminosity, for a large sample of ultraluminous infrared galaxies (Tran et al. 2001). The dotted line indicates the separation between starburst- and AGN-dominated objects. There is a trend towards AGN dominance at the highest luminosities.

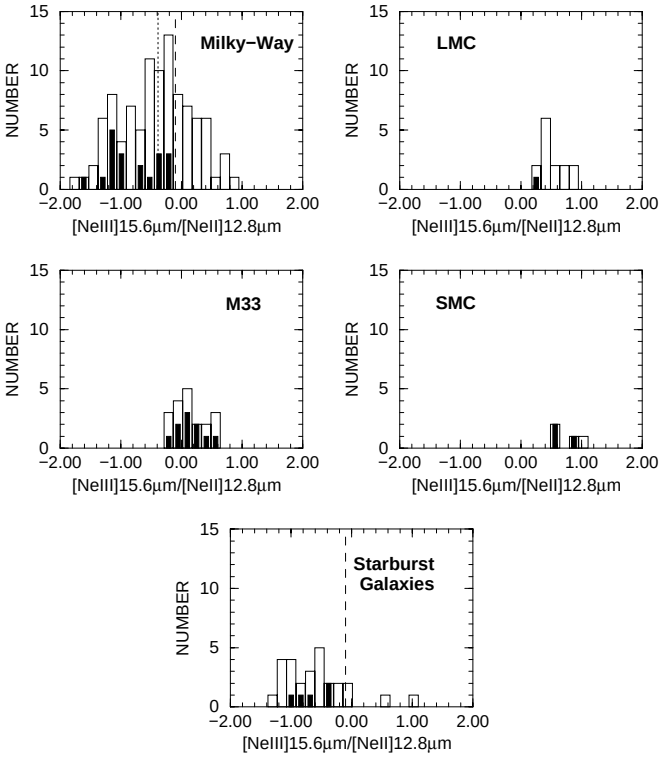

Figure 5. A comparison of the excitation of the neon fine structure line spectrum of starburst galaxies with individual H II regions in the Milky Way and local group galaxies (Giveon et al. 2002).

diagrams solely based on emission lines (Sturm et al. 2002; see Fig. 3 for an example). In underlying physics, the latter are fully equivalent to traditional optical diagnostic diagrams (e.g. Veilleux & Osterbrock 1987) but with much reduced sensitivity to dust obscuration.

The major application of these diagnostic diagrams has been in the study of the power sources of ultraluminous infrared galaxies (ULIRGs). Sensitivity reasons have limited the application of emission line diagnostics to about a dozen objects (Genzel et al. 1998), but the lower resolution diagnostics based on emission features have allowed to extend this to larger samples that cover a wider range of luminosities and probe for evolutionary effects (Lutz et al. 1998, Rigopoulou et al. 1999, Tran et al. 2001). Most ULIRGs are found to be predominantly starburst powered, but with a trend towards AGN dominance at the very highest luminosities (Fig. 4).

5. THE STELLAR POPULATION OF STARBURSTS

A number of key questions are related to the hot star population in starbursts. Is the Initial Mass Function similar to the one in our Galaxy? How do starbursts evolve? Do they continue until they have consumed all their gas fuel or are they stopped in other ways? ISO studied the hot star content by analysis of nebular emission, benefiting from relative insensitivity of the mid infrared lines to extinction and electron temperature. Thornley et al. (2000) have carried out an SWS survey of the [Ne III] 15.55μm and [Ne II] 12.81μm lines in 27 starbursts. The neon line ratio in these starburst galaxies is typically somewhat lower than in individual galactic H II region templates (e.g. Fig. 5, from Giveon et al. 2002). Thornley et al. (2000) have carried out a quantitative analysis, modelling a starburst as an ensemble of evolving star clusters photoionizing the surrounding interstellar medium. Spectral energy distributions for each cluster are derived from an evolutionary synthesis using Geneva tracks and recent non-LTE unified stellar atmospheres (Pauldrach et al. 2001). Nebular emission is predicted from these SEDs and photoionization modelling with CLOUDY. The modelling results suggest that most of these starbursts are presently deficient in the most massive stars, either because they did not form in an IMF invoking an upper mass cutoff, or because they disappeared due to aging effects. The considerable overlap between excitation of starbursts and Galactic H II regions and direct evidence for the presence of very massive stars in nearby starburst templates suggest aging effects to be dominant while the IMF is likely normal. In that framework and using the ratio of infrared (bolometric) and Lyman continuum luminosity as an additional constraint, most starbursts must be short-lived ($<\sim 10^7$ years), only a few O star lifetimes. The most likely cause for this short lifetimes is a strong negative feedback of star formation. Disruption of the interstellar medium by stellar winds and supernovae will be faster than simple gas consumption. Such short bursts are consistent with spatially resolved near-infrared studies (Förster Schreiber et al. 2001).

A number of studies are applying similar methods to Galactic H II regions (Giveon et al. 2002, Peeters et al. 2002, Martín-Hernandez et al. 2002). In addition to analysis of our Galaxy, they can provide important tests of the methods and assumptions of starburst studies. The adequacy of the most recent hot star model atmospheres by the Munich group, for example, appears to be good (Giveon et al. 2002). In addition, comparison to galactic H II regions can help constraining the role of metallicity in determining the starburst spectra (Verma et al. 2002).

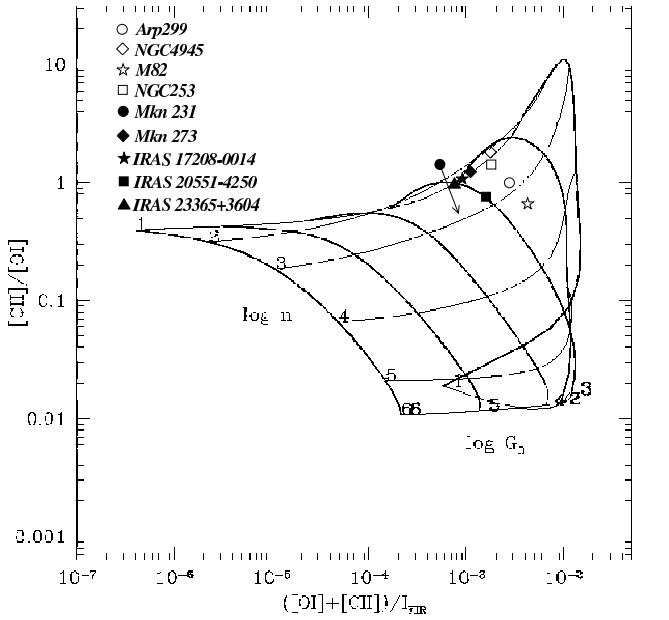

Figure 6. Plot of the [C II] 158μm / [O I] 63μm ratio versus the ratio of ([C II] 158μm + [O I] 63μm) / I_{FIR} emitted from the surface of a PDR. Five ultraluminous infrared galaxies (filled symbols) and several lower luminosity comparison objects are shown (Luhman et al. 2002). The arrow on the black filled circle (Mrk 231) indicates the effect of considering absorption in the [O I] 63μm line, which may be present in this and other ULIRGs.

6. THE [C II] DEFICIT

A key finding of ISO spectroscopy was the relative weakness of [C II] 157.7μm emission in luminous and FIR-warm galaxies that was somewhat of a surprise early during the ISO mission (Malhotra et al. 1997, Luhman et al. 1998), and has strong implications on the potential use of [C II] as a star formation tracer for high redshift studies. One strong contributor to this effect is most likely a reduced photoelectric heating efficiency in the very intense UV fields of PDRs in these galaxies, but diagnostics to reliably measure the physical conditions in these PDRs or investigate alternative scenarios are largely lacking at this point. Spectroscopy with Herschel will better reach the fainter PDR diagnostics, and its higher spectral resolution will allow to test the possible role of [C II] self-absorption in this effect (See the example of Sgr B2, Cox et al. 1999).

Luhman et al. (2002) have recently analysed all 15 ULIRGs with available LWS [C II] spectra, supplementing this analysis with data on the [O I] 63μm and 145μm lines and PAH fluxes where available. The [C II] deficit is confirmed for this enlarged sample. A PDR analysis combining [C II] and [O I] data indicates that a high ratio of UV field intensity and gas density ('G/n') plays a role but is not satisfactory to explain all observations. A key observation here is the weakness of the [O I] 145μm line in Arp 220 which, unlike weakness of the [O I] 63μm line, cannot be ascribed to self-absorption. The analysis of Luhman et al. (2002) suggests increased absorption of UV photons by dust in the H II regions, rather than by gas in the H II region and PDR, i.e. 'dust-bounded' H II regions. The fraction of dust absorbed photons is well known to rise with increasing ionisation parameter U (e.g. Voit 1992b). Given the high concentration of star formation in ULIRGs and the similarities between the 'radiation density / gas density' parameters U (ionizing photons inside the ionisation front) and G/n (UV photons in the PDR outside the ionisation front), it is natural to assume that both effects are linked and contribute to the ULIRG [C II] deficit.

A parameter requiring special attention in view of future high redshift studies is metallicity: Strong [C II] emission observed in local low metallicity systems (e.g. Madden et al. 1997, Hunter et al. 2001) may indicate better prospects for the use of this line than inferred from the local ULIRGs.

ACKNOWLEDGEMENTS

Much of this contribution is based on the joint efforts of many members of the MPE infrared group and collaborators. We acknowledge support for the ISOSDC at MPE by DLR under grant 50 QI 0202. ISO spectroscopy of galaxies is supported by Verbundforschung under grant 50 OR 9913 7.

REFERENCES

Alexander D.M., et al. 1999, MNRAS, 310, 78
Chiar J., et al. 2000, ApJ, 537, 749
Clavel J., et al. 2000, A&A, 357, 839
Contursi A., et al. 2002, this proceedings
Cox P., et al. 1999, in: The universe as seen by ISO, eds. P. Cox and M.F. Kessler, ESA-SP 427, p.631
Fischer J. 2001, in: The Promise of the Herschel Space Observatory, eds. G.L.Pilbratt et al., ESA-SP460, p. 131
Förster-Schreiber N., et al. 2001, ApJ, 552, 544
Giveon U., et al. 2002, ApJ, 566, 880
Genzel R., et al. 1998, ApJ, 498, 579
Haas M., Klaas U., Bianchi S. 2002, A&A, 385, L23
Helou G., et al. 2000, ApJ, 532, L21
Helou G., Malhotra S., Hollenbach D.J., Dale D.A., Contursi A. 2001, ApJ, 548, L73
Hunter D.A., et al. 2001, ApJ, 553, 121
Laurent O., et al., 2000, A&A, 359, 887
Le Floc'h E., et al. 2001, A&A, 367, 487
Luhman M., et al. 1998, ApJ, 504, L11
Luhman M., et al. 2002, ApJ, submitted
Lutz D., et al. 1998, ApJ, 505, L103
Madden S.C. et al., 1997, ApJ, 483, 200
Malhotra S., et al. 1997, ApJ, 491, L27
Martin-Hernandez N.L., et al. 2002, A&A, 381, 606
Mirabel I.F., et al., 1998, A&A, 331, L1
Mirabel I.F., et al. 1999, A&A, 341, 667
Moorwood A.F.M., 1999, in: The Universe as seen by ISO, eds. P.Cox, M.F.Kessler, ESA-SP427, p. 825
Pauldrach A.W.A., Hoffmann T.L., Lennon M., 2001, A&A, 375, 161
Peeters E., et al. 2002, A&A, 381, 571
Rigopoulou D., et al. 1999, AJ, 118, 2625
Rigopoulou D., Kunze D., Lutz D., Genzel R., Moorwood A.F.M. 2002, A&A, 389, 374
Roussel H., Sauvage M., Vigroux L., Bosma A. 2001, A&A, 372, 427

Spoon H.W.W., Koornneef J., Moorwood A.F.M., Lutz D., Tielens A.G.G.M. 2000, A&A, 357, 898
Spoon H.W.W., et al. 2001, A&A, 365, L353
Spoon H.W.W., et al. 2002, A&A, 385, 1022
Sturm E., et al. 2000, A&A, 358, 481
Sturm E., et al. 2002, A&A, in press (astro-ph/0207381)
Thornley M.D., et al. 2000, ApJ, 539, 641
Thuan T.X., Sauvage M., Madden S., 1999, A&A, 516, 783
Tran D., et al., 2001, ApJ, 552, 527
Veilleux S., Osterbrock D.E. 1987, ApJS, 63, 295
Verma A., et al., 2002, this proceedings
Voit G.M. 1992a, MNRAS, 258, 841
Voit G.M. 1992b, ApJ, 399, 495

LUMINOUS DUST EMISSION IN ACTIVE GALAXIES AS SEEN BY ISO

Martin Haas

Max-Planck-Institut für Astronomie (MPIA), Königstuhl 17, D-69117 Heidelberg, Germany

ABSTRACT

This review summarises imaging and photometry results obtained with ISOCAM and ISOPHOT on various active galaxy classes which turn out to be IR luminous having $L_{3-1000\mu m} > 10^{10}$ $L_\odot$ ($H_\circ$ = 75 km/s/Mpc).

Key words: (U)LIRGs, quasars, radio galaxies

1. INTRODUCTION

Before plenty of ISO observations of various galaxy classes are referred to, in this section a guideline is given in order to facilitate our current understanding of dust in galaxies.

Because of limited spatial resolution of FIR imaging, in many cases we focus on the spectral energy distribution (SED) describing the total dust emission of a galaxy. Fig. 1 illustrates the SEDs of various galaxy classes, including already our new knowledge based on ISO. The thermal spectrum has been decomposed into (modified) blackbody components. The relation between the galaxy classes can naturally be discussed in terms of these components:

Left column, top row: The SED of a normal (i.e. not active, quiet) spiral galaxy peaks at wavelengths longer than 100 μm, it is dominated by a cold dust component of T $<$ 20 K. This cold component is accompanied by a lukewarm one for which we adopt here T $\approx$ 40 K. While the energy for the cold component is provided by the interstellar radiation field, the lukewarm component is heated by massive star formation. Both of these dust components can be seen only in the FIR ($\lambda > 60$ μm), with coarse spatial resolution.

Right column, top row: In starbursts the emission of the cold dust component becomes negligible and, in addition to the lukewarm dust, a warm component at T $\approx$ 100 K shows up, observable in the MIR ($\lambda \approx 15$ μm) with good spatial resolution. Actually both the lukewarm and the warm component are attributed to very small dust grains transiently heated and not in thermal equilibrium (Desert et al. 1990). But the flux ratio $f_{15\mu m} / f_{60\mu m}$ is not constant, therefore here we consider two components.

Another component are the PAH features, which are widely distributed throughout spatially resolved normal galaxies (e.g. Mattila et al. 1996, Mattila, Lehtinen & Lemke 1999) and seem to be related more with the cold dust, i.e. cirrus or molecular clouds in a pre-starburst phase (*Right column, 2. row:*), than with the warm starburst dust (Haas, Klaas & Bianchi, this vol.).

Left column, 2. row: Closely interacting and colliding galaxy pairs get what we call IR luminous ($L_{IR} = L_{3-1000\mu m} \approx 10^{10...11}$ $L_\odot$). Starbursts provide the increase of the lukewarm and warm dust emission, while the cold cirrus emission (and probably also the PAH output) is only little affected. Compared with normal galaxies, the 40 K component is clearly prominent. If it outshines the 20 K component, then it is difficult to establish the existence of cold (pre-starburst) dust not yet affected by the starbursts.

Left column, 3. row: The ultraluminous IR galaxies are subdivided into two groups, the "cool" and the "warm" ones. In cool ULIRGs the SEDs appear similar to that of galaxy pairs, but often the 40 K component outshines any other dust emission. (Before ISO it seemed that most of the dust mass is affected by the starbursts, but this needs not to be the case as will be shown later.)

Left column, 4. row: In the SEDs of warm ULIRGs a new component, the hot AGN heated dust torus, shows up via a power-law like IR flux increase. The near- and mid-IR continuum may be so bright, that it outshines the PAH emission. Nevertheless, the resulting upper limits still allow for a PAH luminosity which is comparable to that of cool ULIRGs.

Right column, 3. and 4. row: Radio-quiet quasars show a large dispersion in their dust emission, from luminous $L_{IR} \approx 10^{11}$ $L_\odot$ to hyperluminous 10^{14} $L_\odot$. The AGN heated dust is more prominent than in the warm ULIRGs, and the coolest dust component, i.e. the long wavelength end of the thermal spectrum seems to rise with luminosity from T $\approx$ 30...40 K to T $\approx$ 80...120 K. Hyperluminous IR galaxies (HyLIGs) are suspected to be starburst powered, since an AGN has not yet been identified, but the SEDs are mostly similar to those of quasars.

Left column, 5. row: Steep spectrum radio-loud quasars are though to be similar as radio-quiet ones, but they exhibit a radio synchrotron component. Its spectrum steeply falls towards shorter wavelengths and it seems that its FIR emission is clearly outshone by the dust emission. Radio galaxies are postulated to be "edge-on" radio-loud quasars, exhibiting a similar SED (at least for $\lambda > 25$ μm).

Right column, 5. row: If a flat spectrum radio-loud quasar is seen pole-on, then according to the unified schemes the IR spectrum is dominated by the boosted synchrotron radiation of the beamed jet. In this case the IR luminosity can reach immense values of about 10^{15} $L_\odot$. Clearly, even a hyperluminous

Proceedings of the Symposium *"Exploiting the ISO Data Archive - Infrared Astronomy in the Internet Age"*, 24–27 June 2002, Sigüenza, Spain (C. Gry, S. B. Peschke, J. Matagne et al. eds., ESA SP-511)

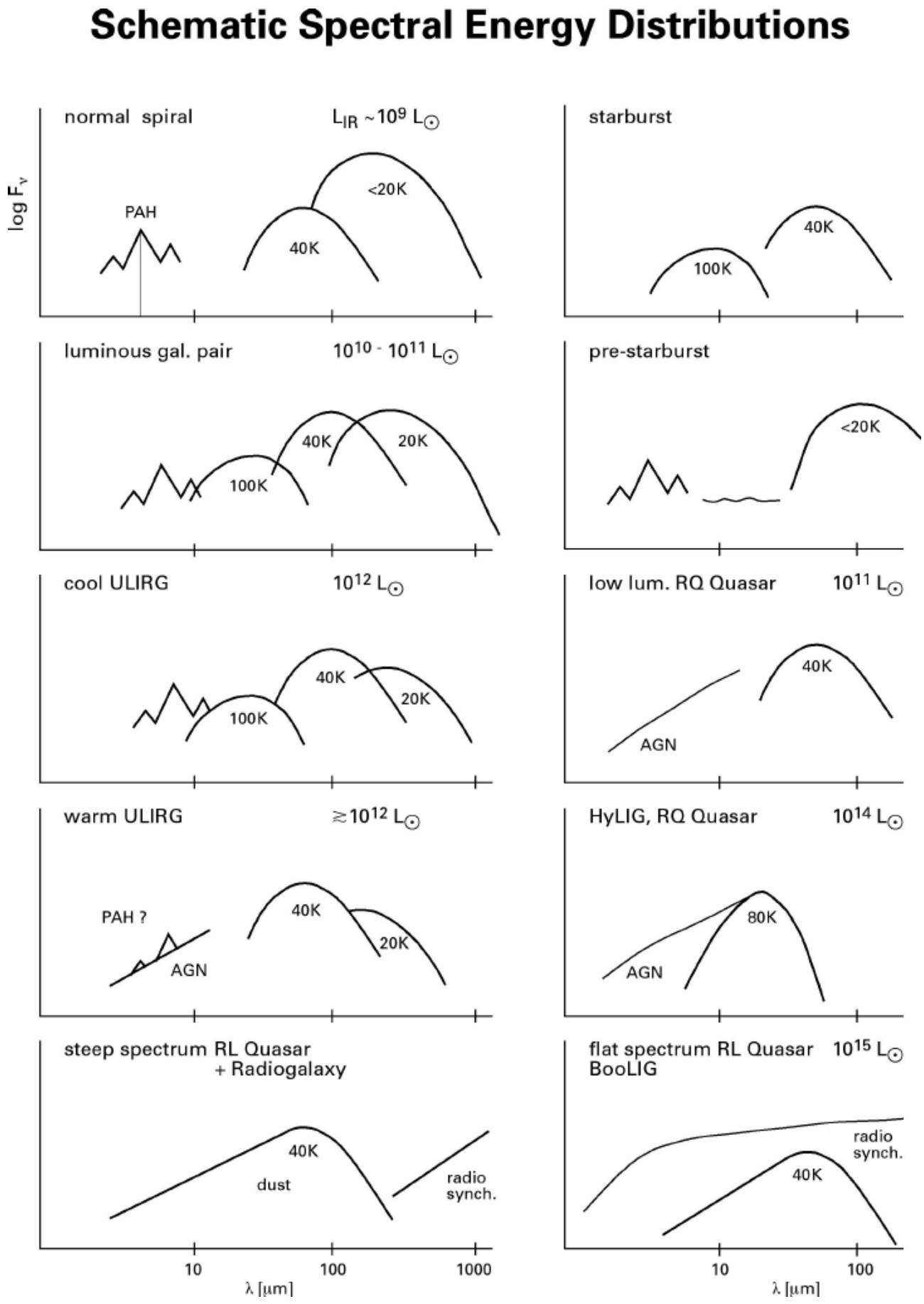

Figure 1. Schematic cartoon illustrating as a guideline the dust components and the galaxy classes.

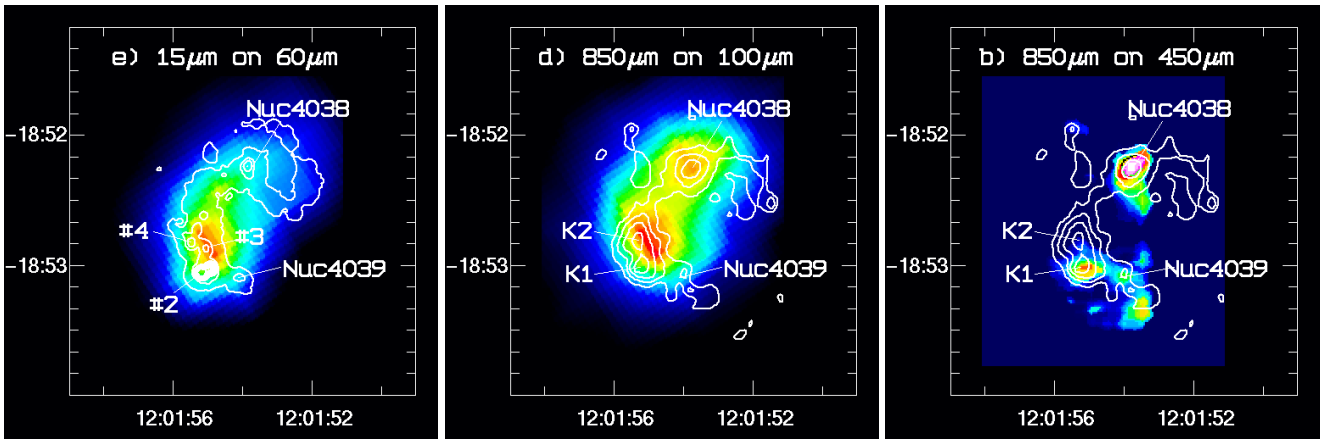

Figure 2. The Antennae galaxies mapped with ISOCAM at 15 μm, with ISOPHOT at 60 and 100 μm, and with SCUBA at 450 and 850 μm. From Haas et al. (2000), with data from Mirabel et al. (1998).

thermal dust emission will be outshone in such boosted IR luminous objects, justifying the name "BooLIGs" for them.

Following this guideline, in the next sections ISO results on each galaxy class are reviewed.

2. INTERACTING GALAXY PAIRS

The classical example of a colliding galaxy pair are the Antennae galaxies (Arp244, NGC4038/4039):

Based on 10-200 μm photometry the luminosity of warm and cold dust emission has been determined for the total galaxy ($6.4 \cdot 10^{10}$ $L_\odot$, Klaas et al. 1997). Between 60 and 200 μm the SED appears also relatively flat and broad, resulting in a "shallow" dust emissivity ($\propto \lambda^{-1.5}$) which alternatively could be fitted by the superposition of a cold and a lukewarm dust component of emissivity $\propto \lambda^{-2}$.

While at optical wavelengths the overlap region of the two galaxy disks appears inconspicuous, MIR radiation could penetrate the pronounced dust lane between the two reddened nuclei. Thus the dark side of star formation within the overlap region was revealed by 6-15 μm imaging of the warm dust near the starbursts (Mirabel et al. 1998). Impressively the brightest starburst complex (Fig. 2e, #2) even outshines both of the two nuclei.

Besides the warm dust heated by active starbursts, also dense concentrations of cold dust (T $<$ 20 K) have been resolved in the overlap region supplementing high-sampled ISOPHOT observations with SCUBA maps (Haas et al. 2000a). Note that the apparent offset of the ISOPHOT maxima with respect to the ISOCAM and SCUBA maxima in Fig. 2 is caused by the large pixels of the FIR detector, as described in Haas et al. The cold dust concentrations (in particular the submillimetre knot K2) are presumably in a pre-starburst phase. Once star formation has been ignited in these clouds, the Antennae may evolve from a luminous IR galaxy into an ultra-luminous one. Thus also the cold side of active galaxies provides interesting aspects.

The simultaneous presence of powerful off-nuclear starbursts & pre-starbursts may be a general feature of colliding galaxies. Further examples of closely interacting galaxy pairs have been mapped at various MIR wavelengths locating the enhancements of emission due to starburst (Xu et al. 2000). The spatial resolution in the FIR is still limited, but the components of each pair could clearly be resolved representing a big step forward in both sensitivity and resolution compared with the IRAS results and work is still in progress (Gao et al. 2001).

3. ULTRA-LUMINOUS IR GALAXIES

Do ULIRGs also have dense cold dust concentrations as found in galaxy pairs, or cold cirrus-like dust as in normal galaxies, or is all the dust already heated up to T $>$ 30 K?

NIR to millimetre SEDs of 41 nearby (z $<$ 0.3) ULIRGs have been obtained by Klaas et al. (2001). The SED shapes between the NIR and 60 μm can clearly be grouped into those for cool and warm ULIRGs (definition of "warm": $f_{25\mu m} / f_{60\mu m}$ $>$ 0.2). While the warm ULIRGs show spectroscopic signatures of AGN, the cool ULIRGs mostly do not (see also Lutz, this vol.). The plenty of filters between 60 and 200 μm used allow to determine accurately the shape of the SEDs, revealing the broad maxima, and the Rayleigh-Jeans tail is constrained by the submillimetre data. Fits with one single modified blackbody yield a high FIR opacity and small dust emissivity exponent $\beta < 2$. However, this concept leads to conflicts with several other observational constraints, like the extended filamentary optical morphology and the low PAH extinction (see Klaas, this vol.). A more consistent picture is obtained using several dust components with $\beta = 2$, low to moderate FIR opacity and cool (50 K $>$ T $>$ 30 K) to cold (30 K $>$ T $>$ 10 K) temperatures. This is illustrated in Fig. 3.

The NIR to millimetre SEDs provide evidence for a 3-stage dust model consisting of hot AGN heated dust, lukewarm/warm starburst heated dust, and cold pre-starburst or cirrus-like dust.

While AGNs and SBs differ in the NIR-MIR, they appear indistinguishable at FIR and submm wavelengths. However, within the sample, which covers only a small range in bolometric luminosity, the relative amounts of warm, cool and cold dust are not correlated with the merger state inferred from the

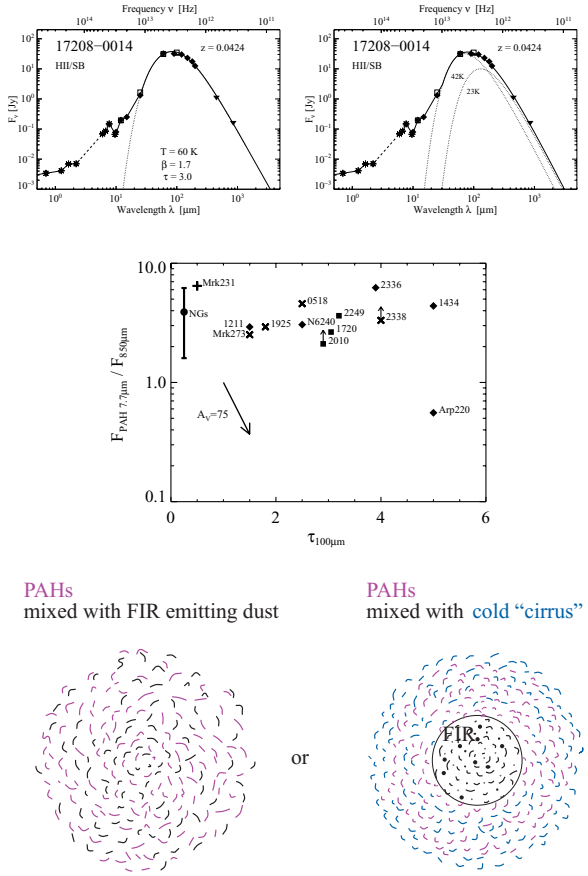

Figure 3. Top: IR-mm SED of the ULIRG IRAS 17208-0014. Left: fitted with a single modified blackbody which would yield very high opacity ($\tau_{100\mu m} \approx 3$). Right: fitted with two optically thin modified blackbodies. Middle: geometric cartoon of the distributions of the PAH, FIR and submm emitting dust particles for the two models fits in the top row. Bottom: flux ratio PAH/850μm as a function of optical depth $\tau_{100\mu m}$ as derived from the single blackbody fit. (Symbols are: cross for Seyfert and diamond for LINER/HII spectra). Apart from one exception (Arp220, see Klaas this vol.) the values for ULIRGs lie in a relatively small horizontal strip at 5±2. For normal galaxies the ratio covers the same range (indicated by the vertical bar labelled "NGs"). With increasing $\tau_{100\mu m}$ the PAH/850μm ratios do not show any decrease parallel to the vector of extinction. This argues against the description of the SED by a single optically thick component. From Klaas et al. (2001).

morphology. Future investigations on larger samples of LIRGs and ULIRGs in the ISO Data Archive may be able to establish such evolutionary trends.

4. HYPER-LUMINOUS IR GALAXIES

The matter of debate on HyLIGs is, how to provide and maintain hyperluminous starbursts with a star formation rate of at least 1000 $M_\odot$ per year. In view of several billion $M_\odot$ gas found in some merging galaxies, it seems a priori not impossible to imagine an "unlimited" star forming rate. On the other hand, the issue is how *sudden* the gas reservoir can really be concentrated and transformed into stars. Mid- to far-infrared SEDs of five IR selected HyLIGs have been studied by Verma et al. (2002, and this vol.), favouring a large fraction of AGN power supply in these sources. Further results are expected from larger samples of HyLIGs and lensed ULIRGS in the ISO Data Archive.

5. SEYFERT GALAXIES

Several samples of Seyfert galaxies (considered to comprise the low luminosity end of quasars) have been studied, and plenty of data are still under work.

Polletta & Courvoisier (1999) investigated 7-200 μm SEDS of four narrow line Seyfert 1s, showing that they are not seen pole-on (as was suggested previously), rather they suffer different degrees of dust absorption consistent with the inclination to the line of sight like in Seyfert 2s.

Spinoglio et al. (2002) investigated the 12 μm AGN sample finding that Sy1s and Sy2s, while different in the MIR range, are indistinguishable at 100-200 μm, consistent with the unified schemes and the idea that the FIR luminosity is mostly powered by starbursts.

6. QUASARS & RADIO GALAXIES

6.1. On the nature of the FIR emission

The first SEDs of 10 radio-quiet and radio-loud quasars with ISO (supplemented by mm data from IRAM) reveal signatures of thermal dust as well as synchrotron emission (Haas et al. 1998). In most cases one of the two components is so dominant that the other remains hidden. The SEDs of the radio quiet and steep spectrum quasars (as well as radio galaxies) show a bump around 60μm and a decline longword of 100μm, strong evidence for thermal emission. On the other hand, in flat spectrum quasars the FIR emission is dominated by the boosted synchrotron component which is more than hyperluminous.

Polletta et al. (2000) confirm the thermal nature of the mid- and far-IR emission of the radio quiet and steep spectrum quasars, which protrudes above a smooth synchrotron spectrum.

6.2. RADIO-QUIET (PG) QUASARS

The SEDs of 17 PG quasars (5 of them having $1 < z < 2$) provide evidence for luminous to hyperluminous dust emission and do not support the existence of dust–free, naked quasars (Haas et al. 2000b). The variety of SED shapes as well as the correlation between mid-and far-infrared luminosities was discussed in the frame of the AGN-starburst connection. As a trend, the coolest dust component, i.e. the break at the long wavelength end of the thermal spectrum, appears warmer in hyperluminous quasars.

Rowan-Robinson (2000) applied AGN and and starburst models to HyLIGs and $z > 1$ PG quasars, finding only little evidence for a significant starburst contribution to power the IR emission of hyperluminous quasars. Furthermore, Nenkova,

Ivezić & Elitzur (2002) presented results on patchy AGN torus models suggesting, in general, a minor role of starbursts for powering the dust of quasars.

Mining the ISO Data Archive Haas et al. (2002) provide the complete ISO view of PG quasars obtaining 64 IR spectral energy distributions, 12 of them having z≈1. Half of the sample was supplemented by MAMBO and SCUBA (sub-)millimetre data. The SEDs support the picture that the IR emission is mainly powered by the AGN and that starbursts play only a minor role. The SEDs exhibit a variety of near-, mid- and far-infrared properties. Following the idea that quasars are preceeded by a dusty ULIRG-like phase, the dust does not disappear at once, hence the sensitive ISO data allow for the first time to see the evolution of the residual dust distribution in the PG quasar sample, thereby explaining the variety of the SEDs.

6.3. Unification of radio galaxies and RLQs

Both radio galaxies and radio-loud quasars show the giant lobes fed by a superluminal jet. But in most radio galaxies one has not yet seen the powerful AGN which is well exposed in the quasars. Are the galaxies intrinsically different from the quasars, perhaps due to a starving black hole? Or is the AGN of the galaxies just hidden behind a thick dust torus seen edge-on, while in the quasars an intermediate torus inclination with respect to the line of sight allows to recognise the central machine? Although the optical light of the central core might be well hidden, if the torus is viewed edge-on, it must heat the postulated dust which in turn emits isotropic infrared radiation. According to the unification, quasars and radio galaxies with equal isotropic luminosities of the radio lobes are expected to show also equal thermal radiation intensities in the mid- and far-infrared range.

Van Bemmel et al. (2000) studied four galaxy/quasar pairs of relatively *low* radio power. In their sample the quasars turn out to be more IR luminous than the galaxies, providing only little evidence for unification.

These differences, however, could be explained as selection effects due to physical evolution of the sources or the circumgalactic medium, as worked out by Haas (2001). This is illustrated in Fig. 4: Firstly, the radio luminosity could be enhanced due to special enviromental conditions (thick vertical arrows). Secondly, a quasar has to evolve from a radio-quiet one into a radio loud one. If a quasar, which has not yet reached maximal radio-loudness, is matched with a radio galaxy (as indicated by the dotted horizontal line), then the quasar will be more IR powerful. For a check of the unified schemes, these biases can be reduced by selecting only the most powerful radio sources for the pairwise galaxy-quasar comparison.

Meisenheimer et al. (2001) obtained the SEDs of 10 galaxy/quasar pairs of high radio power (and redshifts reaching z ≈ 1). The high detection rate and the quality of the SEDs allowed to discern the thermal dust component from the synchrotron part beyond doubt (Fig. 5). The galaxies and quasars are indistinguishable in their thermal IR properties, providing the first successful evidence in the IR favouring the unification.

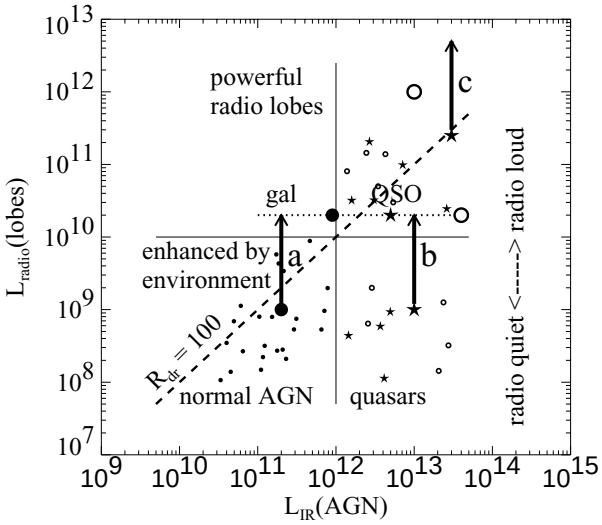

Figure 4. Schematic diagram of radio luminosity against dust luminosity, in order to illustrate selection effects, when unifying radio galaxies and quasars. The symbols are: ⋆ = quasar, ○ = edge-on quasars (radio galaxy with powerful quasar-like AGN), ● = radio galaxy with less powerful 'normal' AGN (irrespective of broad lines or aspect angle). From Haas (2001).

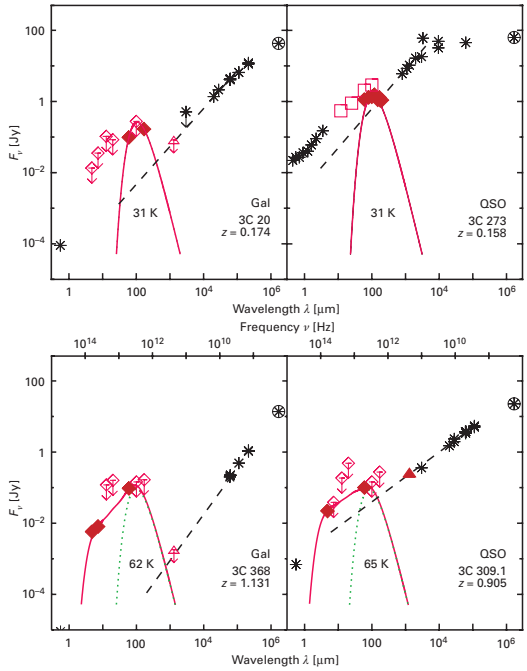

Figure 5. SEDs for two pairs of galaxies and quasars, one at low and one at high redshifts. Each pair has the same isotropic radio lobe flux (encircled asterisk at $\lambda \approx 10^6$ μm). The thermal dust emission (red) is well detected above the synchrotron spectrum (dashed line). For each pair the dust emission has similar properties. Also, consistent with the unified schemes, the quasars show a stronger beamed synchrotron emission than the galaxies. Note also the variability of 3C 273 between the IRAS (open squares) and the ISO observations, the latter being performed during a synchrotron minimum. From Meisenheimer et al. (2001).

The unified scheme has been tested even further. If the relation between radio galaxies and radio-loud quasars is determined solely by the geometric unification and not in addition by evolution or the circumgalactic medium, then the ratio of the infrared to the radio emission should be about the same for all sources. With a few exceptions at low redshift this ratio lies between 100 and 300. Since the dust luminosities range over more than 3 orders of magnitude, the scatter of the infrared/radio luminosity ratio is small and therefore confirms the essential role of geometric unification in describing the relation between radio galaxies and radio-loud quasars. In view of the complexity of the objects the identification of additional effects remains a challenging task for future explorations, which could start with the ISO Data Archive.

6.4. Evolution of radio galaxies

Are compact steep spectrum (CSS) radio galaxies young, having not yet reached their final radio lobe size? Or is their lobe expansion obstructed by dense material? Such dense material is expected to be accompanied by FIR emitting dust. Therefore Fanti et al. (2000) studied a sample of 17 CSS radio galaxies and a control sample of 16 extended radio galaxies between 60 and 200 μm. They find no FIR dust excess for the CSS sources. In a straight forward interpretation, this argues against dense material and favours the youth of the compact radio sources. As pointed out by Fanti et al., a closer look to the power of the driving AGN and the theoretically expected luminosity turn over of the evolving lobes requires further investigations on various larger samples - perhaps contained in the ISO Data Archive.

7. SUMMARY

Mid- and far-infrared imaging and photometry with ISOCAM and ISOPHOT have substantially improved our view of various active galaxy classes all of which are IR luminous. The high spatial resolution, in particular, in the MIR allowed for detailed dust mapping in nearby sources. The superb sensitivity in the mid- and far-infrared, the plenty of filters and the broad wavelength coverage up to the extreme range of 200 μm by ISOPHOT allowed for determining the physically important parts of the SEDs in unprecedented detail. The resolved MIR maps and the MFIR photometry have been supplemented ideally with ground-based (sub)-millimetre observations.

Currently, about 30% of the data have been evaluated, and the ISO Data Archive contains another 30% of valuable data, keeping us busy for the next years. SIRTF may reach higher sensitivity, but offers only a small number of FIR filters. Real quantum steps may have to await the Herschel Satellite and the NGST.

ACKNOWLEDGEMENTS

The ISOPHOT Data Centre at MPIA is supported by Deutsches Zentrum für Luft- und Raumfahrt e.V. (DLR) with funds of Bundesministerium für Bildung und Forschung.

REFERENCES

Desert F.-X., Boulanger F., Puget J.L. 1990, A&A 237, 215
Fanti C., Pozzi F., Fanti R., et al. 2000, A&A 358, 499
Gao Y., Xu C., Lu N. Y., Tuffs R., Sulentic J. 2001, BAAS 198, 3603
Haas M., Chini R., Meisenheimer K., et al. 1998, ApJ 503, L109
Haas M., Klaas U., Coulson I., et al. 2000a, A&A 356, L83
Haas M., Müller S.A.H., Chini R., et al. 2000b, A&A 354, 453
Haas M., 2001, "Habilitationsschrift" Univ. Heidelberg
Haas M., Klaas U., Müller S.A.H., et al. 2002, A&A submitted
Klaas U., Haas M., Heinrichsen I., Schulz B. 1997, A&A 325, L21
Klaas U., Haas M., Müller S.A.H., et al. 2001, A&A 379, 823
Mattila K., Lehtinen K., Lemke D., 1999, A&A 342, 643
Mattila K., Lemke D., Haikala L.K. et al. 1996, A&A 315, L353
Meisenheimer K., Haas M., Müller S.A.H., et al. 2001, A&A 372, 719
Mirabel I.F., Vigroux L., Charmandaris V., et al. 1998, A&A 333, L1
Nenkova M., Ivezić Z., Elitzur M. 2002, ApJ 570, L9
Polletta M., Courvoisier Th. 1999, A&A 350, 765
Polletta M., Courvoisier Th., Hooper E.J., Wilkes B.J. 2000, A&A 362, 75
Rowan-Robinson M. 2000, MNRAS 316, 885
Spinoglio L., Andreani P., Malkan M.A. 2002, ApJ 572, 105
van Bemmel I., Barthel P., de Graauw Th. 2000, A&A 359, 523
Verma A., Rowan-Robinson M., McMahon R., Efstathiou A., 2002, MNRAS accepted, astro-ph 0204524
Xu C., Gao Yu, Lu N.Y., et al. 2000, ApJ541, 644

A MIR SPECTROSCOPIC SURVEY OF STARBURST GALAXIES

Aprajita Verma[1], Dieter Lutz[1], Eckhard Sturm[1], Amiel Sternberg[2], and Reinhard Genzel[1]

[1] Max-Planck-Institut für extraterrestrische Physik, Postfach 1312, D-85741 Garching-bei-München, Germany
[2] School of Physics and Astronomy, Wise Observatory, Raymond and Beverly Sackler Faculty of Exact Sciences, Tel Aviv University, Ramat Aviv, Tel Aviv 69978, Israel

ABSTRACT

We present a mid-infrared (MIR) spectroscopic survey of starburst galaxies as an example of analysis of scientifically focused samples selected from the ISO Data Archive (IDA). We use fine structure lines (FSL) ratios of Ne, Ar and S to construct diagnostic excitation diagrams and, in combination with hydrogen recombination lines (HRL), we determine their elemental abundances. For Ne and Ar, we find that excitation indicators are positively correlated with each other and negatively with abundance. On comparison with a complementary sample of galactic H II regions we find that starbursts are generally of lower excitation. Starbursts exhibiting Wolf-Rayet (WR) features are separated both in excitation and abundance from the remaining starbursts. Most surprisingly, S is found to be underabundant by a factor of ~ 3 in our low excitation starbursts with respect to the Ne and Ar, contrary to expectations from nucleosynthesis theory. Our results are combined with those of a related sub-sample of Seyfert galaxies (Sturm et al. 2002) to derive diagnostic diagrams discriminating the two types of activity on the basis of excitation traced by MIR lines. The data presented will be useful as a reference for observations of fainter and/or higher redshift sources with future IR observatories such as SIRTF, SOFIA and Herschel.

Key words: galaxies: starburst, galaxies: abundances, infrared: galaxies, Galaxies: ISM

1. INTRODUCTION

Starburst galaxies are energetically dominated by massive young hot stars ionising the interstellar medium but the properties and evolution of this population are difficult to constrain for dusty objects where the direct stellar UV radiation is unobservable. Metallicity, the IMF and evolution will all affect integrated (observable) properties such as luminosities, colours and line strengths. In addition, both stellar evolutionary tracks and nebular properties (including excitation) show a dependence on metallicity, suggesting that elemental abundances should be considered when interpreting starbursts. To date, abundance and excitation studies have been based primarily on optical and near-infrared data mainly due to observational limitations from the ground. Infrared spectroscopy, probing the dominant obscured regions of objects at the dusty end of this sequence, is needed for a complete understanding of the local starburst population with implications for the extensive populations of starbursts at higher redshift detected both in the UV/optical and infrared.

Here, we present analysis of ISO SWS spectra (between 2.38 and $45\mu m$) for 12 starburst regions. Our investigation is focused upon the gas phase abundances of neon, argon and sulphur. These elements emit the brightest lines in the MIR spectra of starbursts. Deriving abundances from a combination of IR FSLs and HRLs has a number of technical advantages that minimise uncertainties. Extinction in this wavelength range is low, and the derived abundances are relatively insensitive to variations in electron temperature and density. For all three elements, the major ionisation stages found in H II regions are covered by the SWS spectra, which minimises the required ionisation correction factors. We relate the results to nebular excitation and thereby probe the hot stellar population. This study complements the numerous existing abundance analyses in the optical/near-infrared with the first comparable MIR systematic study of a comprehensive sample of starburst galaxies.

2. SAMPLE & DATA REDUCTION

Our sample consists of 12 starburst regions in 11 local galaxies ($v_{med} = 787 kms^{-1}$) with both FSL and HRLs in their IR spectra. This is a pre-requisite since a HRL is used as the reference line for the abundance estimation. Our starburst sample encompasses a variety of morphological types and includes six starbursts exhibiting WR spectral features (Schaerer et al. 1999).

The IDA was used to collate *all* of the SWS grating spectra available for each galaxy. The SWS instrument (de Graauw et al., 1996) performed spectroscopic measurements between 2.38 to $45.2\mu m$ producing spectra of medium to high resolution. Within its operational wavelength range lie a number of previously seldom-observed emission lines. We used the SWS interactive analysis (IA3[1]) to reduce the data sets from the edited raw data products. We could enhance the quality of the reduced product by using interactive tools in IA3 for dark current subtraction, correction between up and down scans and outlier masking. The resultant reduced spectra were then sub-

[1] IA3 is a joint development of the SWS consortium. Contributing institutes are SRON, MPE, KUL and the ESA Astrophysics Division.

Proceedings of the Symposium *"Exploiting the ISO Data Archive - Infrared Astronomy in the Internet Age"*, 24–27 June 2002, Sigüenza, Spain (C. Gry, S. B. Peschke, J. Matagne et al. eds., ESA SP-511)

ject to further processing in ISAP[2] to remove further outliers and to perform flat-fielding and fringe removal to produce the final spectral line profiles.

3. RESULTS

We detect a number of FSL, HRL and transitions of molecular H within the SWS spectra. Here, we concentrate on the analysis of the results, namely the excitation and abundances of Ne, Ar and S in our starburst sample.

We corrected our fluxes for extinction based upon the ratios of $Br\beta/Br\alpha$ and $[SIII]18.7/33.5$ where available for which the intrinsic ratio has been previously determined. We assumed that the obscuring material and emitting gas are uniformly mixed which is likely to be more appropriate for obscured starbursts than a simple foreground screen (McLeod et al., 1993). We used the Galactic centre extinction law of Lutz et al. (1999) between 3-8.5μm and adopted a Draine (1989) extinction law at all other wavelengths, with a normalisation of the silicate feature of $\tau_{9.6}/\tau_V = 0.122$.

To determine the electron density of our sources we used the ratios of [SIII]18.7μm/33.5μm and [NeIII]15.6μm/36μm and compared them to theoretical values obtained from a solution to the rate equations. Assuming a one-zone ionisation model, we found that all of our starbursts lie in the low density limit (i.e. well below the critical density), within the errors, suggesting $n_e \sim 6 - 600cm^{-3}$. We adopted a median representative value of $n_e = 300cm^{-3}$.

We sought electron temperatures in the literature, yielding accurate millimetre based temperatures for M82, NGC 253 ($T_e = 5000 \pm 1000K$) and radio measurements for NGC 5253 ($T_e = 11000 \pm 1000K$) and II Zw 40($T_e = 12500 \pm 900K$). As we do not have accurate temperature estimates for the entire starburst sample and, in order to allow meaningful intercomparisons between the starbursts, we elected a single representative temperature $T_e^R = 5000K$. This value was chosen based on the assumption that M82 and NGC 253 are *archetypal* starbursts. Deviations from this 'representative' temperature are present and will affect absolute abundances, thus distorting the trends derived in the inter-comparisons. We indicate the effects of moving from T_e of 5000 $\sim 10000K$ by an arrow (which are largest for high T_e objects) in the figures following.

We also compare our data to H II regions from Giveon et al. (2002). We recalculate extinctions for his sample assuming a uniform foreground screen and the same interstellar extinction law used for the starbursts to eliminate discrepancies due to differing assumptions. As excitation increases with galactocentric radius (Giveon et al. 2002, Martín-Hernandez et al. 2002) we split the galactic sample of Giveon et al. into 'inner' and 'outer' sources at the median galactocentric radius of the sample.

[2] The ISO Spectral Analysis Package (ISAP) is a joint development by the LWS and SWS Instrument Teams and Data Centers. Contributing institutes are CESR, IAS, IPAC, MPE, RAL and SRON.

4. ANALYSIS

We may investigate excitation within the starburst sample using ratios of FSL fluxes of different ionic species of the same element. The difference in ionisation potentials between the ionic species means that ratios of these lines are sensitive to the shape of the spectral energy distribution (SED) of the ionising source. We have used (and combined) ratios of some of the strongest lines, $[NeIII]15.5/[NeII]12.8$, $[ArIII]8.9/[ArII]6.9$ and $[SIV]10.5/[SIII]18.7$, from our MIR survey. Ar^+, S^{++} and Ne^+ have ionisation potentials corresponding to ~ 2, ~ 2.5 and ~ 3 Rydbergs, respectively. Therefore these line ratios can constrain the ionising spectra over a range of a few Rydbergs.

We have formed excitation planes by combining the FSL ratios (Fig. 1). The starbursts are relatively spread out across all three excitation planes. The majority of sources occupy the lower left corner of the planes, which indicates that these have low excitation. Extending to higher excitation in both axes are the BCD galaxies and those that exhibit WR features. This result is consistent with existing knowledge of both of these source types (Schaerer et al. 1999). The distribution of the starbursts is well matched with the H II region data. The locations of the 'inner' H II regions is similar to those of low excitation starburst galaxies. The exceptions are the WR and BCD galaxies which are located in regions similar to those of the 'outer' and extragalactic H II regions.

In Fig. 2 (left & middle) we show that starburst excitation and abundance are negatively correlated for Ne and Ar. The WR galaxies have the highest excitation and the lowest abundance. In general, the non-WR starbursts in our sample have super-solar metallicities $(X/H) \sim 1 - 3(X/H)_\odot$ (where X is Ne or Ar) whereas the WR and BCD galaxies are sub-solar. Our adopted 'representative' electron temperature of 5000 K is only a good assumption for high metallicity starbursts and high metallicity H II regions. By adopting a more appropriate electron temperature, the absolute infrared-derived abundances of the low metallicity BCDs are close to the optically-derived values $[0.2X/H_\odot]$. Overall, the effect on the excitation/abundance diagrams of adopting individual electron temperatures (which are unavailable for the entire sample) for each starburst would be to tilt the correlation: the high excitation / low metallicity end would move to $\sim$2 times lower abundance, while the high metallicity/low excitation end remains unchanged.

As 'primary' products of stellar nucleosynthesis, the abundances of neon and argon are expected to be correlated. The overall abundance relation between Ne and Ar is shown in Fig. 2 (right) which indeed shows an above solar, constant ratio of [Ne/Ar] (for which the T_e effects for the two elements largely cancel) that holds for all objects in our sample, from the BCDs and WR galaxies to the dusty starbursts. This implies that the ISM of these galaxies has been enriched by similar processes for both elements.

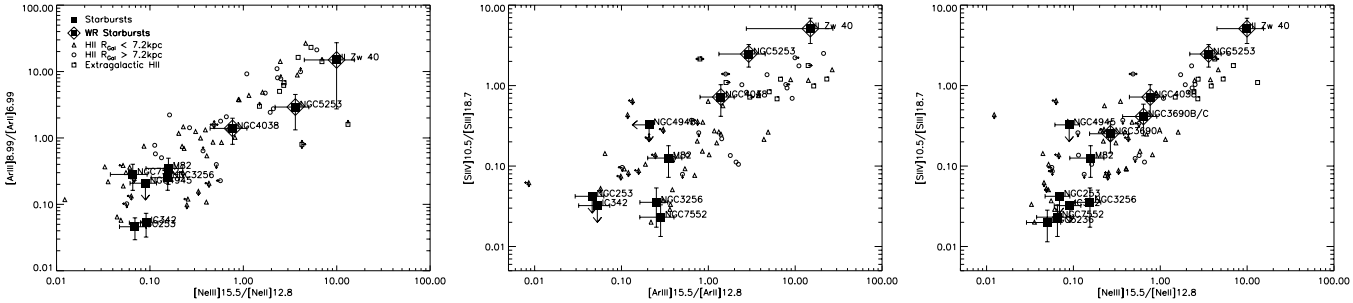

Figure 1. Starburst excitation probed by [NeIII]15.5/[NeII]12.8, [ArIII]8.9/[ArII]6.9 and [SIV]10.5/[SIII]18.7

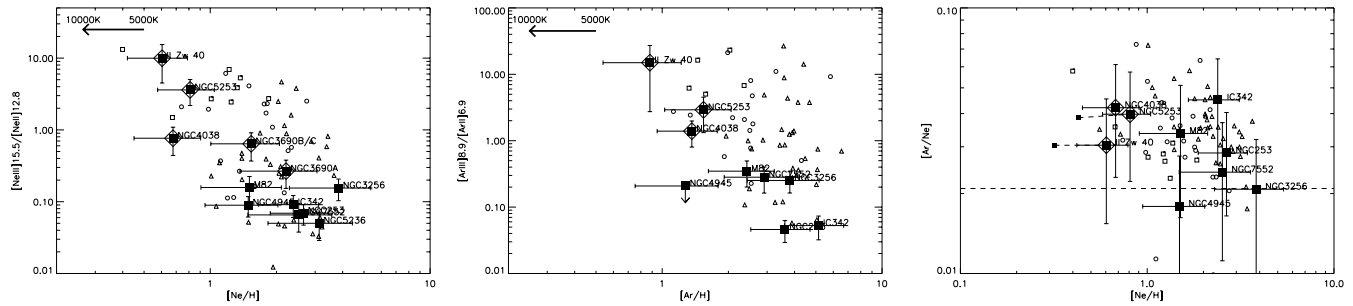

Figure 2. Left: Ne abundance versus excitation, Middle: Ar abundance versus excitation, Right: Ne/Ar against Ne abundance

4.1. SULPHUR

We discuss the abundance of sulphur separately since we do not see the clear correlation between excitation and abundance that is seen in Ne and Ar for the starbursts (Fig. 3 left). In addition, *all* galaxies appear to have sub-solar sulphur abundances, with NGC 4945 being anomalously low. Furthermore, on comparison to the abundances of Ne and Ar, we find that the galaxies not showing WR features have lower S abundances ($< [S/H] >= 0.6$) than expected from their typically high Ne and Ar abundances ($< [Ne/H] >= 2.4,\ < [Ar/H] >= 2.7$). Yet the S abundances for the WR galaxies are similar to that expected from their Ne and Ar abundances ($[X/H] \sim 0.2$).

Fig. 3 (middle & right) compare the temperature independent abundance ratios [S/Ne] and [S/Ar] with the Ne and Ar abundance. S is expected to be correlated with Ne and Ar since they are all primary products of stellar nucleosynthesis. However, our [S/Ne] and [S/Ar] ratios are well below the solar ratio. The plots also show a trend towards a stronger sulphur 'deficiency' at increased Ne or Ar abundance. S is often referred to as an excellent tracer of metallicity (e.g. Oey & Shields 2000) and in studies of the ISM is commonly used as a non-depleted element.

The weakness of the S lines in high metallicity systems has practical implications for future observations of dusty starbursts both locally and at high redshift: sulphur lines are less favoured in comparison to the [Ne II] line as tracers of starburst emission than one would assume from nebular models. The low derived S abundance suggests that S is *not* a good tracer of metallicity in low excitation starburst galaxies.

We discount uncertainties in electron temperature and density to be the cause of this underabundance since they would similarly affect Ne and Ar. We also discount errors in the ionisation correction factor as the presence of significant quantities of [SII] for the excitation range of our sources is unlikely based on photoionisation modelling. A third possible source could be the current theory for nucleosynthesis of S, although little evidence exists to support this argument. Erroneous atomic data may be a plausible explanation however, our calculations are based on the most up-to-date atomic data available.

A consistent explanation of both extragalactic and Galactic observations would be a tendency of S to be more strongly depleted onto dust than the noble gases Ne and Ar. However, UV absorption measurements in the diffuse interstellar medium often suggest most S exists in the gas phase with low depletion ($\sim 30\%$ e.g. Wilms, Allen & McCray 2000). For molecular regions, strong S depletion is predicted by chemical models (e.g. Ruffle et al. 1999). Unfortunately little is known about the H II regions probed by our observations. While depletion is a natural explanation of the failure of the S abundance data to trace the noble gas abundances, a quantitative understanding under the conditions of our higher than solar metallicity H II regions remains to be obtained. Clearly, depletion would have to depend on ISM conditions to explain both the low metallicity dwarfs (with no S deficit both from our results and numerous optical studies) and the higher metallicity starbursts. While noting these open questions, we consider depletion of S onto grains the best explanation for the observed underabundance in low excitation sources.

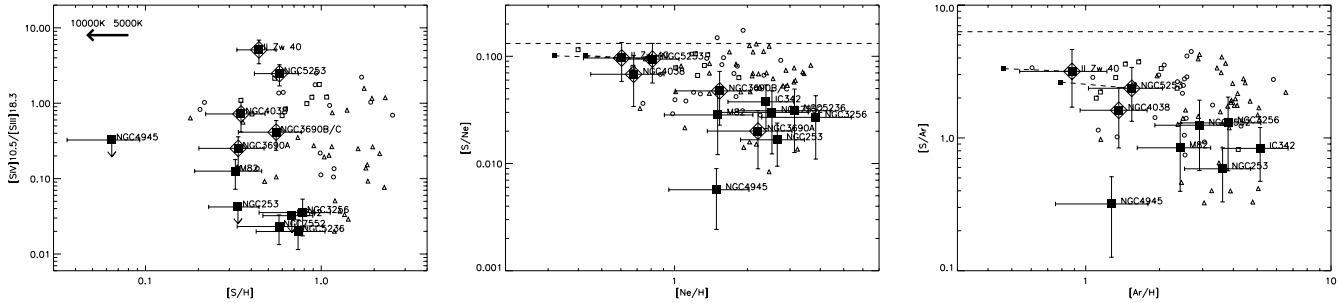

Figure 3. Sulphur: Left: S abundance against excitation, Middle: Ne/S against Ne, Right: Ar/S against Ar

5. STARBURST-AGN DIAGNOSITC DIAGRAM

Sturm et al. (2002) use a MIR analogue (Fig. 4) to the optical excitation diagnostic diagrams of Veilleux and Osterbrock (1987). MIR diagnostics are desirable to classify sources which are heavily obscured and therefore will be a useful tool for the sources detected in future IR missions (i.e. SIRTF, SOFIA and Herschel).

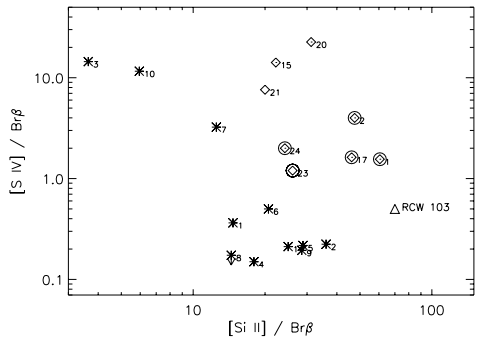

Figure 4. A MIR diagnostic diagram from Sturm et al. (2002, Fig. 9) to distinguish starbursts and AGNs in dusty galaxies. AGNs are shown as diamonds, starburst galaxies as stars.

6. CONCLUSIONS

From our investigation of starburst excitation and abundance determined by Ne, Ar and S MIR lines, we conclude:
a) The positive correlation between excitation ratios implies regions between 2 and 3 Rydbergs are related.
b) A negative correlation between excitation and abundance exists for starbursts. For a given metallicity, starbursts are of lower excitation than H II regions. The excitation of MIR starbursts is governed by a combination of metallicity and other effects like ageing of the population, which should be accounted for in modelling starbursts as composite H II regions.
c) S is ~ 3 times underabundant in low excitation sources. The S abundance also does not correlate well with Ne and Ar, contrary to expectations based on nucelosynthetic arguments. We favour depletion onto dust grains as the most likely cause of this relative underabundance. The low abundance and weak S lines imply that S is not a good tracer of metallicity for low excitation starbursts.
d) A new MIR excitation diagnostic (Sturm et al. 2002) can be used to identify powering mechanisms of obscured sources which will be detected in future IR surveys.
e) Similar scientifically focused samples (using cross-proposal data) remain largely unexploited in the IDA.

Complete descriptions of the starburst and Seyfert ISO programmes and analysis may be found in Verma et al. (2002) and Sturm et al. (2002) respectively.

ACKNOWLEDGEMENTS

The ISO spectrometer Data Center at MPE is supported by DLR under grant 50 QI 0202. This research is partly supported by the German-Israeli Foundation (grant I-0551-186.07/97).

REFERENCES

de Graauw, T. et al. 1996, A&A, 315, L49
Draine, B. T. 1989, in 'Infrared Spectroscopy in Astronomy', ed. B. Kaldeich, ESASP-290, 93
Giveon, U. et al. 2002, ApJ, 566, 880
Lutz, D. 1999, in 'The Universe as Seen by ISO', ESA SP-427, Eds. P. Cox & M. F. Kessler.
McLeod, K.K. et al., 1993, Ap.J., 412, 111
Martín-Hernández, N. L. et al. 2002, A&A, 381, 606
Oey, M. S. & Shields, J. C., 2000, ApJ, 539, 687
Ruffle, D. P., et al., 1999, MNRAS, 306, 691
Schaerer, D., et al. 1999, A&A supp., 136, 35
Sturm, E., et al., 2002, A&A, 393, 821
Veilleux, S. & Osterbrock, D. E. 1987, ApJ supp., 63, 295
Verma, A. et al,. 2002, A&A submitted
Wilms, J., Allen, A., & McCray, R. 2000, ApJ, 542, 914

MID-IR RADIATION OF 3C RADIO GALAXIES: I. OBSERVATIONS AND MODELS

Ralf Siebenmorgen[1], **Wolfram Freudling**[2], **and Endrik Krügel**[3]

[1]European Southern Observatory,Karl-Schwarzschild-Strasse 2, D-85748 Garching b. München, Germany
[2]Space Telescope - European Coordinating Facility, European Southern Observatory, Karl-Schwarzschild-Strasse 2, D-85748 Garching b. München, Germany
[3]Max Planck Institute f. Radioastronomy, Auf dem Hügel 69, D-5300 Bonn, Germany

ABSTRACT

We have carried out a mid-infrared survey of 3CR radio galaxies by extracting all ISOCAM observations of such objects from the ISO archive. The goal of this survey is to investigate the prevalence of hot dust in galaxies at a typical redshift of about 1. The data were calibrated in a uniform manner. A total of 79 radio galaxies were detected. To analyze these data, we have constructed a set of synthetic spectral energy distributions by solving the radiative transfer equations of dust clouds with AGN as primary heating source. We will discuss the motivation and application of these models to our survey.

Key words: ISOCAM – radio galaxies – dust

1. INTRODUCTION

In this paper we want to investigate core properties of radio galaxies at different redshifts. One important issue is the unification theme of radio galaxies which states that the observed radio lobes and jets are excited from an active nucleus which is deeply enshrouded by a dusty torus. A further probe of this scenario may come from high sensitivity and angular resolution observations in the infrared. These instrumental requirements are today best fulfilled by ISOCAM data. By combining mid infrared observations with data at other wavelengths one may hope to derive a better physical understanding of the energetic processes in the nucleus of radio galaxies and to answer the basic questions whether the infrared (IR) radiation of radio galaxies is dominated either by synchrotron or dust emission?

2. FIELD SELECTION

The goal of this paper is to investigate core properties of radio galaxies by means of new infrared observations which we combined with data at other wavelengths. Our objects are from the third update of the revised third Cambridge catalogue (hereafter 3CR) by Spinrad et al. (1985). They are well observed at optical, near infrared and radio wavelengths and individual objects have optical identifications. The 3CR catalogue contains 298 sources with save identification of 195 radio galaxies and 53 radio quasars.

In the infrared the highest sensitivity data available today were obtained with the long wavelength array (LW) of the infrared camera ISOCAM (Cesarsky et al. 1996) on board of the *infrared space observatory* (ISO, Kessler et al. 1996). We searched in the ISO post mission archive and extracted all ISOCAM LW observations where at least one 3CR source is in the field of view of the ISOCAM image. A total of 146 ISOCAM observations have been found.

Most of the observations have been performed in so called mini-raster mode where different ISOCAM detector pixels saw the same part of the sky (see ISO Handbook Vol.II for a description of observing modes, Leech & Pollock, 2001). In addition there are nine staring observations and one beam switch (C03). Of those three used circular variable filter scans (CVF, C04) and one was in polarimetric mode (C05). The pixel scale of the 32×32 detector is 1.5, 3 and $6''$ and a total field of view of 48, 96 and $180''$, respectively. The broad band filter LW10 with bandwidth of 8–15μm and central wavelength at 12μm is used most frequently but there are also observations with LW1 (4–5, 4.5μm), LW2 (5–8.5, 6.7μm), LW3 (12–18, 14.3μm), LW7 (8.5–11, 9.6μm) filter and CVF scans (5 - 17μm) at spectral resolution of $\lambda/\Delta\lambda \approx 50$. In one observing template often more than one filter has been selected.

3. DATA REDUCTION

The data were reduced with the ISOCAM interactive analysis tool (CIA, Ott et al. 1996). We used the default data reduction steps as provided by CIA of version April 2000: They are dark current subtraction, initial removal of cosmic ray hits (glitches), detector transient fitting, exposure coaddition, flat fielding. Except for staring modes, the coadded images at each raster position were sky projected and corrected for field distortion.

4. SOURCE IDENTIFICATION

Sources detected in the final reduced images need astronomical identifications. Generally this is done by matching the celestial position with those of the catalogue. However, for ISOCAM images this is more difficult because of uncertainties in the absolute astrometry. This uncertainty is caused by a jitter of the ISOCAM's lens wheel and the absolute astrometry can be off by as much as 2–3 pixels. This translates for the $6''$ lens to a positional error of $\leq 18''$ (see ISOCAM Handbook, Blommaert et al. 2001). The astrometric uncertainty is a global shift, so that if one or more field stars in an image can be identified it is possible to shift the image and to correct the astrometry to a precision as good as the pointing accuracy of the ISO space craft, which is $\leq 2''$ (Leech & Pollock 2001).

Proceedings of the Symposium *"Exploiting the ISO Data Archive - Infrared Astronomy in the Internet Age"*,
24–27 June 2002, Sigüenza, Spain (C. Gry, S. B. Peschke, J. Matagne et al. eds., ESA SP-511)

Therefore sources visible in the final ISOCAM maps were first cross correlated with optical sky plates (Digitized Sky Survey). We corrected for the lens wheel jitter by applying a shift of the ISOCAM image to match the DSS. Extragalactic sources were identified by overlaying on the ISOCAM image the positions of the galaxies as found in the NASA/IPAC Extragalactic Database (NED). All sources from the 3CR catalogue detected with ISOCAM were marked for later photometric extraction.

5. DETECTED SAMPLE

In total we detected with ISOCAM 79 radio galaxies at redshift range up to $z = 3.5$. In Fig. 1 we present the radio flux at 178 MHz as well as the redshift distribution of the 3C catalogue. For comparison we plot in the same diagrams those 3C sources where we could derive ISOCAM photometry. Both the original and the ISOCAM selected 3C catalogue show similar distributions in radio flux and redshift.

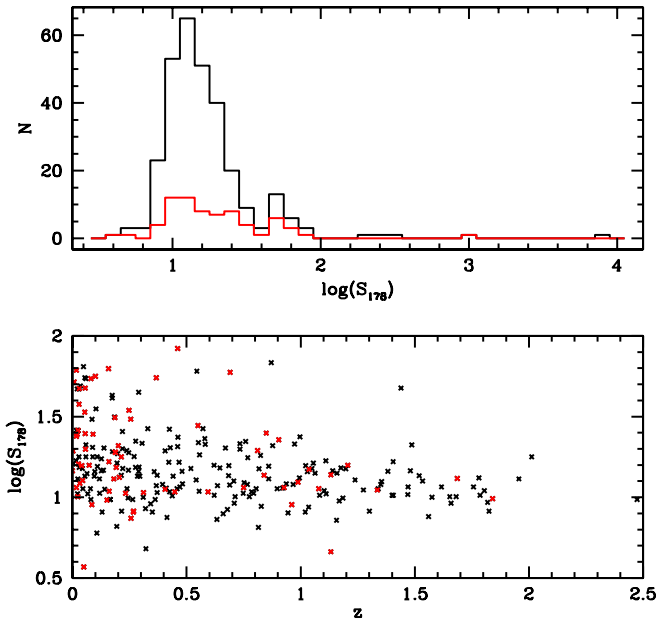

Figure 1. Histogram of the 178 MHz radio flux (top) and redshift distribution (bottom). The parent catalogue of 3CR sources (Spinrad et al. 1985) is shown in black and 3C sources detected by ISOCAM in red.

6. SPECTRAL ENERGY DISTRIBUTION

In case of a positive detection, the data were combined with those at other wavelengths. Often ISOCAM provides the only photometric data point in the IR. In Fig.2 we give a typical example. One can crudely make out three components: optical and near infrared ($\leq 5\mu$m), mid and far infrared ($5\mu\text{m} \leq \lambda \leq 1000\mu$m), and radio ($\geq 1$mm). Optical and near IR data are for most 3CR galaxies dominated by starlight (Best et al. 1998), while radio data are dominated by synchrotron emission. It is important to use the radio core fluxes (Giovanni et al. 2001) and to consider bolometric submillimeter fluxes of the radio core whenever available.

7. RADIATIVE TRANSFER DUST MODEL

Any model based on only a few observed fluxes has, of course, to be very simple and transparent. As a first attempt we consider spherical symmetry although this is not in agreement with the unified theory of active galactic nuclei according to which the energy source is surrounded by an accreting disk or a torus and the phenomenological type is determined by the viewing angle of the observer. Such a configuration is intrinsically two–dimensional.

A second reason to try at this preliminary stage spherically symmetric models stems from the well known fundamental difficulty that disks have in explaining the 10μm–silicate band. This resonance lies in a spectral region covered by ISOCAM. When viewed face–on, disks should show the feature in emission, contrary to what is being observed. Spherical models, on the other hand, are not plagued to much by this problem.

As a third argument in favour of spherical models, we point out that for one of the best known AGNs, in the Circinus galaxy, such a model proved as efficient in reproducing the observed infrared spectral energy distribution and the wavelength dependence of the infrared size (Siebenmorgen et al. 1997) as did two–dimensional models (Ruiz et al. 2001). The reason for its relative successfulness lies in the fact that most infrared data are at present still of low resolution.

For synthetic AGN spectral energy distributions we follow the procedure developed for the Circinus galaxy (Siebenmorgen et al. 1997). For the AGN a power law spectrum $F_\nu \propto \nu^{-0.5}$is assumed. For the dust we consider: large carbon and silicate grains and polycyclic aromatic hydrocarbons (PAH). A recent review of the dust model is given by Siebenmorgen et al. (2001). In the nucleus we apply a constant dust density distribution up to a galactic radius of 250 pc. The inner radius is roughly at 0.25 pc but depends on the detailed computation of the photo–destruction zone of the grains which can be as large as $\sim 1-2$ pc for the PAH. In Fig.3 and Fig.4 some IR spectra of AGN are shown. They are scaled to a distance of 50 Mpc. We consider a visual extinction, $1 \leq A_\mathrm{V} \leq 50$ mag and an AGN luminosity of $L_\mathrm{AGN} = 10^{7-13}$ $\mathrm{L}_\odot$. By applying a constant dust to gas ratio one may convert A_V to a total gas mass M_gas. For AGN the PAH bands are relatively weak. However, they become more pronounced for lower luminosities. This has two reasons: i) PAH destruction by the central engine is less efficient and ii) large grains get heated to lower temperatures only so that they emit less in the mid IR and consequently the PAH band to continuum contrast becomes stronger. Between 15–40μm different AGN luminosities give for a wide range of visual extinction quite similar spectra. Finally one needs to correct the observed fluxes of mid infrared passband filters at different redshifts so that we calculated the K correction factors.

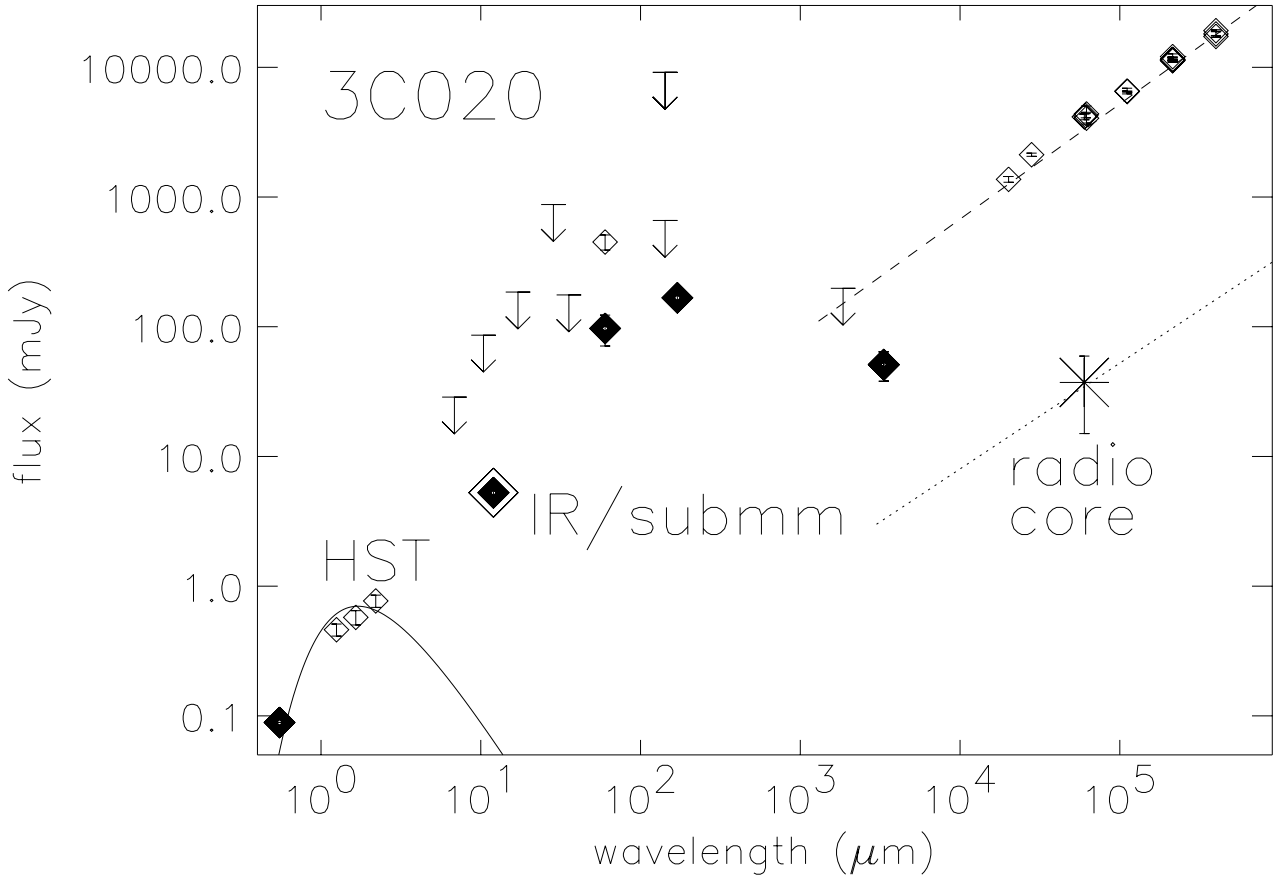

Figure 2. Flux density distribution of 3C20 from optical to radio wavelengths. HST observations suggest a stellar contribution to the near IR data (de Koff et al. 2000). We connect total radio data by a power law fit and apply same exponent to indicate the synchrotron emission of the radio core (Giovanni et al. 2001). The ISOCAM data shown as large diamond (this work) and far IR/submm data (Meisenheimer et al. 2001) points towards dust emission.

8. MODEL PARAMETERS

We consider only three basic parameters: total luminosity, linear source size, and total dust (or gas) mass. Assuming a constant density to keep the geometry as simple as possible, we may alternatively choose for the three parameters: luminosity L, cloud radius $r_{\rm gal}$, and visual optical depth $\tau_{\rm V}$. The influence of the model parameters is shown in Fig.3 and Fig.4 for our set of of synthetic AGN dust spectra[1]. We note that any data point in the ISOCAM wavelength range gives constrains to the infrared luminosity of the models, while far IR or submillimeter observations constrain the total gas mass and size of the dusty radio core. For application of the model to the 3CR sources detected by ISOCAM and preliminary conclusions see Freudling & Siebenmorgen (this proceeding).

ACKNOWLEDGEMENTS

This research has made use of the NASA/IPAC Extragalactic Database (NED) which is operated by the Jet Propulsion Laboratory, California Institute of Technology, under contract with the National Aeronautics and Space Administration. CIA is a joint development by the ESA Astrophysics Division and the ISOCAM Consortium. The ISOCAM Consortium is led by the ISOCAM PI, C. Cesarsky. This publication makes use of data products from the Two Micron All Sky Survey, which is a joint project of the University of Massachusetts and the Infrared Processing and Analysis Center/California Institute of Technology, funded by the National Aeronautics and Space Administration and the National Science Foundation. The research makes use of the Online Digitized Sky Surveys (DSS 1 & 2) server at the ESO/ST-ECF Archive.

[1] Synthetic AGN dust spectra available at rsiebenm@eso.org

REFERENCES

Best P.N., Longair M.S., Röttgering H.J.A., 1998, MNRAS 295, 549

Blommaert J., Siebenmorgen R., Coulais A., et al., 2001, "ISO Handbook Volume III (CAM)", SAI-99-057/Dc, http://www.iso.vilspa.esa.es

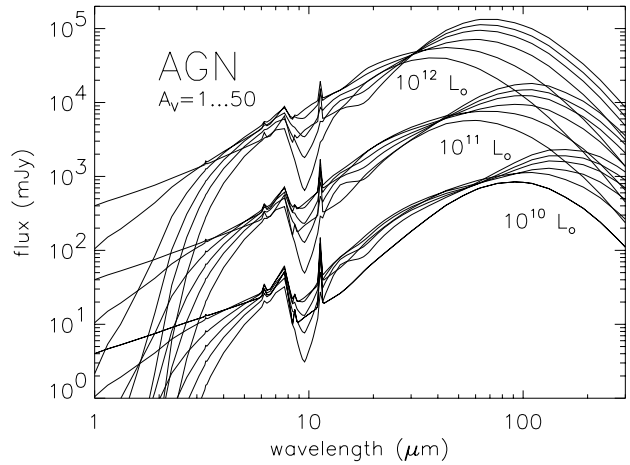

Figure 3. AGN model spectra are shown for visual extinctions of $A_{\rm V} = 1, 5, 15, 25, 35, 50$ *and luminosities of* $L = 10^{10}, 10^{11}$ *and* $10^{12}\ L_{\odot}$ *at distance of 50 Mpc. The galactic radius is fixed at* $r_{\rm gal} = 1$ *kpc.*

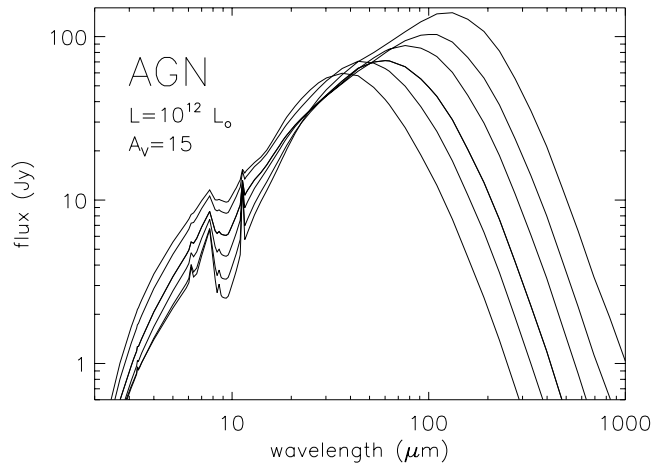

Figure 4. The influence of the galactic radius on the AGN model spectra is shown for $r_{\rm gal} = 0.25, 0.5, 1, 2, 4$ *and 8 kpc. The visual extinction is* $A_{\rm V} = 15$ *and the luminosity is* $L = 10^{12}\ L_{\odot}$ *at distance of 50 Mpc.*

Cesarsky C., Abergel A., Agnèse P. et al., 1996, A&A 315, L32
de Koff S., Best P., Baum S.A., Sparks W., Rottgering H., et al., 2000, ApJS 129, 33
Freudling W., Siebenmorgen R., 2002, this volume
Giovannini G., Cotton W.D., Feretti L., Lara L., Venturi T., 2001, ApJ 552, 508
Kessler M.F., Steinz J.A., Andregg M.E., et al., 1996, A&A 315, L27
Leech K., Pollock A.M.T. , 2001, "ISO Handbok Vol. II", SAI-99-082/Dc, http://www.iso.vilspa.esa.es
Meisenheimer K., Haas M., Müller S. A. H., et al., 2001, A&A 372, 719
Ott S., Abergel A., Altieri B., et al., 1996, ASAP Conference series, Vol. 125, 1997
Ruiz M., Efstathiou A., Alexander D. M., Hough J., 2001, MNRAS 325, 995
Siebenmorgen R., Moorwood A., Freudling W., Käufl H.U., 1997, A&A 325, 450.
Siebenmorgen R., Krügel E., Laureijs R., 2001, A&A 377, 735
Spinrad H., Djorgovski S., Marr J., Aguilar L., 1985, PASP 97, 932

MID-IR RADIATION OF 3C RADIO GALAXIES: II. RESULTS

Wolfram Freudling[1,2] **and Ralf Siebenmorgen**[2]

[1]European Southern Observatory,Karl-Schwarzschild-Strasse 2, D-85748 Garching b. München, Germany
[2]Space Telescope - European Coordinating Facility, European Southern Observatory, Karl-Schwarzschild-Strasse 2, D-85748 Garching b. München, Germany

ABSTRACT

The spectral energy distribution of 3C galaxies was constructed by compiling measurements in optical, near IR, far-IR and at mm bands for galaxies detected in our ISOCAM survey. Exploiting the models discussed by Siebenmorgen et al. (2002, hereafter SFK), we argue that for a large fraction of the detected galaxies, hot dust is the most likely explanation for the mid-infrared emission. Where this is the case, we have derived the total infrared luminosities, dust mass and limits on the dust temperatures. Taking into account selection biases in our sample, we discuss the frequency and properties of hot dust in radio galaxies at high redshift.

Key words: ISO – AGN – radio galaxies

1. INTRODUCTION

In SFK we presented ISOCAM mid-IR fluxes of 3C galaxies. We have searched the literature for photometric data on the ISOCAM detected galaxies in optical to far-IR and radio bands. While the MIR emission detected by ISOCAM is typically concentrated towards the nucleus of the galaxies, most other photometric measurements include emission from the whole galaxy. Examples of constructed SEDs are shown in Fig. 1. ISOCAM measured fluxes are shown as filled squares, whereas triangle mark data from the literature.

2. ESTIMATION OF DUST CONTENT

2.1. MODEL FITTING

Assuming free-free emission can be neglected, there are three potential contributions to the ISOCAM fluxes. First, there is the contribution from stars within the galaxies. Second, in some cases there might be come synchrotron emission from the AGN. Finally, there is a contribution from dust emission. In order to distinguish dust from the other contributions, we adopted the following procedure. First, we drew a redshifted T=4000K black body curves through the optical and near-IR points. They are shown as dashed lines in Fig. 1. The interpretation of this curves depends on the size of the optical image of the galaxy relative to the size in the ISOCAM images. For cases where the sizes are comparable, the extrapolation of the stellar fluxes to the ISOCAM bands was directly subtracted. For cases where the optical flux measurements presented a much larger region than the ISOCAM measurements, the stellar component was considered as an upper limit to a stellar component within the ISOCAM apertures. Next, we identified the few cases where synchrotron radiation might contaminate the ISOCAM fluxes. For that purpose, we used core fluxes at radio wavelength where available, or estimated the core flux from global radio properties. The later estimates are marked as asterisks in Fig. 1. The slope of the global radio properties was then used to extrapolate the core flux to the ISOCAM bands.

We selected model from our model library (see SFK) which are consistent with our data by first requiring that the models smoothed to the ISOCAM bandwidths predict the measured ISOCAM fluxes to within 10% accuracy. Next, we rejected models which violate any 3σ upper limit. Of the remaining models, we choose the ones which best fit the optical to mid-IR data in a least square sense. These models are shown as solid lines in Fig. 1.

2.2. TEST OF PROCEDURE

Our method as outlined above fits the same dust model heated by a central engine to all galaxies. The reason for adopting this procedure is that for most galaxies in our sample, we have no information on the details of the heating process. However, for a few galaxies, the heating mechanism has been studied in much more detail. One such case is M82. It is well known that our model is only a crude approximation to the physical processes in this galaxies. We tested how good an approximation the global parameters derived with our procedure are by comparing our selected model with the much more detailed modeling of the dust contents by Krügel & Siebenmorgen (1994). Their more realistic models simultaneously accurately predict both the SED and the spatial extend of the IR core emission as a function of wavelength. Fig. 2 shows the available data for M82. Superimposed are both the model selected from our library and the more detailed model. We conclude that the global parameters of the model in our library selected with our adopted procedure agree with parameters derived from more realistic models within about a factor of 3.

An independent test of our procedure is the comparison of predicted sizes with direct imaging of dust where available. The sizes in our models essentially determine the relative contribution of hot and cold dust for a given total input power. If our model parameters reflect the physical environment in out tar-

Proceedings of the Symposium *"Exploiting the ISO Data Archive - Infrared Astronomy in the Internet Age"*,
24–27 June 2002, Sigüenza, Spain (C. Gry, S. B. Peschke, J. Matagne et al. eds., ESA SP-511)

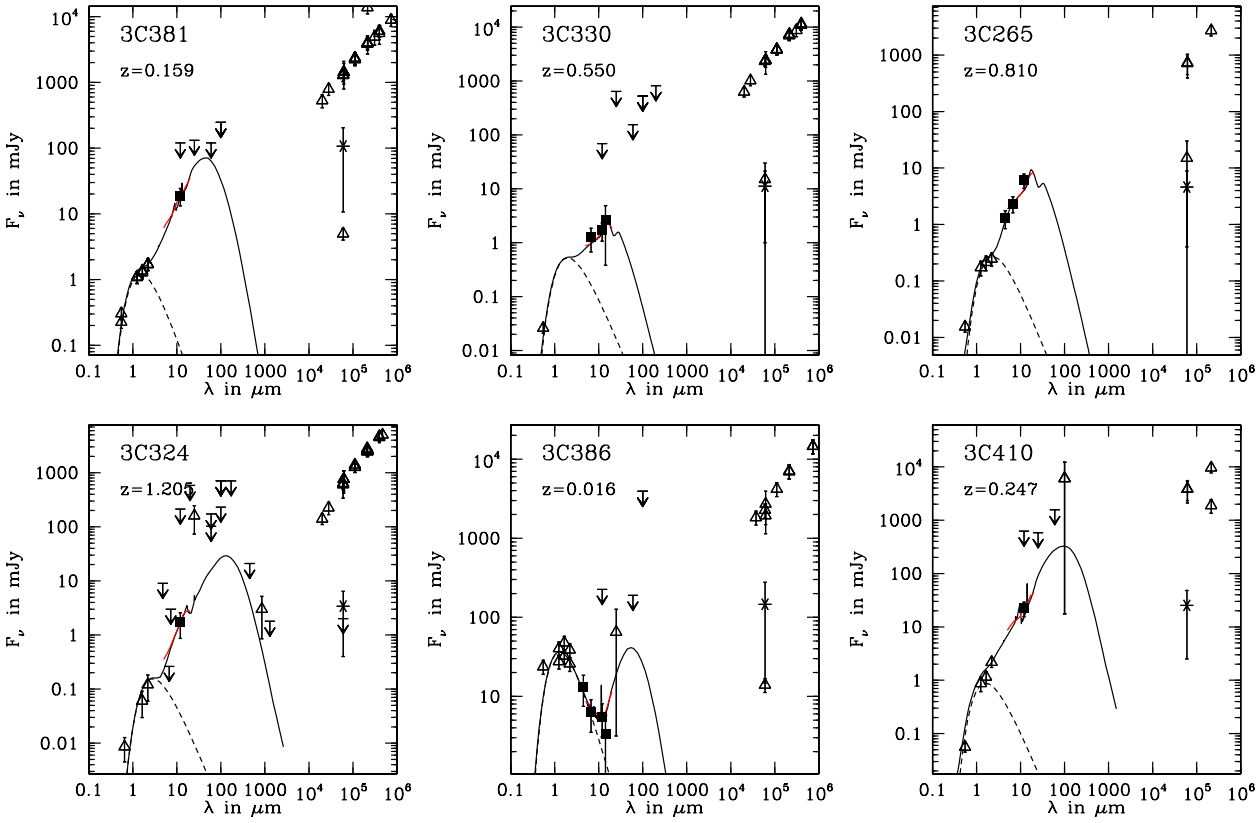

Figure 1. Six examples of SEDs from our catalogue. Each plot includes the adopted stellar contribution and the best fitting model as described in the text.

gets, then the radii of the dust spheres in our models should be similar to the extend of the visible dust distribution. In Fig. 3 we show two examples of HST images superimposed with the radius of the best fitting sphere. Again we conclude that model prediction compare well with observed quantities.

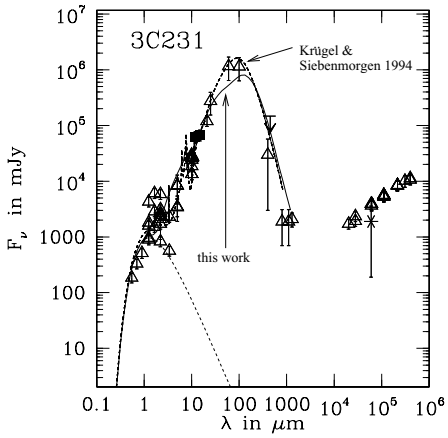

Figure 2. SED of M82. Superimposed are SED models from Krügel & Siebenmorgen and from this work.

3. RESULTS

3.1. Detection Rate

We extracted a total of 84 positions with 3C galaxies from the ISOCAM archive. Of those, 67 galaxies were detected by ISOCAM. We visually identified all SEDs with clear evidence for dust emission. A total of 53 galaxies were judged to contain dust.

Fig. 4 compares the redshift distribution of galaxies with clear indication of dust with that of all detected galaxies. It can be seen that the fraction of dusty galaxies does not depend much on redshift. We therefore conclude that the majority of all 3C galaxies up to a redshift of about 1 contain significant amount of hot dust.

3.2. Total Luminosity

Each fitted SED model is characterized by a total "dust luminosity". This luminosity comprises the energy injected by the central engine and re-radiated by dust (see Siebenmorgen et al.2002). The upper panel of Fig. 5 shows this luminosity as a function of redshift for all detected galaxies. This plot is dominated by selection effects. Since the 3C catalogue is flux limited at radio wavelength, any correlation of the MIR fluxes with the fluxes used to select the sample will lead to an apparent corre-

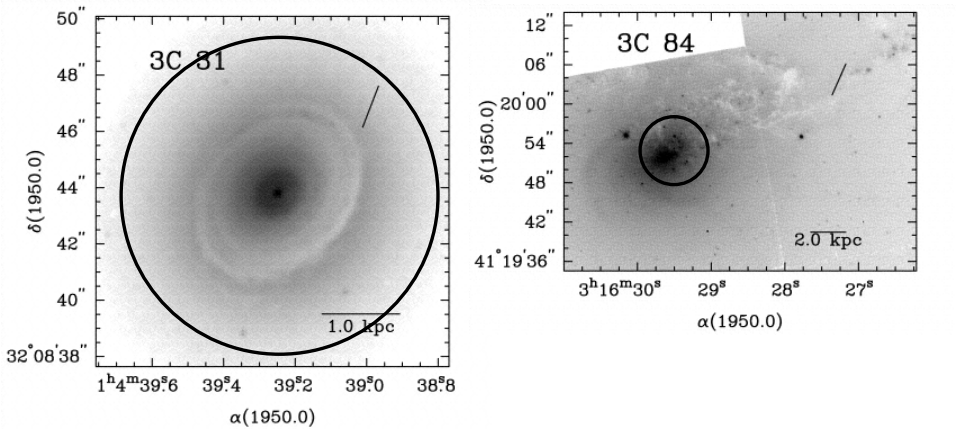

Figure 3. HST images (Martel et al., 1999) of 3C31 and 3C84. The superimposed circles mark spheres with the radii of the best fitting model for each galaxy.

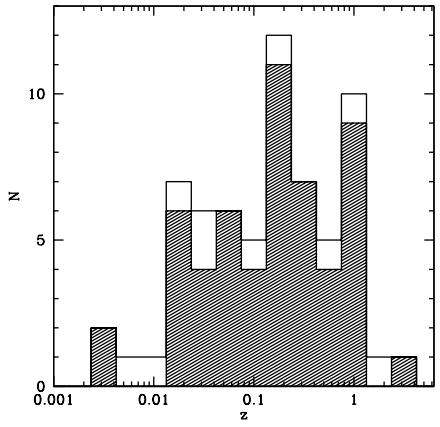

Figure 4. Redshift distribution of all galaxies in our sample. The hashed part of the histogram shows those galaxies with clear evidence of dust.

lation of flux with distance. To minimize selection effects, we related the dust luminosities to the luminosity of stars within the ISOCAM aperture. This was achieved by converting the fits of our black body curves to relative luminosities. The lower panel of Fig. 5, we show the dust luminosities divided by the stellar luminosities. The solid points in both panels of the plot are galaxies with stellar luminosities detectable at all distance bins. It can be seen that there is still a distance dependent effect. This might be due to remaining selection effects or evolution of dust contents.

4. CONCLUSION

ISOCAM was remarkably successful in detecting a large fraction of all 3C galaxies which were within its field of view. We suggest that this is due to a large relative hot dust component in these galaxies.

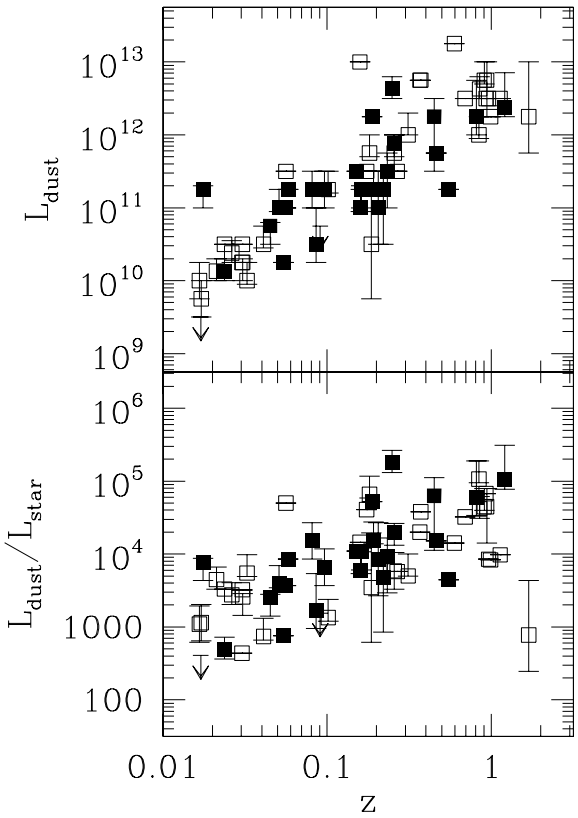

Figure 5. Upper panel: Dust luminosity of detected galaxies as a function of redshift. Lower panel: Dust luminosity divided by luminosity of stars as a function of redshift.

REFERENCES

Siebenmorgen, Freudling, Krügel, 2002, this volume.
Krügel, Siebenmorgen, 1994, AA 288, 929.
Martel et al., 1999, ApJS 122, 81.

MULTI-WAVELENGTH ANALYSIS OF THE DUST EMISSION IN THE SMALL MAGELLANIC CLOUD

Caroline Bot[1,2], François Boulanger[1], Koryo Okumura[3], and Bertrand Stepnik[1]

[1]Institut d'Astrophysique Spatiale, Université Paris-Sud, F-91405 Orsay, France
[2]Observatoire Astronomique de Strasbourg, Université Louis Pasteur, F-67000 Strasbourg, France
[3]Service d'Astrophysique, CEA-Saclay, F-1191 Gif-sur-Yvette, France

ABSTRACT

This paper investigates dust properties in the Small Magellanic Cloud(SMC). For this study, the IRAS maps at 12, 25, 60 and 100 μm were complemented with a 170 μm map built from the ISOPHOT data, retrieved from the ISO Data Archive.

The comparison at 170 μm and 100 μm data leads to a mean equilibrium temperature of 25.5 K for the SMC dust. This temperature implies a mean interstellar radiation field for the SMC ten times greater than for the solar neighbourhood.

ATCA/Parkes combined data were used to compare the dust spatial distribution with the one of neutral hydrogen. There is a tight spatial correlation between dust far infra-red brightness and hydrogen column density, from which we derive the mean dust emissivity per hydrogen atom: $\epsilon(\lambda)_{/H} = 2 \cdot 10^{-27} (\frac{\lambda}{250\mu m})^{-2} cm^2$, fifty times lower than in the solar neighbourhood. This difference is larger than that on the metallicity, which implies a lower depletion than in the Galaxy.

Within the bar, excess in infra-red emission with respect to dust emission in the neutral hydrogen are observed. They can be understood as emission from dust associated with cold H I and molecular gas.

Key words: ISM:clouds – ISM:dust – Galaxies: Small Magellanic Cloud – Infrared: ISM

1. INTRODUCTION

The Small Magellanic Cloud (SMC) is a dwarf galaxy about 50 kpc away. This relative proximity allows an understanding of dust properties at different spatial scales. The SMC is a young galaxy which shows a lower metallicity and a higher star formation activity than the Milky-Way. Studying the SMC and comparing it to our galaxy reflects the effects of the metallicity and star formation activities on dust properties. The ISOPHOT data at 170 μm of the SMC, together with ancillary data (IRAS, ATCA/Parkes) allow us to study the SMC's dust properties at large spatial scales and to compare them to those of the Galaxy. The first section presents the data we used. Section 2 describes the analysis of these data and the results are discussed in section 3.

2. THE DATA

2.1. THE ISOPHOT DATA

The ISO Data Archive provided us a large set of PHOT mapping observations at 170 microns carried out with the P22 AOT. We reduced these data with a standard method and combined the different maps into a large one (Fig. 1). The covered area is a large part of the Small Magellanic Cloud.

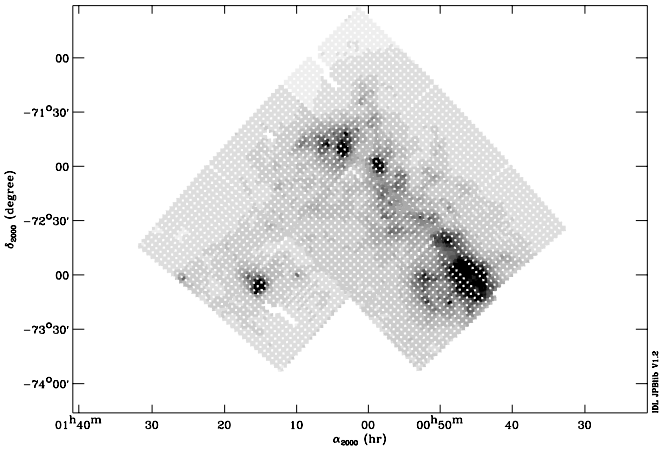

Figure 1. Mosaic of 9 ISOPHOT 170 μm maps, covering a large fraction of the SMC

2.2. ANCILLARY DATA

Together with the ISOPHOT data, we used an IRAS map at 100 μm (Fig. 2). This map is a combination of the IRAS survey and Additional Observations in the SMC. We also used an H I column density map to determine the dust abundances with respect to hydrogen. This map was deduced from ATCA/Parkes combined observations, assuming that the H I is optically thin.

Finally, in order to identify the star formation regions we took an Hα map from G. D. Bothun, smoothed with a median filter in order to suppress stars.

All these data enabled a multi-wavelength analysis of the large dust grains emission in the SMC.

Proceedings of the Symposium *"Exploiting the ISO Data Archive - Infrared Astronomy in the Internet Age"*, 24–27 June 2002, Sigüenza, Spain (C. Gry, S. B. Peschke, J. Matagne et al. eds., ESA SP-511)

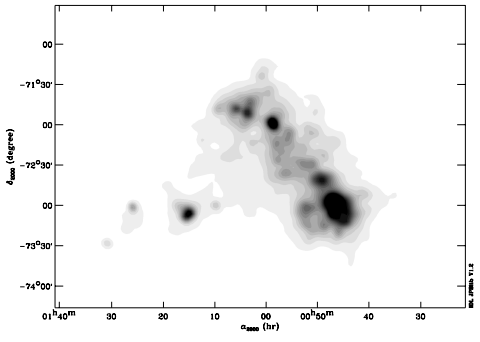

Figure 2. IRAS 100 μm map of the SMC

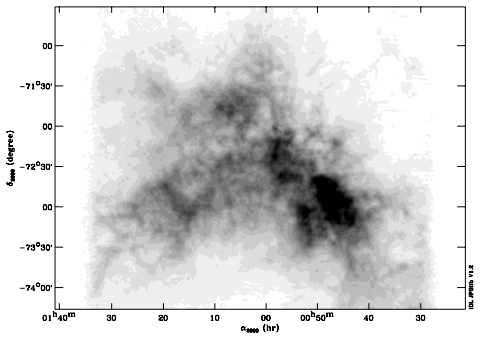

Figure 3. H I map of the SMC from combined ATCA/Parkes data

3. DATA ANALYSIS

We used the two infra-red maps (at 170 μm and 100 μm) to compute the large dust grains temperature and emissivity per hydrogen atom at large scale for the SMC.

3.1. LARGE DUST GRAINS EMISSION

Dust grains receive energy from the UV radiation field, their temperature rises and they re-emit this energy at infra-red wavelengths as thermal emission. Large grains are at thermal equilibrium and their emitted intensity at a frequency ν can be expressed as:

$$I_\nu = N_H \epsilon(\nu)_{/H} B_\nu(T_{dust}) \quad (1)$$

where N_H is the column density of the hydrogen and $\epsilon(\nu)_{/H}$ is the emissivity of the grains per hydrogen atom.

At first, we will assume that all the dust is in the H I, which is optically thin to the UV radiation. We also assume that the emissivity of dust grains in the far infra-red follows a power law:

$$\epsilon(\nu)_{/H} = \epsilon(\nu_0)_{/H} \left(\frac{\nu}{\nu_0}\right)^\beta \quad (2)$$

and we take $\beta = 2$ as found for Galactic emission (Lagache et al. 1999).

3.2. LARGE DUST GRAINS TEMPERATURE

We plotted the ISOPHOT 170 μm data versus the IRAS 100 μm data and tried to fit the data where it correlates (Fig. 4).

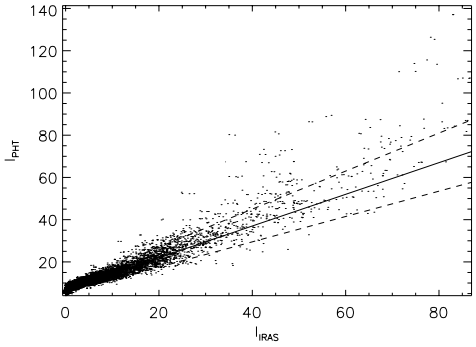

Figure 4. ISOPHOT/IRAS correlation plot with lines fitted on the correlation. The solid line represents the best fit for $I_{\rm IRAS} < 20$ MJysr^{-1} *and is taken as a reference for the temperature calculation. The dotted lines correspond to minimum and maximum slopes that can be fitted to the same region. Infra-red excess can be seen for high intensity and most of them correspond to star formation regions where the dust is heated.*

The slope of the fitted solid line provides a measure of the big grains temperature in the SMC. We find an average grains equilibrium temperature for the SMC of:

$\mathbf{T}_{dust}$ **=25.5 K**.

Using the dust equilibrium temperature in the solar neighbourhood of 17.5K (Boulanger et al. 1996) as a reference, this equilibrium temperature leads to a radiation field $\chi_{SMC} = 10$ which is consistent with a direct estimate from UV observations.

3.3. LARGE DUST GRAINS ABUNDANCES

We plotted the ISOPHOT 170 μm data versus the 21 cm data and tried to fit the data where it correlates (Fig. 5).

The slope of the fitted straight line leads to a determination of the emissivity per hydrogen atom of the big grains in the H I in the SMC.

For an equilibrium temperature of 25.5 K, we find an emissivity per hydrogen atom for the SMC of:

$\epsilon(\lambda)_{/H} = 2. \cdot 10^{-27} (\frac{\lambda}{250\mu m})^{-2} cm^2$.

This value is 50 times lower than the galactic value, to be compared with a difference in metallicity which is less than 10 (Dufour 1984) and a difference in $\frac{E(B-V)}{N_H}$ of about 20 (Bouchet et al. 1985). This result implies a low depletion of the dust elements. Welty et al. 2001 suggested this too, finding Mg and Si to be essentially undepleted. It was also reported in Blue Compact Dwarf Galaxies (Lisenfeld & Ferrara 1998). An interpretation of this effect has been proposed by (Hirashita et al. 2002) with a model of the dust life cycle, where grains are more frequently destroyed by SNe in such galaxies.

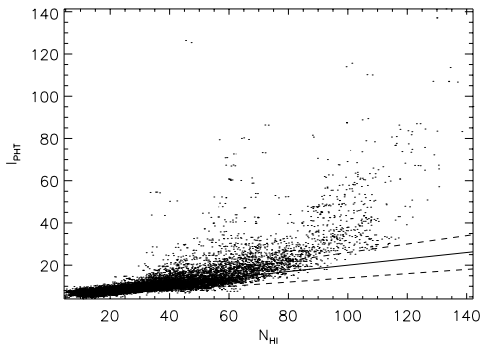

Figure 5. ISOPHOT/H I correlation diagram with lines adjusted on the data for $N_{\rm HI} \leq 30.10^{20}$ atoms cm−2. As for the ISOPHOT/IRAS correlation, the solid line correspond to the best fit and the dashed ones to the minimum and maximum slope that can be adjusted to the correlation.

3.4. LARGE DUST GRAINS SPECTRUM

We computed the spectrum of large dust grains at the equilibrium temperature of 25.5 K and an emissivity of $\epsilon(\lambda)_{/H} = 2. \cdot 10^{-27}(\frac{\lambda}{250\mu m})^{-2} cm^2$. The comparison of this spectrum with IRAS data at 12, 25 and 60 μm shows the importance of the small grains in emission at this wavelength. This emphasizes the contribution of ISOPHOT data for studies on dust grains emission.

Fig. 6 shows this dust emission spectrum together with the galactic one (Reach & Boulanger 1998), both normalized to $N_H = 1.10^{20}\mathrm{cm}^{-2}$. We can see the emissivity difference (vertical shift) and the temperature difference (horizontal shift) between the SMC and the Galaxy.

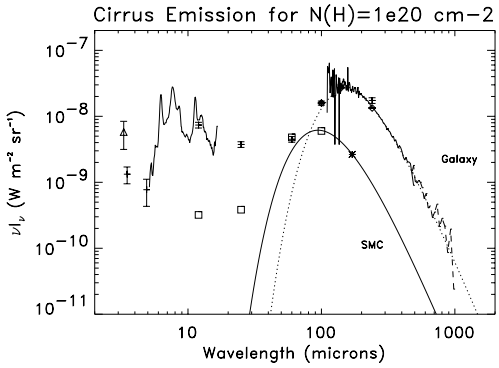

Figure 6. Comparison of the infra-red emission spectra of the SMC and the Galaxy. The brightness is normalised to an interstellar gas column density of $10^{20} cm^{-2}$. The galactic spectrum is composed of COBE/FIRAS data (above 100 μm, shown here with the corresponding thermal equilibrium grains spectrum in dotted line), ISOCAM data (below 20 μm) and photometric measurements from COBE/DIRBE and Arome. The SMC spectrum is composed of IRAS (squares) and ISOPHOT (star) data The thermal equilibrium spectrum associated with it is also shown (continuous line).

We used the dust model of Desert et al. 1990 to quantify in mass the grain size distribution in the SMC (see Fig. 7). Mass abundances relative to hydrogen, compared with galactic values (Desert et al. 1990) are summarized in table 1. Fig. 7 shows the dust emission modeling together with the observed values.

Table 1. Mass abundance relative to hydrogen in the SMC and in the Galaxy. The grain size distribution is assumed to be the same in both cases.

Componant	Galaxy $\frac{m}{mH}$	SMC $\frac{m}{mH}$
PAH	$4.3 \cdot 10^{-4}$	$1.4 \cdot 10^{-6}$
VSG	$4.7 \cdot 10^{-4}$	$4.9 \cdot 10^{-6}$
BG	$6.4 \cdot 10^{-3}$	$1.2 \cdot 10^{-4}$

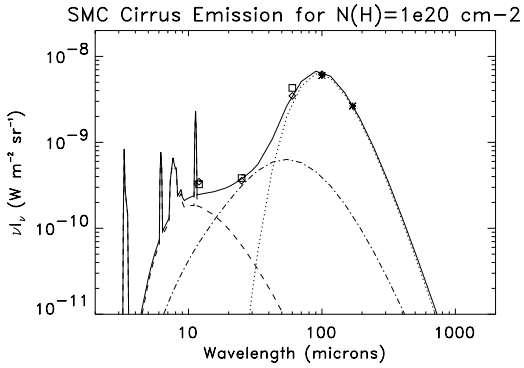

Figure 7. The model resulting spectrum (continuous line) is the sum of three components that are PAHs (dashed line), VSGs (mixed line) and BGs (dotted line). IRAS observations (squares) and ISOPHOT observation (star) have to be compared with the fitted model values at the same wavelength (diamonds)

4. DISCUSSION

To go further in the analysis of the scatter in the 170 μm/HI correlation diagram we divided the SMC in 3 bins according to the Hα emission. We find that part of the scatter is due to dust heating in star forming regions but another part is due to dust in cold H I and molecular gas not traced by the H I emission.

4.1. THE DIFFUSE MEDIUM

As for the whole SMC, we compute the temperature and the abundances for the diffuse medium in the outer part of the galaxy. We also find $T_{dust} = 25.5\ K$ and $\epsilon(\lambda)_{/H} = 2 \cdot 10^{-27}(\frac{\lambda}{250\mu m})^{-2} cm^2$ but correlations are tightened.

4.2. THE SMC BAR

For the bar, we found a dust temperature very slightly higher than in the diffuse medium and we can make the assumption

that the dust emission per hydrogen atom is the same in the bar than in the outer parts.

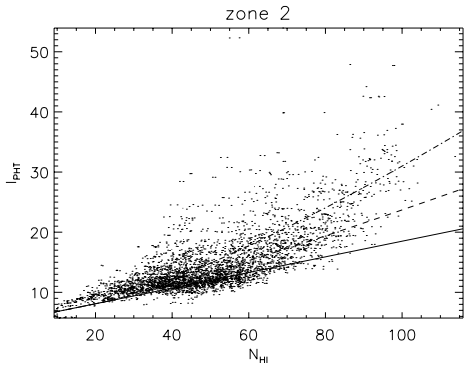

Figure 8. ISOPHOT/H I correlation diagram. The solid line fits the correlation for the diffuse emission. The dotted line represents this correlation taking into account a cold H I component, according to the Dickey et al. correction. The mixed line represents this correlation taking into account a cold H I component and an H_2 component. This two components can explain part of the infra-red excess in the correlations.

However there is significant scatter in the 170μm/H I correlation diagram above the dust emission expected in the H I gas (solid line). Based on H I absorption measurement, Dickey et al. 2000 have estimated the fraction of cold ($\approx$ 40K) H I not seen in emission to be:

$$f_{cold} = (1 + 0.667(\log N_{H_I} - 21.4)) \quad (3)$$

for $N_{H_I} \geq 30 \cdot 10^{20}$atoms cm^{-2} The dashed line shows the expected dust emission if we take this cold gas into account. We can also expect a contribution from dust in molecular clouds. The dash-dotted line illustrates this contribution with the arbitrary assumption that the fraction of molecular gas follows the same law than f_{cold}. This interpretation is confirmed by a spatial correlation between these infra-red excess and CO seen with NANTEN (Mizuno et al. 2001).

Thus, we show that an H I and an H_2 component are seen at large scales and can explain infra-red excess non related to star formation regions. Note that within this interpretation the fraction of gas mass in H_2 would be comparable to that of cold H I, about 15% of the mass traced by the H I emission.

From this result, we can conclude that H_2 in the SMC is more abundant than what was seen by FUSE. This can be explained as far as their study was on line of sights among hot stars, which is not where molecular hydrogen is dissociated.

5. CONCLUSION

We retrieved nine ISOPHOT maps at 170 μm from the ISO Data Archive, covering a large part of the SMC. These maps were reduced and arranged into a mosaic. Together with IRAS maps at 12, 25, 60 and 100 μm and an H I map from ATCA/-Parkes, we characterised the properties of large dust grains.

We found an equilibrium temperature of 25.5 K which leads to a radiation field ten times higher than in the solar neighbourhood. At this temperature, we found the mean dust emissivity to be $2.10^{-27}\left(\frac{\lambda}{250\mu m}\right)^{-2}$ cm^2 per hydrogen atom. This low value is partly accounted for the SMC's low metallicity, but also requires a lower gas depletion than in the Galaxy.

The Hα emission allows us to divide the SMC into three regions: the diffuse medium surrounding the SMC bar, the SMC bar and the star formation regions. 170μm/100μm and 170μm/H I correlations studies were performed for the two first regions. We also found $T_{\rm dust} = 25.5$ K and $\epsilon(\lambda)_{/H} = 2 \cdot 10^{-27}(\frac{\lambda}{250\mu m})^{-2} cm^2$ for the diffuse medium. In the bar, we observe infra-red excess that can not be associated with heating effects. If we assume that dust properties are the same in the whole SMC, we can explain this excess taking into account the distribution of cold atomic and molecular gas, not seen in emission.

All data used for this study were retrieved in different databases and combined, allowing a multi-wavelength view of dust and gas. This is thus a science case of what can be done via a Virtual Observatory for extended emission.

ACKNOWLEDGEMENTS

We acknowledge S. Stanimirovic for providing us the H I data and her help in using it.

REFERENCES

Bouchet et al., 1985, A&A 149, 330
Boulanger F. et al., 1996, A&A 312, 256
Dickey J.M. et al., 2000, ApJ 536, 756
Dufour R.J., 1984, in IAU Symp. 108, 353
Hirashita H. et al., 2002, A&A 388, 439
Lagache G. et al., 1999, A&A 344, 322
Lisenfeld U. & Ferrara A., 1998, A&A 496, 145
Okumura K., 1993, Ph.D. Thesis, Univ. Paris-Sud
Staveley-Smith L. et al., 1997, MNRAS 289, 225
Welty D.E. et al., 2001, ApJ 554, L75
Tumlinson J. et al., 2002, ApJ 566, 857

INVESTIGATING THE [CII]-PAHS RELATION IN A LARGE SAMPLE OF LOCAL GALAXIES

Alessandra Contursi[1], **James Brauher**[2], **and George Helou**[2]

[1]Max-Planck-Institut für Extraterrestrische Physik, Giessenbachstraße, 85748, Garching, Germany
[2]SIRTF Science Center, California Institute of Technology, Mail Code 314-6, 1200 East California Boulevard Pasadena, CA 91125

ABSTRACT

We present preliminary results about the linear correlation existing between the Mid Infrared (MIR) Aromatic Features seen in emission (AFEs) and the emission of the main cooling line of the neutral atomic medium, [CII] at 158 μm, for a sample of 140 galaxies. A similar analysis on a smaller sample of normal galaxies only, has been already published by Helou et al. (2001). The final aim of the work presented here is to further investigate the physical origin and implications of such a relation and to see if the same results hold for a much wider variety of galaxy types and activities. When only spiral galaxies are considered, we confirm the results already obtained in previous works by Malhotra et al. (2001) and Helou et al. (2001) : there exists a difference between the behavior of the [CII]/FIR and [CII]/AFE ratios as a function of the 60 μm /100 μm IRAS colors: while [CII]/FIR decreases with the IRAS color, the [CII]/AFE ratio stays constant. The same result seems to hold also for early-type and irregular galaxies although they show a much higher dispersion in the [CII]/AFE ratio. As first step of the analysis, we concentrate on understanding the origin of the dispersion in order to separate intrinsic physical behavior from errors in the ISOCAM photometry. There exist few outsiders with a [CII]/AFE ratio lower than the main trend outlined from late spiral and irregular galaxies, although, at this preliminary stage of the analysis, we are not yet able to explain the physical origin.

Key words: galaxies: ISM, atoms, dust, lines and bands

1. INTRODUCTION

The interplay between ISM and star forming processes is the key to understanding galaxy evolution. One way to approach this topic is to study the energy budget in nearby galaxies, *i.e.* the energy input provided by stars to the ISM and the resultant cooling of the ISM. Interstellar dust is heated by stellar radiation and cools by re–radiating at infrared wavelengths. The heating and cooling of the interstellar gas are more complicated processes because, they depend on its phase (molecular, atomic, neutral or ionized), chemical composition and temperature.

[CII] (158 μm) and [OI] (63 μm) are the main cooling lines of the neutral atomic gas. In normal galaxies, [CII] usually dominates energetically, carrying a luminosity $\sim$ 0.3–1 percent of the FIR luminosity (Crawford et al. 1985, Stacey et al. 1991). [OI] and [CII] emission from the neutral ISM arise in photodissociation regions (PDRs), *i.e.* those regions in which the chemical and heating processes are dominated or induced by interaction with FUV photons. In PDRs the gas is heated by energetic photo–electrons ejected by dust grains after absorption of FUV (6 eV $<$ hν $<$ 13.6 eV) photons (Hollenbach & Tielens 1999) or, for dense ($n > 10^4$ cm^{-3}) gas regions, via collisional deexcitation of vibrationally excited H_2 (Sternberg & Dalgarno 1989). Since smaller grains are more efficient at photo–electron production, the smallest grains (sometimes referred to as Very Small Grains) or even large molecules (those responsible for the Aromatic Features observed in Emission (AFEs) between 5 μm and 20 μm often attributed to Polycyclic Aromatic Hydrocarbons or PAHs) are likely to be the main sources of photo–electrons and thus of gas heating in PDRs (Bakes & Tielens 1994).

The general scenario described above was actually observationally confirmed by works based on Kuiper Airborne Observatory (KAO) data (Poglitsch et al 1991, Stacey et al. 1991, Madden et al. 1993, 1997, Nikola et al. 1998) of the Milky Way and close-by galaxies. With the advent of the Infrared Space Observatory (ISO, Kessler et al. 1996) it was possible to carry out Far Infrared (FIR) fine structure line observations of galaxy samples wider than before and therefore to addres in more detail the role of the different grain populations in the heating process of the gas and the relation between interstellar medium and star forming processes. One of such studies has been carried out on a sample of Normal Galaxies (ISO–KP on Normal galaxies Helou et al 1998), observed at MIR wavelengths with ISOCAM (Dale et al. 2000) and in a wealth of FIR infrared structure lines with ISO-LWS (Malhotra et al. 2001). One important result from the analysis of these data is that, while the [CII]/FIR ratio decreases with the IRAS 60/100 μm colors, which to first order traces the heating intensity of the system (Malhotra et al. 2001), the [CII]/AFE ratio is remarkably constant (Helou et al. 2001). This suggests that there is a difference in the role of different dust grain populations in the gas heating process such that there exists a special conncetion between the Aromatic Feature carriers and the [CII] emission. On the other hand, the physical origin of this tight connection has not been completely understood; it might reflect that the carriers responsible for the Aromatic Features are indeed the most efficient in the gas heating process or/and that the FIR and the MIR emission are probing different layers of the HII-

Proceedings of the Symposium *"Exploiting the ISO Data Archive - Infrared Astronomy in the Internet Age"*,
24–27 June 2002, Sigüenza, Spain (C. Gry, S. B. Peschke, J. Matagne et al. eds., ESA SP-511)

PDR-Molecular cloud complex (Helou et al. 2001).
In order to understand these open issues, and to check whether the above results still hold for other than normal galaxies, we continue this analysis, expanding the sample of galaxies to include all kind of morphologies and activities. The ISO archive is the perfect tool for such a project, as we could gather all data available on galaxies observed with both ISO-LWS and ISO-CAM.

2. THE SAMPLE

All ISO-LWS data on FIR fine structure lines of galaxies available in the ISO-archive (228 galaxies, including the ISO-KP Normal Galaxies sample) have been reduced at IPAC and the data will be made available to the community soon by Brauher (2003, in preparation). From this huge project we started a side-project aimed at studying the physical relation between dust and gas in galaxies of all types and activities in the Local Universe. Of the whole ISO-LWS extragalactic sample, we have reduced the ISOCAM data of all targets observed either with LW2 (λ_c=6.7 μm) or LW3 (λ_c=14.3 μm) or both filters (80 galaxies).
In order to have consistency on the MIR photometry of the whole sample, we reduced from scratch the ISOCAM data of the ISO-KP sample. The new reduction strategy provides an improved photometry over the previous published data set by Dale et al. (2000). The main difference lies in a more careful flat-field correction with respect to the recipe followed in Dale et al. (2000). As was pointed out in Roussel et al. (2001), Dale et al. (2000) photometry was underestimated due to a non-complete masking of the source in the flat field created from the data. The agreement on a sub-sample of ISO-KP galaxies and Virgo galaxies published by Roussel et al. (2001) and our new photometry is within 20 per cent.

Due to the above selection criteria it is obvious that the whole sample (140 galaxies) does not meet any completeness criteria but provides a large variety of galaxies in morphology, FIR/B ratio, IRAS 60/100 colors and presence of nuclear activity. Fig. 1 shows ISOCAM images of some of the galaxies in the sample. The diameter of each circle corresponds to the FHWM of the LWS beam at 158 μm (75″). From these few examples it is clear the variety of the sources and also that some targets are extended and some are not with respect to the LWS beam. The ISOCAM and IRAS flux in the LWS beam at each pointing of the extended galaxies have been calculated as described in Contursi et al. (2002).

3. RESULTS

Upper panel of Fig. 2 shows the [CII]/FIR ratio of galaxies belonging to the two samples (ISO-KP in blue and the present sample in black) as a function of the 60 μm/100 μm IRAS ratio which traces the heating intensity of the systems. The two samples agree very well confirming the results of Malohtra et al. (2001): the [CII]-FIR ratio decreases as the IRAS color ratio increases probably because of the decreasing of the photoelectric

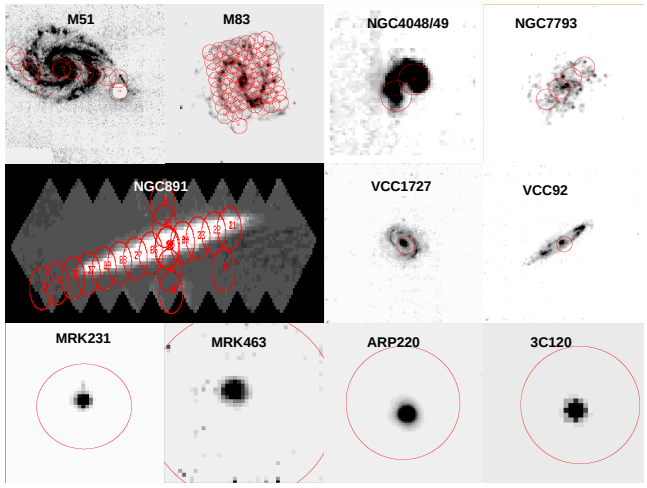

Figure 1. LWS coverage at 158 μm of some of galaxies in the sample. Gray-scales are ISOCAM images and circles indicate the LWS pointings. The circle's diameters correspond to the ISO-LWS FHWM at 158 μm.

efficiency due to positive grain charging as the heating intensity becomes high. Bottom panel of Fig. 2 shows a similar plot but for the [CII]/AFE ratio. This plot confirms the result by Helou et al. (2001) that in galaxies, AFE and [CII] scale together regardless of their IRAS colors, although the overall dispersion of the present sample is higher than the dispersion obtained considering Normal Galaxies only. However, we note that the dispersion decreases significantly if only spirals are considered (circles). This is better shown in Fig. 3 where the histograms of the [CII]/FIR and [CII]/AFE ratios are shown separately for early-type, spirals and irregular galaxies (see caption of Fig. 2 for details on how these three classes are defined). Although the histogram width corresponding to spirals is the smallest for both ratios, the [CII]/AFE histogram clearly shows that this ratio is remarkably constant in spirals. This is even more striking considering that these data refer to regions either inside galaxies, spiral arms, inter arms and nuclear regions, or to the whole galaxy emission (Fig. 1), suggesting that [CII] and AFE always scale together in regions very different in stellar populations, and physical conditions of the ISM.

Before concluding that the differences in the [CII]/AFE ratio of different galaxy types reflect real physical differences in the heating/cooling process of the atomic gas, we have to understand why the [CII]/AFE relation followed by other than spiral galaxies has a large dispersion. The average [CII]/AFE ratio of early-type galaxies is lower than the ratio of later types regardless of their IRAS colors (triangles in Fig. 2 bottom panel). This can be due to a significant stellar photosphere contribution in the LW2 filter in most of the early-type galaxies: this flux is obviously not directly related to the atomic gas heating such that there is more flux at 7 μm than one would expect simply scaling from the [CII] emission. In principle, one can

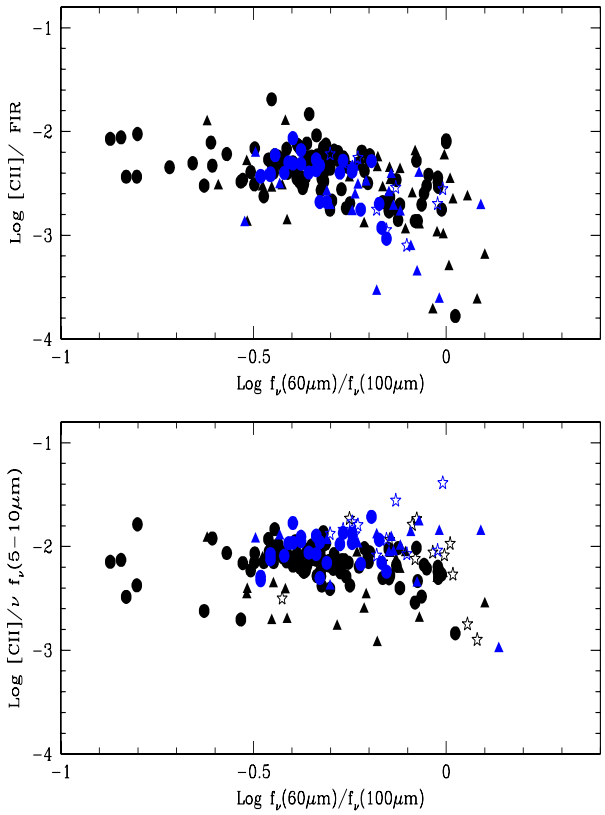

Figure 2. Top Panel: the [CII]/FIR ratio as a function of the IRAS 60 μm/100 μm ratio for the whole sample (140 galaxies). The two samples, the ISO-KP published by Malhotra et al. (2001) (blue symbols) and the present sample agree very well confirming the decreasing of the [CII]-FIR ratio for high IRAS colors. We divided the galaxies in three morphological classes according to the following division (types T are form RC3): early-type (filled-triangles) with T < 0; spirals with 0≤ T ≤ 8 (filled circles); irregulars with T≥9 (empty stars). Bottom Panel:the [CII]/AFEs (PAHs) ratio as a function of the IRAS 60 μm/100 μm color ratio for the whole sample. Symbols and colors have the same meaning as in top panel. Note that in both figures, both extended and not extended sources with respect to the LWS beam are plotted.

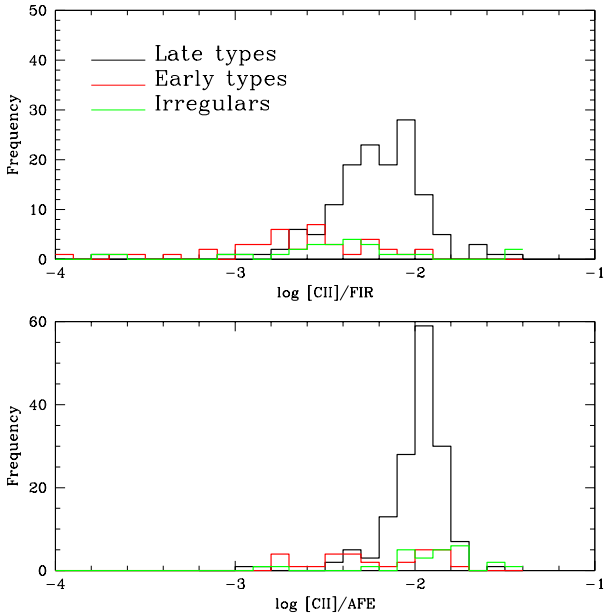

Figure 3. The [CII]/FIR (top) and [CII]/AFE (bottom) ratio histograms of the whole sample divided in the three morphological types we have described in figure 2.

estimate the stellar contribution from Near Infrared photometry. In the forthcoming work we will verify this hypothesis and quantify the stellar contribution using 2MASS data.

At the highest IRAS color range (Log (60 μm/100 μm) > 0) in the [CII]/AFEs relation in Fig. 2 there are 4 objects with [CII]/AFE ratios significantly lower than the main trend followed by spirals and irregulars suggesting that they behave differently from the bulk of the sample. One of this galaxy is an early type and therefore we cannot state that it has a [CII] deficiency with respect to its AFE emission until we correct for the stellar contribution at 7 μm. The other three objects (MRK231, MRK463 and IRAS01589-2524) are all classified as Seyfert galaxies. In order to check whether the [CII]/AFE deficiency is the signature of AGN activity, we have investigated where the Seyfert galaxies lie on the plot: if indeed a low [CII]/AFE ratio is an indication of AGN presence and activity, one would expect Seyfert and AGNs grouping at lower [CII]/AFE levels. This is not seen in our data (not shown here); active galaxies are spread out all over the whole IRAS color range and do not differ in any way from the main trend. At this stage of the analysis we are not yet able to understand whether these galaxies are peculiar with respect to the rest of the galaxy sample or if we just see the same phenomenon seen in Fig. 1 for the [CII]/FIR ratio but at extremely warm IRAS colors.

Finally , some of the irregulars show a high [CII]/AFE ratio. This was already noted by Hunter et al. (2001) and Contursi et al. (2002) and it probably depends on the fact that the contribution from ionized gas (either diffuse or in HII regions) to the total [CII] emission is higher in irregulars. Indeed, the observed [CII] emission of all galaxies in the sample should be corrected for this contribution and we expect this to reduce the dispersion. This will be done using the [NII] emission line at 122 μm as shown in Malhotra et al. (2001) for the galaxies of the sample observed at this wavelength with the ISO-LWS instrument.

4. CONCLUSION AND FUTURE WORK

In this paper we have presented preliminary results on the analysis of the [CII]-AFE (PAH emission) relation in a big sample of local galaxies. The final aim of this project is to better understand which is the role of the different dust grain populations in

the heating process of the atomic gas in galaxies and therefore its connection with the star forming process. Such a research on an extended galaxy sample has been possible only thanks to the ISO data archive where we could gather MIR images and FIR fine structure lines data for 140 galaxies.

We confirm the fact that at least for spirals, [CII] and AFE scale together as already found on a sample of Normal Galaxies by Helou et al. (2001); the remarkable result here is that the [CII]-AFE linearity still holds despite the fact we included in our sample galaxies of very different types, star forming rates and nuclear activities, and we probe both different regions inside the galaxies and their global emission. Nevertheless, some differences have been found in the behavior of the [CII]/AFE ratio as a function of $60\mu m/100\mu m$ IRAS colors for early, spiral and irregulars galaxies, with spiral galaxies having the smallest dispersion. Before concluding that these differences arise from different physical relations between the carriers responsible for the AFEs and the atomic gas heating, we have to understand whether there exist other possible contributions able to alter the main [CII]-AFE relation followed by spirals. We have reason to believe that indeed this is the case: the [CII]/AFE ratio of early-types is lower than the [CII]/AFE ratio of spirals probably because of a significant contribution of stellar emission at 7 μm. Irregular galaxies tend to have higher [CII]/AFE ratio, probably because of a contribution of [CII] arising in ionized gas to the total observed emission. Therefore the first next step of the analysis will be to correct from these extra contributions not arising from either the Aromatic Feature carriers or atomic gas to see if their dispersion in [CII]/AFE-IRAS color plot decreases. Secondly, we will use the other FIR fine structure lines data as a tool to understand if the difference observed in the behavior of the [CII] with respect to FIR and MIR emission arises from the fact that FIR and MIR are probing different ISM phases: the FIR is mostly produced in denser and quiter regions, the MIR on layers closer to the heating sources. Most of the galaxies in the sample have been observed also in the [OI] line at 63 μm, which should probe layers in the molecular cloud-PDR complex denser than the layers where [CII] arises.

REFERENCES

Bakes, E.L.O., & Tielens, A.G.G.M., 1994, ApJ, 427, 822

Contursi, A., Kaufman M. J., Helou G., et al, 2002, AJ, 124, 751

Crawford M. K., Genzel R., Townes C.H., et al., 1985, ApJ, 291, 755

Dale, D.A., Silbermann, N. Helou, G., et al., 2000,AJ, 120, 583

Helou, G., 1998, Highlights of Astronomy Vol. 11A, Ed. Johannes Andersen. Kluwer Academic Publishers, p.1134

Helou, G., Malhotra, S., Hollenbach, D., et al., 2001, ApJl, 548, L37

Hollenbach, D. J., & Tielens, A.G.G.M., 1999, Rev. Modern Phys., 71, 173

Hunter, D. A., Kaufman, M.J., Hollenbach, D.J., et al., 2001, ApJ, astro–ph/0012354

Kessler M. F., Steinz J. A., Anderegg M. E., 1996, A&A, 315, 27L

Madden S. C., Geis N., Genzel R. , et al., 1993, ApJ, 407, 579

Madden S. C., Poglitsch A., Geis N., 1997, ApJ, 483, 200

Malhotra, S., Kaufman, M.J., Hollenbach, D., et al., 2001, ApJ, 561, 766

Nikola, T.; Genzel, R.; Herrmann, F, 1998, ApJ, 504, 749

Roussel, H., Vigroux, L., Bosma, A., et al., 2001, 369, 473

Poglitsch A., Stacey G. J., Geis N., 1991,, ApJ, 374, 33

Stacey, G.J., Geis, N., Genzel, R., et al., 1991, ApJ, 373, 423

Sternberg, A., & Dalgarno, A., 1989, ApJ, 338, 197

WHAT POWERS THE PAH EMISSION IN GALAXIES?

Martin Haas[1], **Ulrich Klaas**[1], **and Simone Bianchi**[1,2]

[1]Max-Planck-Institut für Astronomie, Königstuhl 17, 69117 Heidelberg, Germany
[2]CNR, Istituto di Radioastronomia, Sezione di Firenze, Largo E. Fermi 5, 50125 Firenze, Italy

ABSTRACT

Our new methodology to study dedicated topics on the ISM is based on the use of the 850 μm continuum as a measure of the full amount of dust, and ISOPHOT-S and ISOCAM observations of the PAH features, which are presumably mixed with the ISM. In this poster we focus on the question: Is the PAH emission in galaxies mainly due to starbursts or due to the interstellar radiation field? For details we refer to the paper by Haas, Klaas & Bianchi (2002). Here we give only a brief outline.

Key words: ISM; PAHs; cold dust

1. RESULTS AND CONCLUSIONS

We investigated five spatially resolved galaxies which cover a range of star forming activities.

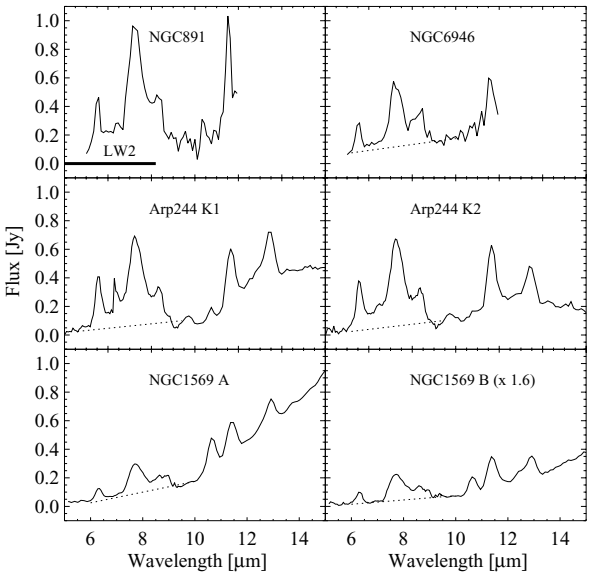

Figure 1. ISOPHOT-S and ISOCAM-CVF spectra at dedicated positions of the galaxies, showing the typical PAH features and the slope of the continuum, in particular longwards of 10 μm. The dotted lines indicate the eyeball-fitted continuum around 7.7 μm. The horizontal bar indicates the bandpass of the LW2 6.7 μm filter.

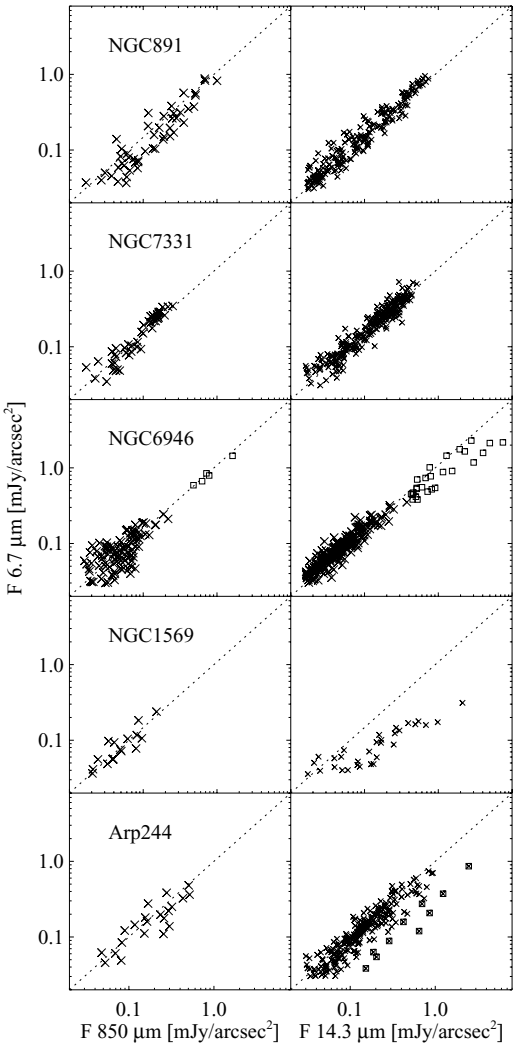

Figure 3. Relation between the fluxes at 6.7 μm versus 850 μm (left column) and 14.3 μm (right column). Each symbol corresponds to an area in a grid covering the galaxies. The apertures are 15-25" and 6-10" for the left and right column, respectively. The ratio between the fluxes is mostly about unity (dotted lines). An exception are the 14.3 μm points for the starbursts regions, in particular, the nucleus of NGC 6946 and the active knot K1 in the overlap region of Arp244 (squares).

Fig. 1 shows MIR spectra taken with ISOPHOT-S and ISOCAM-CVF for dedicated positions in the galaxies. Using suitable

Proceedings of the Symposium *"Exploiting the ISO Data Archive - Infrared Astronomy in the Internet Age"*, 24–27 June 2002, Sigüenza, Spain (C. Gry, S. B. Peschke, J. Matagne et al. eds., ESA SP-511)

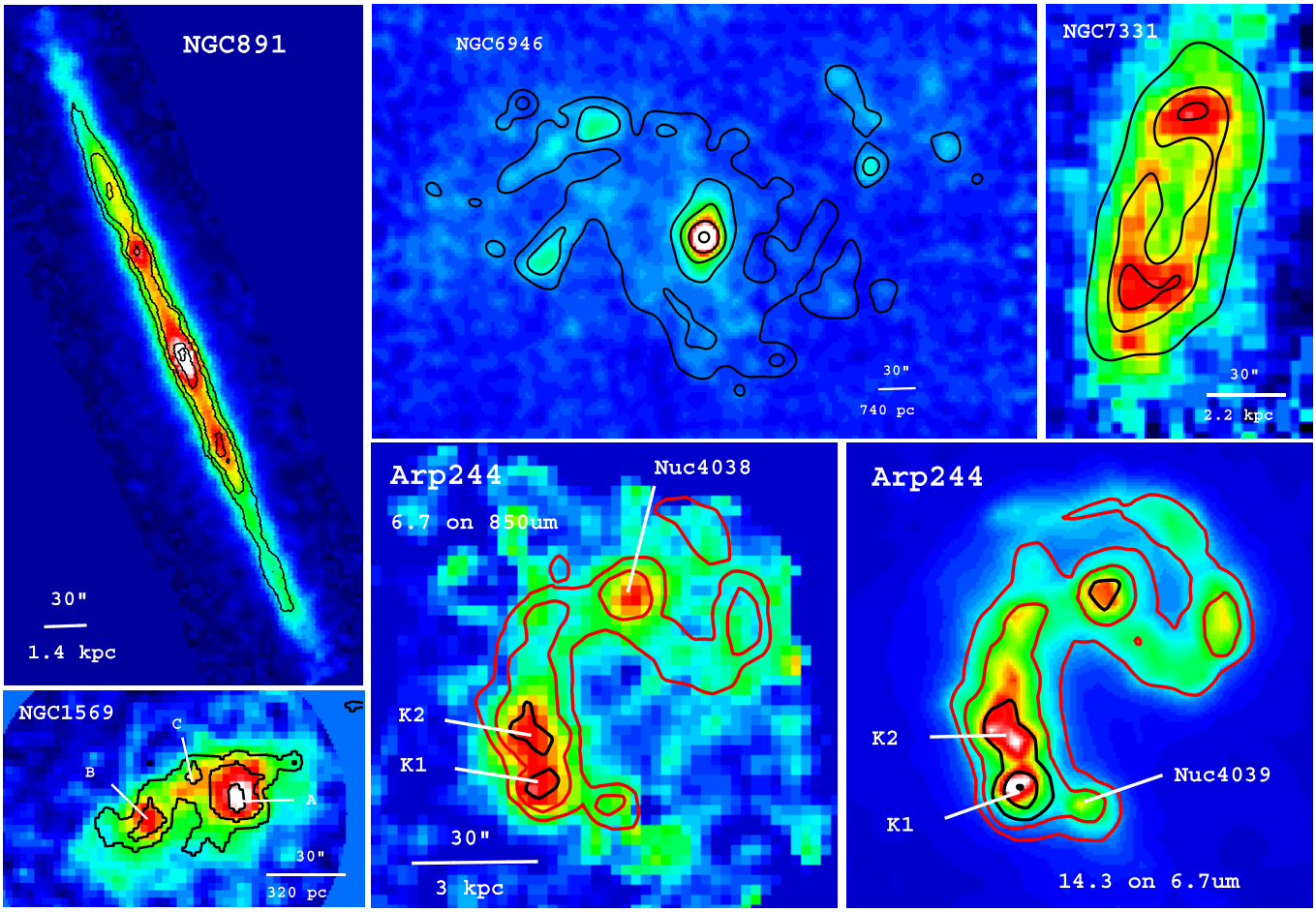

Figure 2. 850 μm maps with 6.7 μm contour overlays showing the good spatial coincidence. North is up, east is left. Bottom right for Arp 244: 14.3 μm contours on a 6.7 μm map, showing the increase of the 14.3 μm emission with respect to that at 6.7 and 850 μm in the starburst area K1.

ISOCAM broad band filters (for the emission of the PAHs as well as the very small grains) a complete coverage of the galaxies is provided.

Fig. 2 shows the SCUBA 850 μm and ISOCAM maps. We find a good spatial coincidence between the 850 μm continuum emission and the strength of the PAH's, traced by the ISOCAM 6.7 μm band.

In order to quantify the spatial coincidence, we compared the fluxes for a grid of suitably sized apertures covering the galaxies. As shown in Fig. 3, the PAHs correlate with cold dust emission, and also with the emission from very small grains at 14.3 μm, but regions with starbursts show an excess in the very small grain emission.

We conclude that the PAH carriers are preferentially related to the regions dominated by cold dust and molecular clouds, where they are excited mainly by the interstellar radiation field. The lack of increased PAH/submm ratio in starburst knots suggests that starbursts play a minor role for powering the entire PAH emission in galaxies.

REFERENCES

Haas M., Klaas U., Bianchi S., 2002, A&A 385, L23

ISOPHOT'S SERENDIPITY SURVEY UNVEILS AN UNUSUAL ULTRALUMINOUS INFRARED GALAXY

Oliver Krause[1], Ute Lisenfeld[2], Ulrich Klaas[1], Dietrich Lemke[1], and Manfred Stickel[1]

[1]Max-Planck-Institut für Astronomie, Königstuhl 17, D-69117 Heidelberg, Germany
[2]Instituto de Astrofísica de Andalucia, Camino Bajo de Huétor 24, E-18080 Granada, Spain

ABSTRACT

We present multi-wavelength observations of the unusual ultraluminous infrared galaxy (ULIRG) ISOSS J 15080+7248. The object was identified using the 170 μm ISOPHOT Serendipity Survey (ISOSS) in the search for cold and luminous extragalactic far-infrared sources. The dust emission of ISOSS J 15080+7248 is associated with a giant elliptical galaxy ($M_V = -22.6$ mag) at redshift z = 0.214. ^{12}CO(1-0) line observations reveal a molecular gas mass of $M_{H_2} = 2 \cdot 10^{10}$ $M_\odot$ which is unusually high for such an elliptical. Peculiar is moreover the absence of any optical line emission from this luminous ($L_{IR} = 2 \cdot 10^{12}$ $L_\odot$) galaxy with a star formation rate of 350 $M_\odot$ yr^{-1}, as inferred from the bolometric infrared luminosity. Our observations contrast with the known population of local ULIRGs, which are virtually all advanced mergers of gas rich spirals and characterized by optical emission line spectra and warm dust emission due to their strong star formation activity. The undisturbed elliptical morphology, the presence of a de Vaucouleur $r^{1/4}$ brightness profile and a low gas-to-dust ratio and dust temperature let us suggest that ISOSS J 15080+7248 is either a giant elliptical merging a gas rich spiral or a relaxed merger between two spirals on the transition into a massive elliptical system. Such sources might have been overlooked in surveys based on the IRAS data, which were biased towards the warm dust emission at the peak of star formation activity.

1. INTRODUCTION

About 2000 galaxies have been detected by the ISOPHOT Serendipity Survey (ISOSS) at 170 μm (Bogun et al. 1996; Stickel et al. 2002, this volume). It provides a unique data base to identify objects with hitherto unusual SED properties. An object class of particular interest are galaxies with increasing energy distributions beyond 100 μm, indicating lower dust temperatures and hence higher dust masses than derived from IRAS data alone. The ISOPHOT (Lemke et al. 1996) Serendipity Surveys allows for the first time to search for such cold FIR emitters. We have performed follow-up observations in order to characterize the nature of these galaxies and here we present a detailed study of ISOSS J 15080+7248, which is one of the most distant cold objects detected in the survey. Its 170 μm flux is 2 Jy.

2. FOLLOW-UP OBSERVATIONS

Our IRAS/ISO photometry is complemented by the following set of observations:

[1] 1.2 mm continuum measurements with the IRAM 30m telescope using the MAMBO bolometer array.

[2] CO(1-0) line observations with the IRAM 30m telescope using the A100 and B100 heterodyne receivers.

[3] Optical long slit spectroscopy obtained with the TWIN double spectrograph at the Calar Alto 3.5m telescope.

[4] CCD R-band images obtained with LAICA at the Calar Alto 3.5m telescope and with the MPIA 0.7m telescope in the Johnson R & I bands.

[5] 21cm continuum observations from the VLA (Condon et al. 1998).

[6] JHK near-infrared photometry from 2MASS (Cutri et al. 2000).

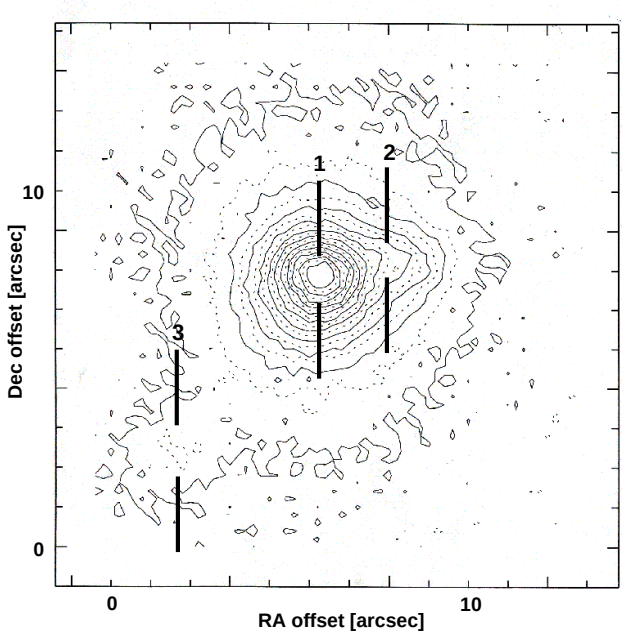

Figure 1. R-Band image of ISOSS J 15080+7259 obtained with LAICA at the Calar Alto 3.5m telescope. The giant elliptical galaxy (1) has a close companion (2) and shows a faint tail of emission (3) towards southeast.

Proceedings of the Symposium *"Exploiting the ISO Data Archive - Infrared Astronomy in the Internet Age"*, 24–27 June 2002, Sigüenza, Spain (C. Gry, S. B. Peschke, J. Matagne et al. eds., ESA SP-511)

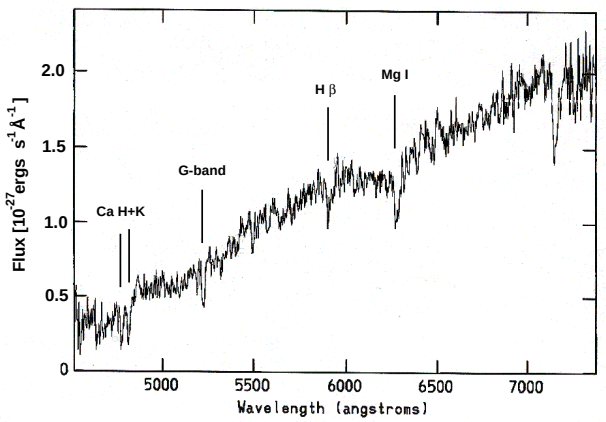

Figure 2. Optical spectrum of the elliptical galaxy (courtesy E. Moran).

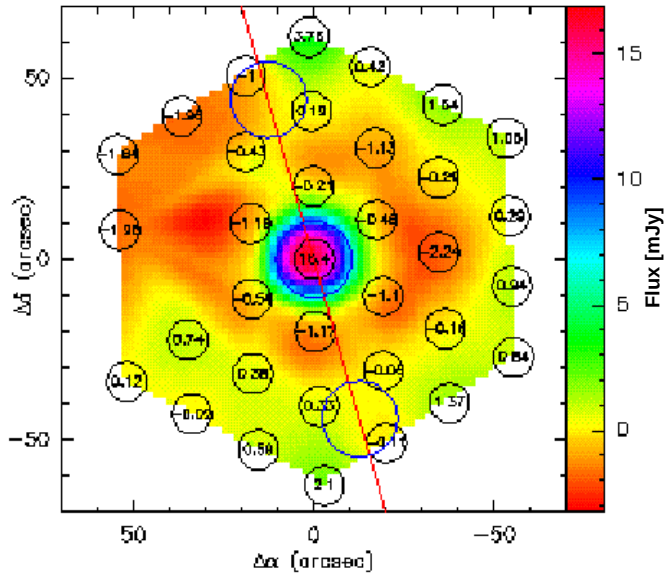

Figure 3. 1.2mm continuum photometry of ISOSS J15080+7259 obtained with the MAMBO bolometer array.

3. RESULTS

The optical R-Band image (Fig. 1) shows extended emission of an elliptical galaxy. Its brightness profile can be well fitted by a de Vaucouleur $r^{\frac{1}{4}}$ law. Two additional peaks of emission can be be seen 2 arcsec W and 6 arcsec SE from the central peak.

Optical long slit spectroscopy reveals a pure absorption spectrum (Fig. 2) towards the elliptical. The redshift derived from the Ca H & K, G-band and Fe 5340 Å features is z = 0.2137 ± 0.0003. In direction of the western brightness peak, an emission line spectrum typical of a star forming spiral is found. It is blue-shifted by 600 km s^{-1} with respect to the central component. Furthermore, the spectral lines are oblique implying rotation.

The 1.2 mm continuum measurement with MAMBO provides a point source flux of 16 mJy (Fig. 3). From the integration over the spectral energy distribution (Fig. 4) we derive a total IR luminosity L_{IR}(8-1000 μm) = $2 \cdot 10^{12}$ $L_\odot$. This corresponds to a star formation rate of 350 $M_\odot$ yr^{-1} (Kennicutt 1998). Our MAMBO observation corresponds to a rest wavelength of 990 μm. The dust mass is then given by $M_d = Fd^2/\kappa_{990\mu m} B_{990\mu m}(T_d)$, where we used a dust mass absorption coefficient $\kappa_{990\mu m} = 0.64$ cm^2 g^{-1} following Lisenfeld et al. (2000). The dust continuum (Fig. 4) can be modeled by either two optically thin components (T_d=20/50 K, dust emissivity β=2, dashed line) or one optically thick component (T_d=45 K, β=1.6, $\tau_{100\mu m}$=5, solid line)

The CO(1-0) observation shows a peak of emission at a redshift of 0.213, coinciding with the optical redshift of the elliptical galaxy. The integrated intensity of the source is 1.35 Jy km s^{-1}, yielding a molecular gas mass $M(H_2) = 2 \times 10^{10}$ $M_\odot$. We used a conversion factor of 4.6 $M_\odot pc^{-2} K^{-1}$, following Solomon et al. (1987). The gas mass corresponds to the values observed for gas-rich spirals. Assuming an atomic-to-molecular gas ratio of $M_{HI}/M_{H_2} \sim 1$, the gas-to-dust ratio for the optical thick dust model is ~ 50.

VLA observations (Condon et al. 1998) show the presence of a compact (FWHM $\sim 3 \times 1$ $arcsec^2$) continuum source, coinciding in position with the optical center of the elliptical galaxy. The measured 21cm flux density $S_{21cm} = 5.3$ mJy follows the FIR-Radio-correlation of star forming galaxies (Sanders & Mirabel 1996). No evidence for an AGN is found from the radio/MIR data.

4. DISCUSSION

ISOSS J 15080+7248 turns out to be an ultraluminous IR galaxy with unusual properties. ULIRGs normally show a much more disturbed morphology and emission line spectra in their centers (Veilleux et al. 1999). Although there is observational evidence that other ULIRGs show elliptical kinematics in the NIR (Genzel et al. 2001), none of them have such a regular appearance as ISOSS J 15080+7248. If ISOSS J 15080+7248 has evolved along the usually assumed merger sequence of two gas-rich spirals then it would be one of the most evolved objects known so far. Alternatively ISOSS J 15080+7248 may be an elliptical galaxy merging with a gas rich spiral inducing a powerful starburst in the center of the elliptical. Both the CO and radio continuum observations indicate that the activity is linked with the central region of the elliptical galaxy. The optically thick dust model would be consistent with a deeply embedded star formation region. In any case the dust temperatures derived from the two dust models are significantly lower than found for nearby ULIRGs (Klaas et al. 2001) and indicate an unusual evolutionary stage.

5. CONCLUSION

Using the ISOPHOT Serendipity Survey we have identified ISOSS J 15080+7248 as a giant elliptical galaxy with a luminosity of $L_{IR} = 2 \times 10^{12}$ $L_\odot$ and a molecular gas mass of $M(H_2) = 2 \times 10^{10}$ $M_\odot$, which is one of the highest ever measured for such an elliptical. Moreover, the object is to our

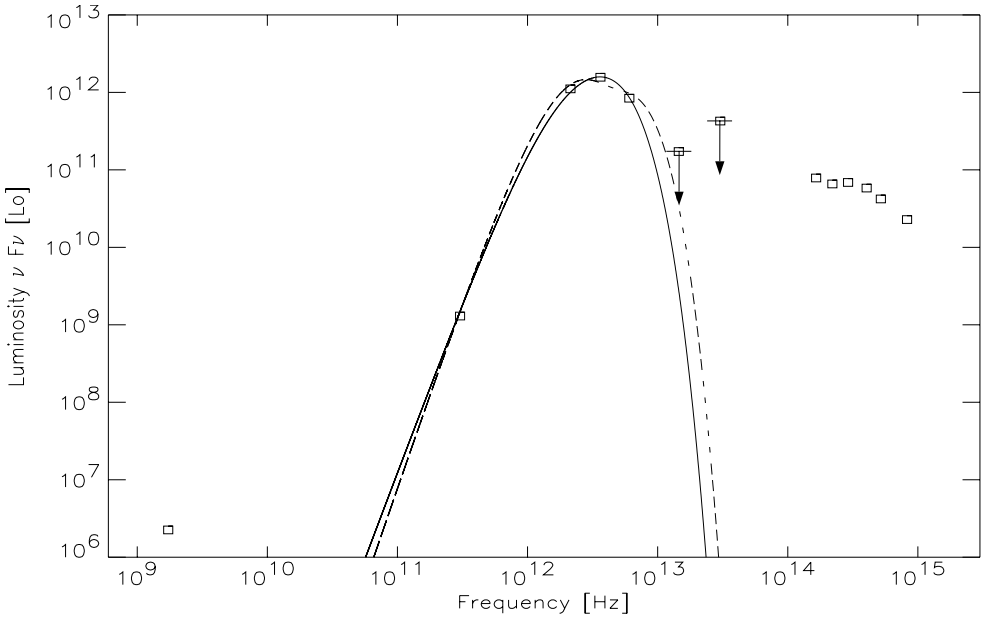

Figure 4. Rest frame spectral energy distribution of ISOSS J 15080+7248. The FIR dust emission can be well characterized by our two dust models (solid: optically thick, dashed: optically thin, see text for details). Upper limits on IRAS 12 and 25 μm photometry are indicated by arrows.

knowledge the only ULIRG so far without the presence of any optical emission lines. This is consistent with our interpretation of the thermal dust emission originating from a deeply embedded starburst. We conclude that ISOSS J 15080+7248 is either an old giant elliptical galaxy merging a gas-rich spiral or a relaxed merger between two spirals. The observations show, that giant elliptical galaxies still undergo phases of strong star formation in the local universe.

ACKNOWLEDGEMENTS

The ISOPHOT Data Centre at MPIA is supported by Deutsches Zentrum für Luft- und Raumfahrt (DLR) with funds of Bundesministerium für Bildung und Forschung, grant No. 50QI0201. OK thanks the Wernher von Braun-Stiftung zur Förderung der Weltraumwissenschaften for financial support. We acknowledge support of this project by M. Grewing, E. Moran and J. Fried. This research has made use of the NASA/IPAC Extragalactic Database (NED), which is operated by the Jet Propulsion Laboratory, California Institute of Technology, under contract with NASA.

REFERENCES

Bogun, S., Lemke, D., Klaas, U. et al., 1996, A&A 315, L71
Condon, J.J., Yin, Q.F., Thuan, T.X. et al., 1998, ApJ 116, 2682
Cutri, R. M., et al. 2000, Explanatory Supplement to the 2MASS Second Incremental Data Release
Genzel, R., Tacconi, L., Rigopoulou, D., 2001, ApJ 563, 527
Klaas, U. et al., 2001, A&A 379, 823
Kennicutt, R., 1998, ARA&A 36, 189
Lemke, D. et al, 1996, A&A 315, L64
Lisenfeld, U. et al, 2000, MNRAS, 312, 433
Moran, E. et al., 1996, ApJSS 106, 341
Sanders, D. & Mirabel, I., 1996, ARA&A, 34, 749
Solomon, P.M., Downes, D., Radford, S.J.E. et al. 1997, ApJ, 478, 144
Stickel, M., Lemke, D., Klaas, U., Krause, O. et al., 2002, this volume
Veilleux, S., Kim, D., Sanders, D., 1999, ApJ 522, 113

THE COMPLEX FAR-INFRARED MORPHOLOGY OF M86

Manfred Stickel

Max–Planck–Institut für Astronomie, Königstuhl 17, D–69117 Heidelberg, Germany

ABSTRACT

The elliptical galaxy M86 (NGC 4406) shows a highly asymmetric X-ray morphology with an extended emission feature, which is likely due to ram pressure stripping of the hot coronal gas. A far-infrared (FIR) source detected by IRAS is offset from the galaxy centre in the same direction. On the basis of this apparent connection between the X-ray and far-infrared morphology, it has been proposed that not only gas but also dust is ram pressure stripped from M86 by the intracluster medium due the large relative velocity. Although elliptical galaxies have much less dust than spiral galaxies, M86 is nevertheless still the only case with some observational evidence for ongoing gas and dust stripping. ISOPHOT imaging of M86 at $60\,\mu$m, $90\,\mu$m, $150\,\mu$m, and $180\,\mu$m reveals a much more complex FIR morphology. A central pair of compact sources with a cold FIR spectrum of about 18 K dust temperature is closely associated with the M86 galaxy itself. A third unresolved source, previously discovered by IRAS, lies about $3.5'$ north-west of M86 and has in contrast a warm FIR spectrum. A fourth source with a cold FIR spectrum and a core-halo morphology lies about $7.5'$ north-west of M86, close to the nearby edge-on spiral NGC 4402. The ISOPHOT data do not support the interpretation that the north-western component is cold dust removed from M86, since it has a rather warm dust temperature of about 60 K, actually lies away from the ridge of the extended X-ray emission, and is positionally coincident with an optically faint unresolved point source, most likely an unrelated background source. Likewise, neither the central double source nor the fourth cold source lying between M86 and NGC 4402 provides support for the ram pressure dust stripping scenario. The former is likely due to the central FIR emission of M86 in conjunction with dust already seen in the optical. The latter likely part of the interstellar medium of NGC 4402 tidally removed during the passage of M86, and represents the first detection of a dust cloud in the intergalactic region between galaxies.

Key words: galaxies: individual: M86 – galaxies: clusters: general – intergalactic medium – infrared: general

1. INTRODUCTION

While there is considerable evidence for the ram pressure interaction of the intracluster medium (ICM) of galaxy clusters with the gas in the interstellar medium (ISM) of cluster members, it is still controversial whether dust mixed with the interstellar gas participates in this dynamical process. A significant dust stripping of spirals near cluster cores was found by Doyon & Joseph (1989), whereas Bicay & Giovanelli (1987) and Contursi et al. (2001) conclude that the FIR properties and the dust content of most cluster galaxies are not affected by the environment. Moreover, a clear case of dust being stripped from an individual spiral galaxy is currently not known.

Observational data suggesting ongoing dust stripping due to the movement of the galaxy relative to the cluster environment is only available for the bright Virgo elliptical M86 (NGC 4406). It shows distorted optical isophotes (Nulsen & Carter 1987; Elmegreen et al. 2000), a high negative adial velocity relative to the cluster ($-1364\,\mathrm{km\,s^{-1}}$, Faber et al. 1989), and is likely the dominant member of a small galaxy group entering the Virgo cluster from the back (Binggeli 1999). X-ray observations of M86 reveal a region of extended emission not coincident with the galaxy center (Forman et al. 2001), which is interpreted as hot ISM stripped from the galaxy (Forman et al. 1979, Rangarajan et al. 1995). IRAS FIR data of M86 showed it to be comprised of two components, one coincident with the optical galaxy, and another $\approx 3.5'$ north-west of the galaxy center (White et al. 1991). The latter off-center $60\,\mu$m FIR emission appeared to be close to the extended X-ray emission while the weaker $100\,\mu$m FIR component was closely coincident with the center of the optical galaxy. The positional association of the off-center FIR and X-ray emission was interpreted as dust in the ISM removed from M86 by ram pressure stripping subsequently being heated and destroyed by sputtering, while the asymmetry in the optical isophotes might be caused by starlight scattered by the stripped dust (White et al. 1991).

Although M86 is a key object for the dynamical process of ram pressure dust stripping, the IRAS data lack sufficient depth and angular resolution to provide the crucial observational evidence for the connection between the extended X-ray and FIR emission. With its much higher sensitivity, higher angular resolution, and increased wavelength coverage FIR observations with the ISOPHOT detector aboard the Infrared Space Observatory (Kessler et al. 1996) give a much more detailed view of the dust distribution, allow a comparison of the FIR morphology with the structures seen at other wavelengths, and shed new light on the different scenarios proposed for the dynamical state of M86, particularly the ram pressure dust stripping. The following gives a summary of the ISOPHOT data on M86, while

Proceedings of the Symposium *"Exploiting the ISO Data Archive - Infrared Astronomy in the Internet Age"*, 24–27 June 2002, Sigüenza, Spain (C. Gry, S. B. Peschke, J. Matagne et al. eds., ESA SP-511)

a much more detailed description of the data and their interpretation can be found in Stickel et al. (2002).

2. OBSERVATIONS AND DATA REDUCTION

FIR observations of M86 were obtained in June and July 1996 with the FIR cameras of ISOPHOT (Lemke et al. 1996; Lemke & Klaas 1999) in P32 chopped mode. The four rectangular maps cover an area of $\approx 15' \times 10'$, two of which were obtained with the 3×3 pixel C100 camera at $60\,\mu$m and $90\,\mu$m wavelengths, while the other two were obtained with the 2×2 pixel C200 camera ($150\,\mu$m and $180\,\mu$m). Total integration times were 2300 s and 2000 s for the C100 $60\,\mu$m and $90\,\mu$m maps, respectively, and 3800 s for both C200 filters.

The derivation of the detector signals made use of the pairwise differences of consecutive ramp read-outs instead of the standard ramp slopes, where all read-outs belonging to a given raster and chopper position were considered as a single entity. As estimator for the signal, the robust outlier-insensitive myriad estimator (Kalluri & Arce 1998), applied to the corresponding pairwise distribution, was used. The signals were subsequently corrected for signal dependence on ramp integration times to be consistent with calibration observations (Laureijs et al. 2000), dark-current subtracted, and finally flux calibrated with PIA[1] Version 9.1 / Cal G Version 6.0 (Gabriel et al. 1997). For the conversion to an absolute flux level, the observations of the ISOPHOT Fine Calibration Source (FCS) obtained at the beginning and end of each scan in each filter were used.

Residual time-dependent pixel-to-pixel sensitivities (flat field) were corrected by robust smoothing of the data stream for each pixel, followed by a time-dependent scaling of each individual data stream to the common mean, and removing any residual time trend with robust low-order polynomial fits.

To utilize the high redundancy of the P32 chopped mode of ISOPHOT, individual full maps with a common pixel size and map centre were made for each detector pixel and chopper throw from the flat-fielded flux calibrated data streams using Drizzle within IRAF. This procedure gives 117 individual images for the shorter wavelengths bands ($60\,\mu$m and $90\,\mu$m) from the C100 detector, and 28 individual images from the longer wavelengths C200 bands ($150\,\mu$m and $180\,\mu$m) bands. These individual maps were subsequently stacked, and a final averaged map created from the stack using a min-max outlier rejection scheme. To get a less blocky appearance of the final stack-averaged maps, the individual maps were resampled to a twice finer grid before stacking, rejecting and averaging, with a pixel size of $15''$ for all four bands. This stack-averaging reduction scheme is quite similar to standard near-infrared data processing and is found to suppress quite effectively small scale detector variability, leading to significantly lower detection limits compared to the standard processing where all detector pixels are simultaneously drizzled onto a single map grid (Stickel et al. 2002).

[1] The ISOPHOT data presented in this paper were reduced using PIA, which is a joint development by the ESA Astrophysics Division and the ISOPHOT Consortium. The ISOPHOT Consortium is led by the Max-Planck-Institute für Astronomie, Heidelberg.

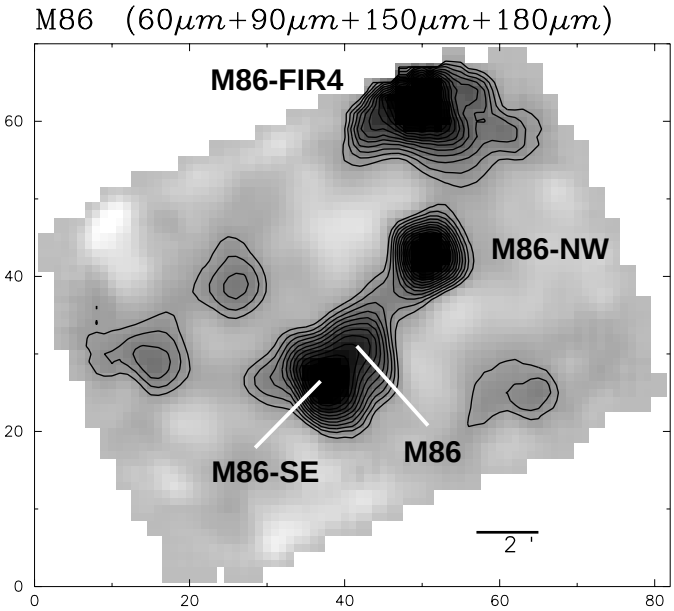

Figure 1. ISOPHOT FIR "white light" ($60 - 180\,\mu$m) image of the M86 field, the mean of the stack-averaged images of the four wavelengths. Final map pixel size is $15''$.

3. RESULTS

The individual maps for the four different wavelengths show a good agreement in the FIR morphology, with resolved as well as unresolved source present (Stickel et al. 2002). The deepest image, obtained by averaging the individual maps of the four wavelengths (Fig. 1), reveals a total of seven distinct sources in the field of M86, all of which are lying within the optical stellar halo of the M86 elliptical galaxy (Fig. 2). This is a quite unexpected complex FIR morphology for an elliptical galaxy, which is supposed to have only little dust.

Near the optical position of M86 lies a compact double source (M86 / M86-SE) separated by $\approx 1.5'$. The western component of this pair is positionally coincident with the M86 galaxy centre. A third, unresolved, FIR source (M86-NW), which was previously discovered by IRAS, lies $\approx 3.5'$ north-west from the central pair. A fourth source (M86-FIR4) lying $\approx 7.5'$ north-west close to the nearby edge-on spiral NGC 4402 is the brightest FIR source long-wards of $90\,\mu$m and consists of a compact central core surrounded by an extended halo. This source lies at the border of the mapped area and likely extends well beyond the covered sky region. Additionally, three faint FIR sources are detected in the field.

Photometry from the four individual maps allow the derivation of the FIR spectral energy distributions (SED) for M86 / M86-SE and M86-NW (Fig. 3). While the fluxes of the components of the central pair can be reconciled with a dust temperature $T_{\rm Dust} \approx 18\,$K, the SED of the offset source M86-NW already detected by IRAS indicates much warmer dust with of

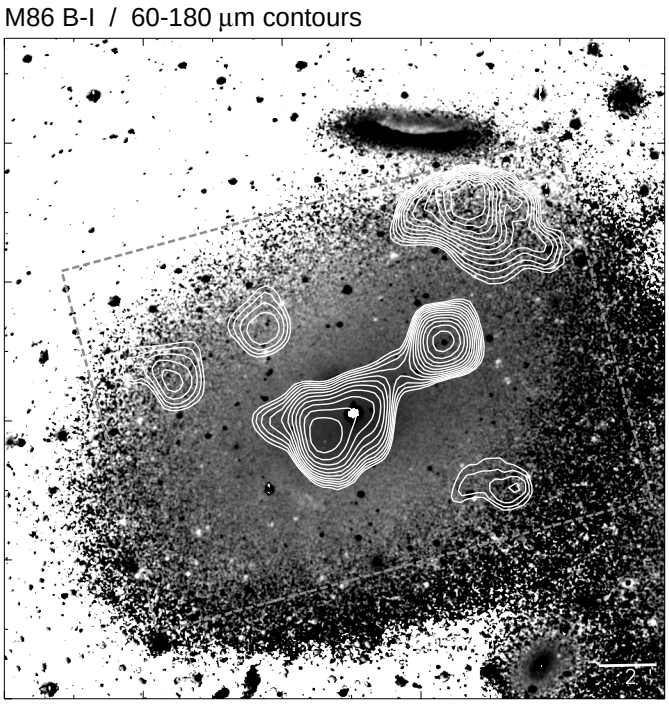

Figure 2. The ISOPHOT FIR "white light" ($60 - 180\ \mu$m) image of M86 (contours) overlaid on a gray-scale representation of the optical B-I color index image. The border of the FIR mapped region is indicated by the dashed rectangle.

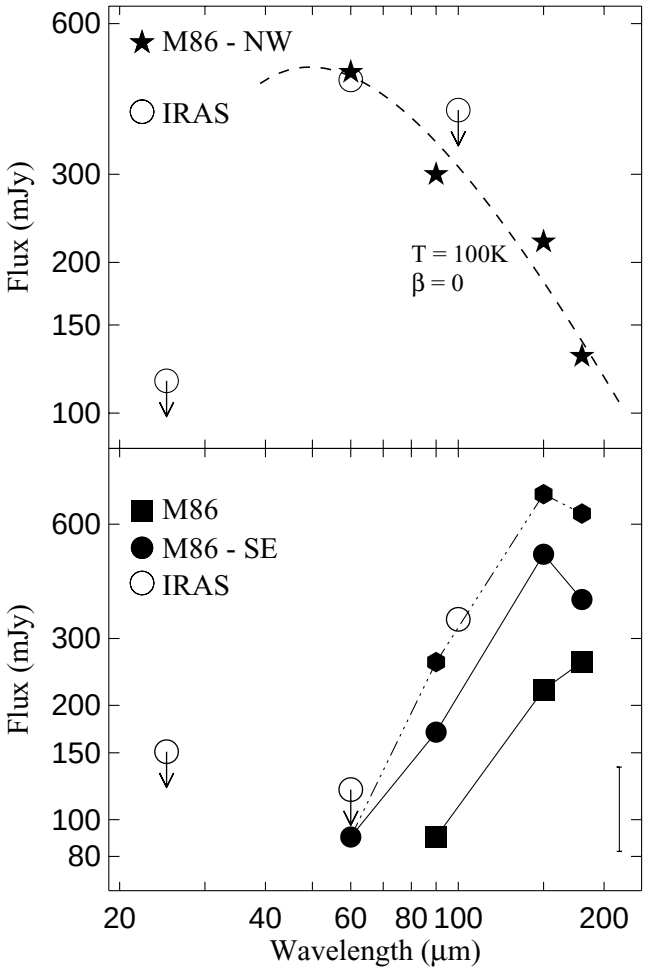

Figure 3. FIR spectra of M86-NW (top) and the compact double source M86 / M86-SE (bottom). Filled symbols indicate ISOPHOT fluxes, while IRAS fluxes are represented by open circles (upper limits with downward arrows). For M86-NW, the dashed curve shows the best fit blackbody spectrum with $\mathrm{T_{Dust}} = 100\ K$ and $\beta = 0$. The dot-dashed in the lower panel is the sum of the M86 and M86-SE SEDs. The dissimilarity of the SEDs is striking, as is the agreement of the ISOPHOT and IRAS fluxes

$\mathrm{T_{Dust}} \gtrsim 60$ K. Due to the incomplete coverage of M86-FIR4, only a crude photometry can be obtained, which gives a rapidly increasing brightness with increasing wavelength, again indicative of cold dust. This is consistent with its non-detection in $60\ \mu$m and $100\ \mu$m IRAS HIRES maps of the M86 field.

The western component (M86 in Fig.1) of the central pair of FIR sources is identified with the FIR dust emission of M86 itself. The eastern component (M86-SE in Fig.1) lies close to dust streamers already discovered in the optical, which in turn are likely due to interstellar matter tidally removed from the close companion galaxy VCC 882. The associated dust masses derived from the $180\,\mu$m fluxes are $\approx 5 \times 10^6\,\mathrm{M_\odot}$ and $\approx 7.5 \times 10^6\,\mathrm{M_\odot}$, respectively. Due to the continuously rising SED beyond the $100\,\mu$m IRAS wavelength limit, the combined dust mass for the central double source M86 / M86-SE ($\approx 1.25 \times 10^7\,\mathrm{M_\odot}$) is about a factor of 10 larger than that derived from the IRAS data alone (Forbes 1991).

The unresolved off-center source M86-NW is positionally coincident with a point-like optical object, and lies away from the extended X-ray emission (Fig. 4). This together with the rather high inferred dust temperature suggests that it is unrelated to M86 and actually a background object such as an ULIRG. Because of its much higher dust temperature, the dust mass of M86-NW would be extremely low ($\approx 3.5 \times 10^3\,\mathrm{M_\odot}$), if it were also located at the distance of M86. Only beyond redshifts of $\mathrm{z} \approx 0.07$ and $\mathrm{z} \approx 0.6$, typical dust masses of $\approx 10^6\,\mathrm{M_\odot}$ and $\approx 10^8\,\mathrm{M_\odot}$, respectively, would be reached. M86-FIR4 has a rather large dust mass of $\approx 1.5 \times 10^7\,M_\odot$, but neither the optical nor B-I color index images nor HI data show a candidate for optical counterpart. Only the distorted outer isophotes of M86 lie roughly at its position.

4. CONCLUSIONS

New ISOPHOT FIR imaging data of M86 revealed a complex morphology consisting of a total of seven resolved and unresolved sources. FIR emission is associated with the M86 galaxy centre and likely also with optically discovered dust streamers east of the centre. Both components have a cold FIR SED with $\mathrm{T_{Dust}} \approx 18$ K, similar to dust in non-active spiral galaxies (Stickel et al. 2000). The off-center source previously discov-

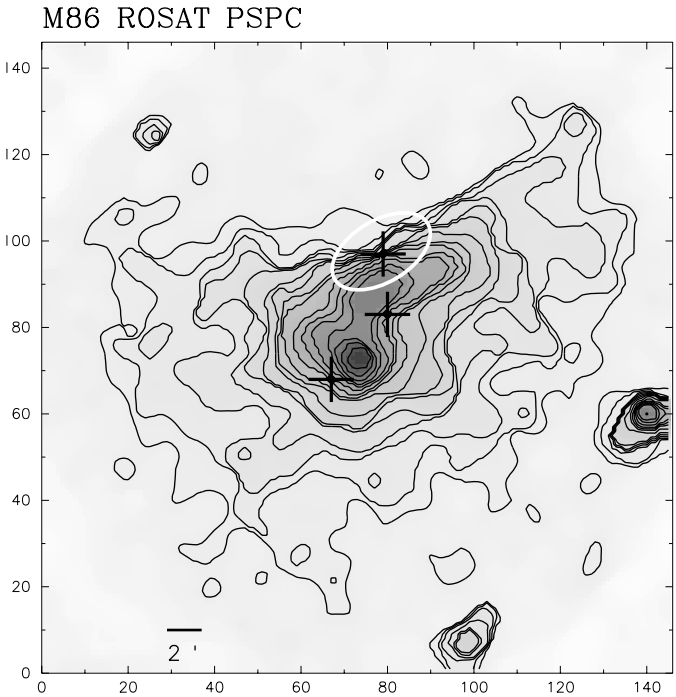

Figure 4. Adaptively filtered ROSAT PSPC (0.2 – 2 kev) image of the M86 field. The positions of the FIR sources M86-NW, M86-SE, and M86-FIR4 (see Fig. 1) are indicated by crosses. A rough outline of the extended halo of M86-FIR4 is indicated by the white ellipse. Image scale is $15'' \, pixel^{-1}$*, north is up and east to the left.*

ered by IRAS is unresolved, is associated with an point-like optical source, has a warm FIR SED with $\mathrm{T_{Dust}} \gtrsim 60\,\mathrm{K}$, and lies away from the asymmetric extended X-ray emission. It is likely a background source rather than dust ram pressure stripped from M86. The most interesting FIR source lies between M86 and the nearby spiral galaxies NGC 4402. At wavelength above $100\,\mu\mathrm{m}$ it is the brightest source in the field, showing a core-halo structure. It is not associated with an optical counterpart and is also undetected in HI. It is the first localized dust cloud lying in the intergalactic space between the two galaxies, possibly causing the strong absorption gradient seen in the X-Ray emission (Fig. 4). Because of the large dust mass, it is likely ISM from NGC 4402 tidally removed by M86, rather than dust originating in M86 itself. Overall, the FIR of M86 is not consistent with the ram pressure dust stripping picture, since none of the FIR sources is associated with the ram pressure stripped X-ray gas. A clear case for the on-going stripping of interstellar dust by intracluster gas has yet to be found.

ACKNOWLEDGEMENTS

The development and operation of ISOPHOT were supported by MPIA and funds from Deutsches Zentrum für Luft- und Raumfahrt (DLR, formerly DARA). The ISOPHOT Data Centre at MPIA is supported by Deutsches Zentrum für Luft- und Raumfahrt (DLR) with funds of Bundesministerium für Bildung und Forschung, grant. no. 50 QI0201.

REFERENCES

Bicay M.D., Giovanelli R., 1987, ApJ 321, 645
Binggeli B., 1999, in *The Radio Galaxy Messier 87*, eds. H.-J. Röser, K. Meisenheimer (Berlin: Springer), p. 9
Contursi A., Boselli A., Gavazzi G., et al., 2001, A&A 365, 11
Doyon R., Joseph R.D., 1989, MNRAS 239, 347
Elmegreen D.M., Elmegreen B.G., Chromey F.R., Fine M.S., 2000, ApJ 120, 733
Faber S.M., Wegner G., Burstein D., et al., 1989, ApJS 69, 763
Forbes D.A., 1991, MNRAS 249, 779
Forman W., Schwarz J., Jones C., Liller W., Fabian A.C., 1979, ApJ 234, L27
Forman W., Markevitch M., Jones C., et al., 2001, astro-ph/0110087
Gabriel C., Acosta-Pulido J., Heinrichsen I., et al., 1997, Astronomical Data Analysis Software and Systems VI, A.S.P. Conf. Ser., Vol. 125, eds. G. Hunt, H. E. Payne, p. 108
Kalluri S., Arce G.R., 1998, IEEE Transactions on Signal Processing 46, 322
Kessler M.F., Steinz J.A., Anderegg M.E., et al., 1996, A&A 315, L27
Laureijs R.J., Klaas U., Richards P.J., Schulz B., Ábrahám P., 2000, The ISO Handbook, Volume V: PHT - The Imaging Photo-Polarimeter, Version 1.1, SAI/99-069/dc
Lemke D., Abolins J., Abraham P., et al., 1996, A&A 315, L64
Lemke D., Klaas U., 1999, in *The Universe as seen by ISO*, eds. P. Cox, M.F. Kessler, ESA-SP 427, p. 55
Nulsen P.E.J., Carter D., 1987, MNRAS 225, 939
Rangarajan F.V.N., White D.A., Ebeling H., Fabian A.C., 1995, MNRAS 277, 1047
Stickel M., Lemke D., Klaas, U., et al., 2000, A&A 359, 865
Stickel M., Bregman J.N., Fabian A.C., White D.A., Elmegreen D.M., 2002, A&A, in press
White D.A., Fabian A.C., Forman W., Jones C., Stern C., 1991, ApJ 375, 35

FAR INFRARED EMISSION FROM ELLIPTICAL GALAXIES: NGC 4649, NGC 4472, AND NGC 4636

Pasquale Temi[1,2], William G. Mathews[3], Fabrizio Brighenti[3,4], and Jesse D. Bregman[1]

[1]Astrophysics Branch, Nasa/Ames Research Center, MS 245-6, Moffett Field, CA 94035
[2]SETI Institute, Mountain View, CA 94043
[3]University of California Observatories/Lick Observatory, Board of Studies in Astronomy and Astrophysics, University of California, Santa Cruz, CA 94064
[4]Dipartimento di Astronomia, Universita' di Bologna, via Ranzani 1, Bologna 40127, Italy

ABSTRACT

We present ISOPHOT P32 oversampled maps and P37/39 sparse maps, of three bright elliptical galaxies in the Virgo Cluster. The maps reach the limiting sensitivity of the ISOPHOT instrument at 60, 100, 170 and 200μm. Two elliptical galaxies show no emission at all far-IR ISOPHOT wavelengths at a level of few tens of mJy. The null detection provides a test of the evolution of dust in elliptical galaxies and its size distribution and composition. As previous studies have shown, in many elliptical galaxies both IRAS and ISO have detected mid-IR excess 6-15 micron emission relative to the stellar continuum indicating emission from circumstellar dust. Under the assumption that these dusty outflows from evolving red giant stars and planetary nebulae are continuously supplying dust to the interstellar medium, we have computed the infrared luminosity at the ISOPHOT bands appropriate for NGC4472. The null far-IR ISOPHOT observations exceed the far-IR flux expected from dust expelled from a normal old stellar population.

Key words: ISO – Infrared: galaxies – Galaxies: Elliptical – Infrared: ISM – ISM: dust

1. INTRODUCTION

In recent years the traditional view of elliptical galaxies as simple systems of non-interacting stars, devoid of interstellar matter, has radically changed. Observations across the electromagnetic spectrum have demonstrated that the interstellar medium (ISM) in elliptical galaxies contains substantial amounts of cold gas and dust in addition to hot gas, the dominant component. Far-IR emission detected by the IRAS satellite and improved optical imaging of elliptical galaxies provide clear evidence for the presence of dust. However, estimates of the total amount of dust, as well as its origin and spatial distribution, remain uncertain and controversial. Optical observations indicate dust masses that are one order of magnitude less than those inferred by IRAS. We have recently embarked on a program to study the infrared emission from early-type galaxies using the large database of observations taken by the ISO satellite. Our principal goals are to observe the spatial location and emission spectrum of dust throughout elliptical galaxies, and with this information, to determine the origin, evolution, and physical properties of dust in massive elliptical galaxies.

2. OBSERVATIONS AND DATA REDUCTION

ISO provides a vast amount of data with good spatial resolution in the mid and far-IR for a large number of elliptical galaxies. A good fraction of these observations have been taken using ISOPHOT in several observing modes (Astronomical Observing Template), including the oversampled maps P32, the P37/38/39 sparse maps and P22 multi-filter photometry data. Here we present data from three very bright ellipticals located in Virgo Cluster: NGC4649, NGC4472, and NGC4636.

NGC4636 has been observed in the P37/39 AOT mode at 60, 100, and 180 μm. Observations were made in each filter with one on-source single point staring mode and one off-source exposure. The background position was located $\sim 10'$ north-east from the target, on blank sky position. Data reduction and calibration were performed with the PIA 9.1 package (Gabriel et al. 1997). The reduction included correction for the non-linear response of the detectors, readout deglitching, and linear fitting of the signal ramps. After resetting of all ramp slopes and subtracting the dark current, the flux densities were extracted using the power calibration of the reference lamps. After sky subtraction the on-source signal was corrected for the fraction of the point-spread function included within the detector's field of view. A color correction was applied assuming that the SED of the galaxy could be approximated by a blackbody curve with temperature of 30 K. We tested the C100 detector response on a number of galaxies observed in the same observing mode as NGC4636. Integrated fluxes from 8 ellipticals were compared to the IRAS values at 60 and 100 μm. Calibrated survey scans from the IRAS satellite were extracted using the SCANPI software from IPAC. A very good linear correlation between the ISO and IRAS fluxes is seen at both wavelengths.

NGC4649 and NGC4472 have been observed in P32 mode in three broadband filters at 60, 90 and 180 μm using the C100 and C200 detectors. The maps were obtained by scanning the spacecraft Y and Z axes in a grid of 4×4 (NGC4649) and 5×4 points (NGC4472). The focal plane chopper was stepped at intervals of one-third of the detector pixel, at each raster position, providing a sky sampling in the Y direction of 15" and 30" for the C100 and C200 detectors. To reduce the P32 data we used a dedicated software package developed at MPI Kernphysik in Heidelberg and supported by the VILSPA ISO Data Center (Tuffs & Gabriel 2002). The new routines allow a proper correction for transients in PHT32 measurements. Both NGC4472 and NGC4649 show no detectable emission at 60, 90, and 180 μm. The maps reach the limiting sensitivity of the ISOPHOT

Proceedings of the Symposium *"Exploiting the ISO Data Archive - Infrared Astronomy in the Internet Age"*, 24–27 June 2002, Sigüenza, Spain (C. Gry, S. B. Peschke, J. Matagne et al. eds., ESA SP-511)

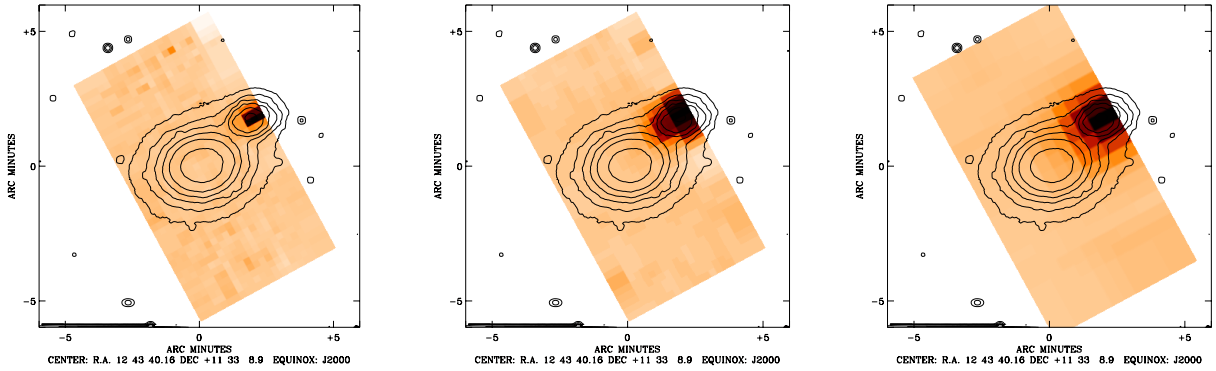

Figure 1. NGC4649 P32 maps at 60, 90, and 180 μm respectively with optical contours superimposed. The galaxy is undetected at all wavelengths observed with ISOPHOT. The bright source at the edge of map is its spiral companion NGC4647 and it is prominent at all three wavelengths. The angular resolution of the oversampled map nicely resolves NGC4647 and shows that there is no contribution from NGC4649 in this aperture centered on the elliptical. At 180 μm the signal from the spiral galaxy extends almost to the location of NGC4649 nucleus, but an analysis of the light profile shows that the emission is clearly coming from the extended far-IR image of NGC4647.

instrument at a level of few tens of mJy and the 3σ upper limits are presented in Tab. 1. Fig. 1 shows the 60, 90, and 180μm maps for NGC4649. The bright spiral companion NGC4647, recorded at the edge of the maps, is well detected at all three wavelengths and is responsible for the high flux detection, erroneously attributed to NGC4649, reported in literature from IRAS observations. In fact the angular resolution and beam size of the IRAS instruments were not able to disentangle the contribution of the two galaxies. Fig. 2 show the 90 μm oversampled map for NGC4472.

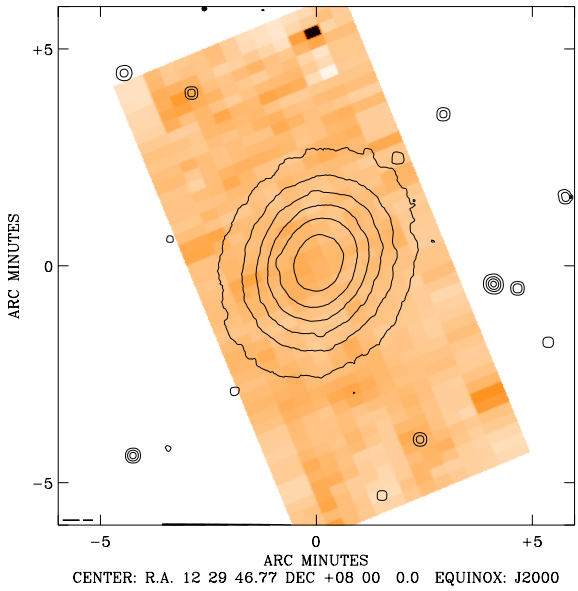

Figure 2. Optical image (contours) superimposed to ISOPHOT 90μm map for NGC4472 . Similar maps at 60 and 180μm show no detectable emission from the bright elliptical.

Table 1. ISOPHOT flux densities.

	Flux (mJy)		
	NGC4649	NGC4472	NGC4636
$F_{60\mu m}$	$< 137^c$	$< 147^c$	187± 57
$F_{90\mu m}$	$< 85^c$	$< 99^c$	491± 64
$F_{180\mu m}$	$< 110^c$	$< 87^c$	790± 71

[c] No detection, 3 σ upper limit flux

3. A MODEL FOR NGC4472

Mid-IR (6 - 15μm) ISO observations of NGC4472 detect strong dust emission that can be understood as emission from circumstellar dust from mass-losing AGB stars at or near the globally expected rate for this galaxy (Athey et al. 2002). Since this dust should emit in the far-IR when it becomes interstellar, it may be significant that NGC4472 is not detected at $\lambda \geq 25\mu$m either by ISO or IRAS (Knapp et al. 1989). We now briefly describe an estimate of the far infrared emission from NGC4472, assuming that the grains are dispersed in the hot interstellar gas before sputtering commences. First we calculate the temperature $T_d(r, a)$ of dust grains of radius a (in μm) at galactic radius r and then determine the grain emissivity and luminosity for a distribution of initial grain sizes. Since the 9.7μm silicate feature is seen in emission in NGC4472, we assume that all grains

have properties similar to astronomical silicates (Laor & Draine 1993).
The grain temperature is determined by both absorption of starlight and by electron-grain collisions:

$$\int_0^\infty 4\pi J_*(r,\lambda)Q_{abs}(a,\lambda)\pi a^2 d\lambda + 4\pi a^2(1/4)n_e\langle v_e E_e\rangle\tau(a) = 4\pi a^2\sigma_{SB}T_d(r,a)^4\langle Q_{abs}\rangle(T_d,a) \quad (1)$$

although we consider each type of heating separately. The mean intensity of starlight at wavelength λ (in μm) is related to the B-band intensity $J_*(r,\lambda) = J_{\lambda B}(r)\phi(\lambda)$ and the SED $\phi(\lambda)$ taken from Tsai & Mathews (1995). $J_{\lambda B}(r)$ is found by integrating over a de Vaucouleurs stellar profile with a "nuker" core of slope $\rho_* \propto r^{-0.95}$ within $0.031R_e$ (Faber et al. 1997). At a distance $d = 17$ Mpc NGC4472 has an effective radius $R_e = 8.57$ kpc and total stellar mass $M_{*,t} = 7.26\times10^{11}\ M_\odot$ assuming $M_{*,t}/L_B = 9.2$ (van der Marel 1991). The second term on the left represents heating by e^--grain collisions including a correction $\tau(a)$ for small grains which do not completely stop the electrons (Dwek 1986). For astronomical silicate grains of radius less than $\sim 1\mu$m we can use the approximations $Q_{abs} \approx a\psi(\lambda)$ and $\langle Q_{abs}\rangle \approx 1.35\times10^{-5}T_d^2 a$. For starlight heating the grain temperature $T_d(r) = 44J_{\lambda B}^{1/6}$ K is independent of a and varies from 26 K at 1 kpc to 16 K at 10 kpc. For e^--grain heating the grain temperature $T_d = 0.662(n_e T^{3/2}\tau/a)^{1/6}$ K varies as $a^{-1/6}$ for $a > 0.04\mu$m where $\tau \approx 1$ but is independent of grain radius for $a < 0.04\mu$m where $\tau \approx 33a$. Fig. 3 shows the calculated dust temperature profile for the starlight heating and the e^--grain heating. For NGC 4472 the collisional heating dominates over the radiative heating for grain sizes $a \lesssim 0.3$ μm.
If grains are expelled from the stars with an initial MRN size distribution

$$S(a,r) = S_o(r)a^{-s}$$

where $s = 3.5$ and a is in μm (Mathis et al. 1977), then the steady state grain size distribution in the hot gas is

$$N(r,a) = \left|\frac{da}{dt}\right|^{-1}\frac{S_o(r)}{(s-1)}a^{1-s} \quad a \le a_{max}. \quad (2)$$

The coefficient

$$S_o(r) = \frac{3\delta\alpha_*\rho_*}{4\pi\rho_g 10^{-12}}\frac{(4-s)}{a_{max}^{4-s}} \quad (3)$$

depends on the rate that the old stellar population ejects mass, $\alpha_* = 4.7\times10^{-20}$ s^{-1}, the initial dust to gas mass ratio scaled to the stellar metal abundance in NGC4472, $\delta = (1/150)z_m(r)$ and the density of silicate grains, $\rho_g = 3.3$ gm cm^{-3}. The grain sputtering rate

$$\frac{da}{dt} = -fn_p 3.2\times10^{-18}\left[\left(\frac{2\times10^6\ \mathrm{K}}{T}\right)^{2.5}+1\right]^{-1}\ \mu\mathrm{m\,s^{-1}} \quad (4)$$

is a fit to the rate of Draine & Salpeter (1979) with an additional correction $f = f(a,T) \ge 1$ to account for the enhanced (isotropic) sputtering from small grains (Jurac et al. 1998). The hot gas temperature T and proton density n_p for NGC4472 are taken from Brighenti & Mathews (1997).

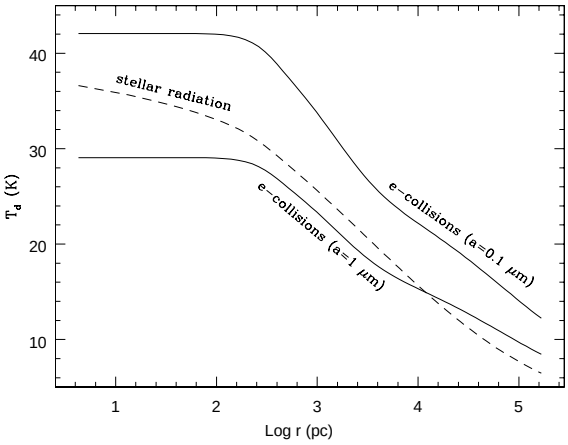

Figure 3. Temperature of dust grains due to starlight heating only (dashed lines), and due to electron-grain collisions only (heavy solid line for grain size $a = 1$ μm; thin solid line for grain size $a = 0.1$ μm). For grains with size $a \lesssim 0.3$ μm the collisional heating is larger than the radiative one.

The infrared emissivity from grains at galactic radius r is

$$j(r,\lambda) = \frac{1}{4\pi}\int_0^{a_{max}} daN(r,a)4\pi a^2 10^{-8}Q_{abs}(a,\lambda) \times\pi B(r,a,\lambda) \quad (5)$$

where $B(T_d(r),a,\lambda)$ is the Planck function.
The total galactic luminosity at wavelength λ is

$$L_\lambda = \int 4\pi j(r,\lambda)(4/3)\pi d(r^3) \quad (6)$$

and the observed flux at λ_μ is

$$F_\nu = 10^{22}\frac{L_\lambda}{4\pi d^2}\frac{\lambda_{\mu\mathrm{m}}^2}{c}\ \ \mathrm{mJy}. \quad (7)$$

Fig. 4 compares the computed far-IR spectra for the cases of stellar radiation heating and collisional heating with the three ISO flux upper limits. The total IR emission (not shown in the figure) is the sum of the contribution of the two heating sources for each value of a_{max}. Grains with an initial MRN distribution having $a_{max} < 1\mu$m are consistent with the null observations of NGC4472 in the far-IR. Grains with radii less than about 0.003μm experience stochastic temperature excursions, but this complication should not greatly change our estimated flux in Fig. 4.

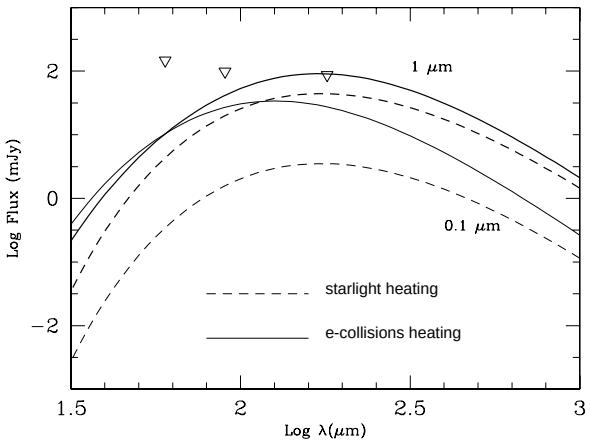

Figure 4. Computed Far-IR flux in mJy from NGC4472 calculated for $a_{max} = 1\mu m$ (heavy lines) and $a_{max} = 0.1\mu m$ (light lines). Solid lines show the grain emission based only on electron-grain heating and dashed lines show the emission from grains that are heated only by stellar radiation. The three ISO upper limits are shown with open triangles.

4. RESULTS

We have assumed that the circumstellar dust observed in the mid-IR from NGC4472 (Athey et al. 2002) ultimately becomes interstellar and is exposed to the mean galactic starlight and to bombardment by thermal electrons in the hot ~ 1 keV gas. Grains receive somewhat more energy from electrons than from stellar photons. The calculated far-IR spectrum peaks at $\lambda \sim 180$ μm, a spectral region not accessible to IRAS, but well covered by ISO. However, the computed fluxes are below the observed upper limits if $a \lesssim 0.5$ μm. Thus the ISO upper limits do not strongly constrain the properties of dust in NGC4472. We are currently developing a model for the far-IR emission for NGC4636 (Temi et al. 2002). This galaxy shows higher far-IR fluxes (Tab. 1) and should allow us to put strong constraints on the origin and the evolution of the interstellar dust.

We thank NASA and NSF for grants that funded this research.

REFERENCES

Athey, A., Bregman, J. N., Bregman, J. D., Temi, P. & Sauvage, M. 2002, ApJ 571, 272

Brighenti, F. & Mathews, W. G. 1997, ApJ, 486, L83

Draine, B. T. & Salpeter, E. E. 1979, ApJ 231, 77

Dwek, E. 1986, ApJ 302, 363

Faber, S. M., Tremaine, S., Ajhar, E. A., Byun, Yong-Lk, Dressler, A., Gebhardt, K., Grillmar, C., Kormendy, J., Lauer, T. R., Richstone, D. 1997, AJ, 114, 1771

Gabriel, C., Acosta-Pulido, J., Heinrichsen, I., Morriss, H., & Tai, W-M., Astronomical Data Analysis Software and Systems VI, A.S.P. Conference Series, Vol. 125, 1997, Gareth Hunt & H. E. Payne, eds., p. 108.

Jurac, S., Johnson, R. E., and Donn, B. 1998, ApJ, 503, 247

Knapp, G. R., Guhathakurta, P., Kim, D-W., Jura, M. A. 1989, ApJS 70,329

Laor, A. & Draine, B. T. 1993, ApJ, 402, 441

Mathis, J. S., Rumpl, W., Nordsieck, K. H. 1977, ApJ, 217, 425

Temi, P., Mathews, W. G., Brighenti, F. and Bregman, J. D. 2002, in preparation

Tsai, J. C. & Mathews, W. G. 1995, ApJ, 448, 84

Tuffs, R. J., & Gabriel, C., 2002, ESA-SP 482, In Press.

van der Marel, R. P., 1991, MNRAS, 253, 710

INFRARED COLOURS OF STAR-FORMING GALAXIES AND A FLUX CALIBRATION OF ISOCAM ELAIS CATALOGUES

Petri Väisänen[1] **and Thierry Morel**[2]

[1]European Southern Observatory, Alonso de Cordova 3107, Vitacura, Casilla 19001, Santiago 19, Chile
[2]Osservatorio Astronomico di Palermo, Piazza del Parlamento 1, 90134 Palermo, Italy

ABSTRACT

We present J and K-band near-infrared photometry of a sample of ISOCAM sources detected by the European Large Area *ISO*-Survey (ELAIS). All of the high-reliability LW2 (6.7μm) sources and 80 per cent of the LW3 (15μm) sources are identified in the near-IR survey reaching $K \approx 17.5$ mag.

The near- to mid-IR flux ratios can effectively be used to separate stars from galaxies in mid-IR surveys: at 6.7μm, 80 per cent of the identified ELAIS objects are stars while at 15μm 80 per cent are galaxies. The stars are then used to perform an accurate new calibration of the ELAIS ISOCAM data at both 6.7 and 15 μm: we adopt values of 1.23 and 1.05 ADU/gain/s/mJy for the LW2 and LW3 filters, respectively.

The ISOCAM ELAIS survey is found to mostly detect strongly star-forming late-type galaxies. We show that near to mid-IR colour-colour diagrams can be used to further classify galaxies, as well as study star-formation. In a $[15/2.2]$ vs. $[6.7/2.2]$ plot the Hubble type of a galaxy can be roughly estimated from its position along the diagonal ($[6.7/15] = 1$) and the star-forming efficiency from a galaxy's departure from the diagonal (eg. $[6.7/15] < 1$).

The ELAIS galaxies yield an average mid-IR flux ratio LW2/LW3 $= 0.67 \pm 0.27$. We discuss this $[6.7/15]$ ratio as a star formation tracer using *ISO* and *IRAS* data of a local comparison sample. The $[2.2/15]$ ratio is also found to be a good indicator of activity level in galaxies and conclude that the drop in the $[6.7/15]$ ratio seen in strongly star-forming galaxies is a result of both an increase of 15μm emission and an apparent depletion of 6.7μm emission.

Key words: ISO – infrared: galaxies – surveys – infrared: stars

1. INTRODUCTION

To understand the history of luminous matter in the Universe it is necessary to study the infrared properties of galaxies. It is also important to tie together the physical processes seen at work in the ISM and stars of the nearby galaxies with the integrated properties of high-redshift galaxies. The European Large Area *ISO* Survey (ELAIS) stands as an important bridge between local and deep *ISO*-surveys.

The mid-infrared truly opened up for study only with the *ISO*-mission (see reviews by Genzel & Cesarsky 2000, Helou 1999). Many studies (eg. Mattila et al. 1999, Helou et al. 2000) have confirmed the complex nature of spectral energy distributions of disk galaxies in the $3 - 20\mu$m range. In addition to a continuum due to hot or warm dust there are bright IR-bands in the MIR, often called the Unidentified Infrared Bands (UIBs) and proposed to be the signature of Polycyclic Aromatic Hydrocarbons (PAHs).

The PAHs are an essential component in forming the mid-infrared $[6.7/15]$ colour ratio which is emerging as a tracer of star forming activity in galaxies (Vigroux et al. 1996, 1999, Sauvage et al. 1996, Dale et al. 2000, Roussel et al. 2001a). The value $[6.7/15] \approx 1$ is expected in quiescent medium and PDRs, while HII regions have $[6.7/15] < 0.5$ (eg. Cesarsky et al. 1996). The $[6.7/15]$ ratio thus remains close to unity for quiescent and mildly star forming galaxies, while it starts to drop for those with more vigorous star formation activity.

A subset of the ISOCAM ELAIS survey with near-IR follow-up observations is presented here (see also Väisänen et al. 2002).

2. OBSERVATIONS AND DATA

The mid-IR ELAIS *ISO*-observations were made with the ISOCAM LW2 and LW3 filters; For a description of the observations, data reduction, and source extraction see Oliver et al. (2000) and Serjeant et al. (2000). The latest version of the source catalogue, the v.1.3 preliminary analysis was used – however, we considered only those detections with near-IR matches.

The J and K-band observations were carried out using the STELIRCam instrument at the 1.2-m telescope of the F. L. Whipple Observatory on Mount Hopkins (see Väisänen et al. (2000). The survey area is approximately 1 square degree, in two separate regions centered at

RA=16h 09m 00s, DEC=$54^\circ 40' 00''$ (N1) and
RA=16h 36m 00s, DEC=$41^\circ 06' 00''$ (N2).

3. ELAIS FLUX CALIBRATION

Most stars could be easily separated by their morphology. However, also the near to mid-IR colour can be used very effectively. Flux ratios of $[2.2/15] > 10$ and $[2.2/6.7] > 2$ were found to define stars (though if using only the latter limit some elliptical galaxies overlap with the stars).

The stars were used for a new and accurate flux calibration of the ELAIS *ISO*-data. The ELAIS catalogue v.1.3 merely uses a one-to-one conversion of ADUs/gain/s to mJy fluxes. B

Proceedings of the Symposium *"Exploiting the ISO Data Archive - Infrared Astronomy in the Internet Age"*, 24–27 June 2002, Sigüenza, Spain (C. Gry, S. B. Peschke, J. Matagne et al. eds., ESA SP-511)

and V-band bolometric magnitudes (Hipparcos, SIMBAD) of stars seen in the ELAIS fields had been used in previous attempts to calibrate the ELAIS fluxes. With good quality near-IR data we potentially have a better chance of deriving the calibration factor because the uncertainty of extrapolating optical magnitudes into mid-IR is greatly reduced.

From our own sample of stars we used only those with the highest mid-IR reliabilitity flag, and in addition we excluded stars with $K < 8$ mag because of saturation in the NIR images. The stars were compared to observationally based stellar spectra used for the extensive ISOCAM and ISOPHOT calibration programs[1]. We calculated near- and mid-IR colours of stars with a range of spectral types from these spectra, which are estimated to be accurate within 5 per cent. The mid-IR fluxes were colour-corrected according to *ISO*-convention.

Fig. 1a shows the stars detected at 6.7μm plotted as $[2.2/6.7]$ vs. $J-K$, with the model stars overplotted as solid symbols. Ignoring the negligible colour-term, from the average difference of $[2.2/6.7]$ ratios of observations and models, we derive a correction factor of 1.22 to the 6.7μm fluxes of the v.1.3 ELAIS catalogue.

Fig. 1b shows the equivalent plot for the 15μm stars – there are much less stars here, but the overall calibration of the v.1.3 ELAIS catalogue appears quite accurate. We derive a 1.05 ADU/gain/s/mJy calibration for the LW3 data. The J-band data can be used as well: panels c and d show the equivalent colour-colour plots with J-band flux. The calibration factors are confirmed, as we find 1.24 and 1.06 ADU/gain/s/mJy for the LW2 and LW3 filters, respectively. We thus adopt values of 1.23 and 1.05 ADU/gain/s/mJy for the LW2 and LW3 filters.

Fig. 2 shows the *predicted* 6.7 and 15μm stellar fluxes (derived from the observed K-magnitude and model colours) against the observed and re-calibrated ELAIS 6.7 and 15μm fluxes. The scatter is seen to be very small, and the relation highly linear over two orders of magnitude. The conversion factors are in good agreement also with the ISOCAM handbook values of 2.32 and 1.96 ADU/gain/s/mJy (Blommaert 1998), where an additional factor of 2 correction for signal stabilization has been included. This lends strong support for the accuracy of the reduction and photometric techniques used in the creation of the ELAIS Preliminary catalogue.

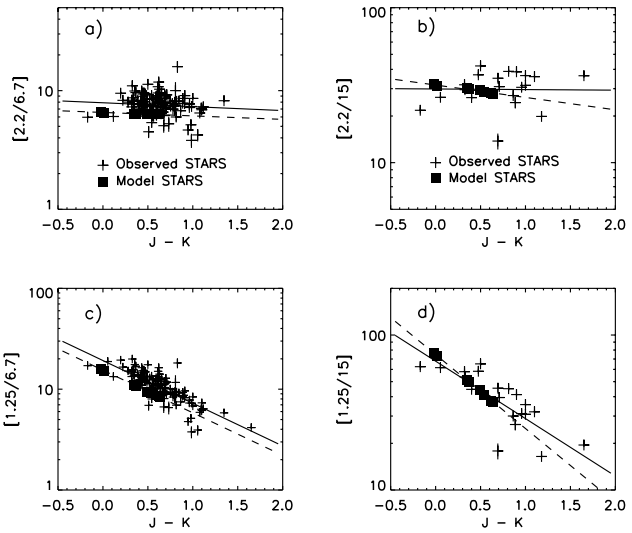

Figure 1. Stars in NIR/MIR vs. $J-K$ diagram. The 6.7 and 15 μm fluxes of the ELAIS v.1.3 catalogue stars (crosses) are in ADUs. The model colours (filled squares, in mJy) have been calculated from stellar spectra templates used in the ISOCAM calibration program. The solid and dashed lines are fits to the observed data and model points, respectively. Constant correction factors for the ADU to mJy conversion are derived from these fits.

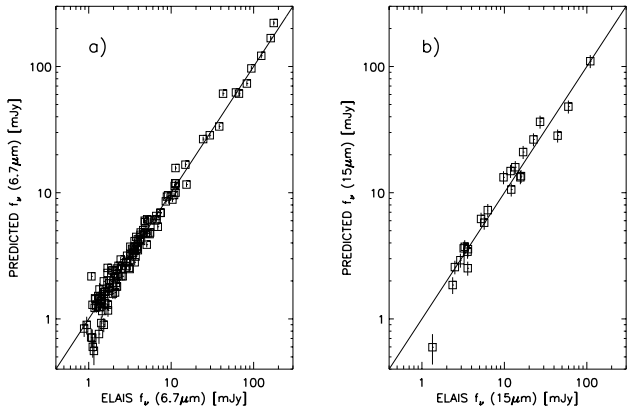

Figure 2. Predicted stellar fluxes vs. the observed ELAIS fluxes.

4. RESULTS

4.1. IDENTIFICATIONS

Table 1 presents the summary of detected and identified ISOCAM sources in our fields. Completeness limits (estimated from expected MIR fluxes of NIR stars) are 1.5 mJy and 2 mJy for the LW2 and LW3 bands, while sources down to 0.7 and 1.0 mJy, respectively, are detected. All of the high-reliability LW2 sources and 84 per cent of the high-reliability LW3 sources are identified in the NIR. The detection efficiencies for identified R=3 sources are lower, and the overall ISOCAM v.1.3 catalogue NIR percentages become 97 and 55 per cent at LW2 and LW3, respectively. 53 sources are common to both ISOCAM filters, and 29 of these turn out to be galaxies.

It is interesting to note the overall proportions of stars and galaxies: in the near- and mid-IR matched catalogue 81 per cent of the 6.7μm sources are stars. At 15μm only 21 per cent of the objects are stars.

4.2. INFRARED COLOURS OF GALAXIES

In general, the emission from galaxies in near-IR bands is due to the stellar contribution, the 6.7μm carries information on the PAH contribution, and any strong 15μm emission would indi-

[1] see http://www.iso.vilspa.esa.es/users/expl_lib/ISO/wwwcal/cam.html/

Table 1. ISOCAM sources in the 1 sq.deg. near-IR survey area within the ELAIS N1 and N2 fields, per band and reliability parameter; R=2 stands for a 'secure' detection and R=3 for a 'probable' detection. Column (Det.) refers to the total number of ISO sources and (Ident.) to the number of NIR identifications.

		Det.	Ident.	Stars	Gals.
N1					
LW3	R=2	47	37	7	30
	R=3	59	12	1	11
N2					
LW2	R=2	170	170	141	29
	R=3	53	47	34	13
LW3	R=2	68	60	19	41
	R=3	115	49	6	43
LW2&3	R=2&3	53	53	24	29
TOTALS					
LW2		223	217	175	42
LW3		289	158	33	125

cate warm dust. Several colour indices may thus be useful in studying the relative strengths of these components and processes in galaxies.

Fig. 3 shows the 6.7 and 15μm fluxes of those galaxies in our sample which are detected in both MIR bands, normalized with the K-band flux, ie. by the stellar contribution to the brightness of the galaxy. Since the K-band is well correlated with the mass of the galaxy, this normalization also corrects for mass-luminosity dependence to first order. GRASIL models (Silva et al. 1998) for different Hubble types are overplotted, with redshift dependence from z=0 (large symbol) to z=1 (open end of curve). The strengths of the mid-IR fluxes are seen to correlate strongly, and the difference in the relative strength of mid-IR flux ranges nearly two orders of magnitude.

The colour-colour plot is divided into four different regions using template colours of local *ISO*-galaxies and models. Using a comparison sample of *ISO*-galaxies from the literature (Boselli et al. 1998, Dale et al. 2000, Roussel et al. 2001a) we verified that the types of galaxies become systematically later upward along the diagonal – however the NIR/MIR is not a good indicator of Hubble type if the galaxy has $[6.7/15]$-ratios much less than unity (i.e. strong star formation, see below). Most of our sources group in the low-redshift, $z = 0.1 - 0.4$, late type galaxy region.

The two mid-IR filters detect surprisingly different populations. Only one third of LW3 galaxies are detected in LW2 and two thirds of LW2 galaxies are detected in LW3. Using arguments from detection limits and expected colours of sources, it is clear that faint late type spirals and starbursts make up the majority of LW2-missed sources. Most of the galaxies missed by the LW3-band are early types with high a $[2.2/6.7]$-ratio.

4.3. MIR and NIR as Star Formation Tracers

The use of MIR fluxes and the $[6.7/15]$ ratio as star formation tracers has been recognized over the past few years. In Fig. 3, a

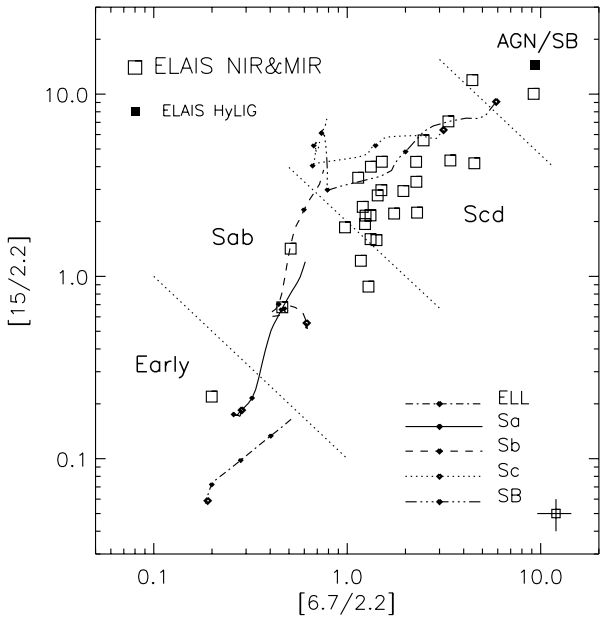

Figure 3. The 6.7 and 15 μm fluxes of our ELAIS galaxies normalized with the K-band flux. Curves show models adopted from the GRASIL library and the dotted lines roughly separate areas for different types of galaxies. A hyper-luminous IR-galaxy detected in another ELAIS region (Morel et al. 2001) is also shown (solid symbol).

departure upward from the one-to-one $[6.7/15] = 1$ diagonal is a measure of star forming activity, i.e. galaxies with $[6.7/15] < 1$ are most active. The ELAIS galaxies yield an average mid-IR flux ratio $[6.7/15] = 0.67 \pm 0.27$.

Roussel et al. (2001b) found a good correlation between MIR emission and $H\alpha$, and thus star formation rate (SFR). Adopting relations therein, and assuming a typical redshift of $z = 0.2$ for the late-type galaxies in our sample, we estimate average SFRs of $\sim 15 - 30 M_{\odot}/yr$ for these galaxies.

Using the same comparison sample mentioned in Section 4.2 and the well known IRAS $[60/100]$ tracer, we checked how the MIR and NIR/MIR flux ratios might trace star formation and activity level of galaxies.

Galaxies from literature are plotted in Fig. 4. First of all, the $[2.2/15]$ value (anti)correlates closely with $[60/100]$. The $[2.2/15]$ colour thus also indicates the activity level of galaxies.

Also, one can see that the $[6.7/15]$ stays constant at low $[60/100]$ but drops at higher heating levels (i.e. high $[60/100]$). This has been noted before (eg. Dale et al. 2000) and has been understood as the rising emission from the very small grains entering the 15μm band. However, since the $[2.2/15]$ does not have a corresponding break in its slope, this can not be the only explanation. Since there is a break in the $[2.2/6.7]$ slope, a flattening beyond $[60/100] \sim 0.4$, the destruction of the PAH emission carriers in this MIR regime is indicated. The ISO-IRAS diagram, i.e. the $[6.7/15]$ vs. $[60/100]$, must then be explained by both the increasing 15μm emission and relatively decreasing 6.7μm emission.

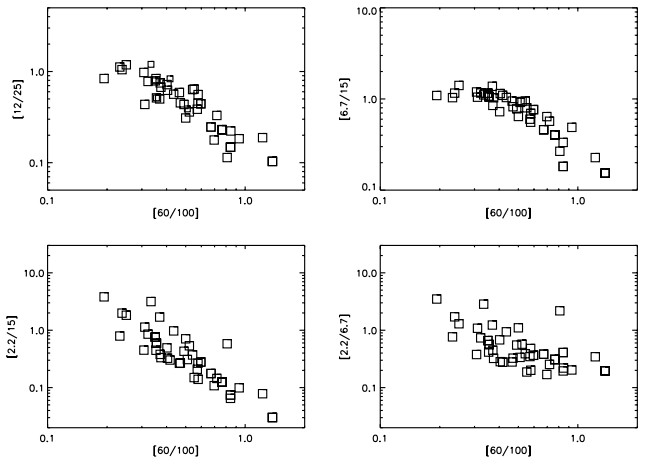

Figure 4. Comparing the IRAS $[60/100]$ colour and star-formation tracer to near- and mid-IR colours. E/S0 galaxies are excluded from this plot.

5. SUMMARY

We have presented photometry of a subsample of the ISOCAM ELAIS survey from the N1 and N2 fields. The near- and mid-IR stars detected in the field were used to perform an accurate new calibration of the ELAIS ISOCAM data at both 6.7 and 15 μm.

Excluding the stars, the mid-IR survey as a whole mainly detects late type spiral galaxies and starbursts. The faintest population of these is missed by the LW2 filter. The few objects missed by the longer mid-IR filter are most probably early type galaxies. Simple arguments indicate that typical redshifts of the sample seen with both mid-IR bands are $z \approx 0.2$.

NIR/MIR colour-colour plots are useful in studying the relative emission strengths of stellar, PAH, and warm dust components in galaxies. In a $[15/2.2]$ vs. $[6.7/2.2]$ plot the Hubble type of a galaxy can be roughly estimated from its position along the diagonal.

Star formation activity can also be estimated. In this same $[15/2.2]$ vs. $[6.7/2.2]$ plot the quiescent galaxies fall on the diagonal where $[6.7/15] \approx 1$. Increasing star formation activity raises the galaxies above the one-to-one curve, i.e. $[6.7/15] < 1$. Comparing with the IRAS $[60/100]$ colour, we have shown that the $[6.7/15]$ drops at high heating levels, and that this is a result of both increasing 15 μm emission and the destruction of the carriers of PAH emission seen in the ISOCAM 6.7 μm band.

ACKNOWLEDGEMENTS

We gratefully acknowledge the work done by the whole ELAIS collaboration – we particularly made use of the data sets made available by colleagues at Imperial College.

REFERENCES

Blommaert, J., 1998, 'ISOCAM Photometry Report V2.1.1', http://www.iso.vilspa.esa.es/users/expl_lib/CAM/photom_rep_fn.ps.gz
Boselli, A., et al., 1998, A&A, 335, 53
Cesarsky, D, et al., 1996, A&A, 315, L309
Dale, D.A., et al., 2000, AJ, 120, 583
Genzel, R., Cesarsky, C.J., 2000, ARAA, 38, 761
Helou, G., 1999, in Cox, P., Kessler, M.F., eds., ESA SP-47, The Universe As Seen by ISO, ESA Publ.Div., ESTEC, Noordwijk, p. 797
Helou, G., Lu, N.Y., Werner, M.W., Malhotra, S., Silbermann, N., 2000, ApJ, 532, L21
Mattila, K., Lehtinen, K., Lemke, D., 1999, A&A, 342, 643
Morel, T., et al., 2001, MNRAS, 327, 1187
Oliver S., et al., 2000, MNRAS, 316, 749
Roussel, H., et al., 2001a, A&A, 369, 473
Roussel, H., et al., 2001b, A&A, 372, 427
Sauvage, M., et al., 1996, A&A, 315, L89
Serjeant S., et al., 2000, MNRAS, 316, 768
Silva, L., et al., 1998, ApJ, 509, 103
Väisänen, P., et al., 2000, ApJ, 540, 593
Väisänen, P., et al., 2002, MNRAS, in press (astro-ph/0208412)
Vigroux, L., et al., 1996, A&A, 315, L93
Vigroux, L., et al., 1999, in Cox, P., Kessler, M.F., eds., ESA SP-47, The Universe As Seen by ISO, ESA Publ.Div., ESTEC, Noordwijk, p. 805

ISO PHOTOMETRY OF HYPERLUMINOUS INFRARED GALAXIES: IMPLICATIONS FOR THE ORIGIN OF THEIR EXTREME LUMINOSITIES

Aprajita Verma[1], **Michael Rowan-Robinson**[2], **Richard McMahon**[3], **and Andreas Efstathiou**[4]

[1]Max-Planck Institut für extraterrestrische Physik, Postfach 1312, D-85741 Garching, Germany.
[2]Astrophysics Group, Blackett Laboratory, Imperial College, Prince Consort Road, London SW7 2BZ, England.
[3]Institute of Astronomy, Madingley Road, Cambridge CB3 0HA, England.
[4]Department of Computer Science & Engineering, Cyprus College, 6 Diogenous Street, P O Box 22006, 1516 Nicosia, Cyprus.

ABSTRACT

We present 7-180μm photometry of a sample of hyperluminous infrared galaxies (HyLIGs) obtained with the photometer and camera mounted on the *Infrared Space Observatory* (ISO). We have used state-of-the-art' radiative transfer models of obscured starbursts and dusty tori to model their broadband spectral energy distributions (SEDs). We find that IRAS F00235+1024, IRAS F14218+3845 and IRAS F15307+3252 require a combination of starburst and AGN components to explain their mid to far-infrared emission, while for TXS0052+471 a dust torus model alone is sufficient. For IRAS F00235+1024 and IRAS F14218+3845 the starburst component is the predominant contributor whereas for IRAS F15307+3252 the dust torus component dominates. The implied star formation rates (SFR) estimated from the starburst infrared luminosities are $dM_{*,all}/dt > 1000 M_{\odot} yr^{-1} h_{50}^{-2}$ and are amongst the highest SFRs estimated to date. We also demonstrate that the well-known radio-FIR correlation observed for extragalactic sources extends into both higher radio and infrared power than previously investigated. The relation for HyLIGs has a mean q value of 1.94. The results of this study imply that better sampling of the IR SEDs of HyLIGs may reveal that **both** AGN and starburst components are required to explain their emission from the NIR to the sub-millimetre.

Key words: infrared: galaxies - radio continuum: galaxies - galaxies: starburst - galaxies: Seyfert

1. INTRODUCTION

Hyperluminous infrared galaxies constitute the most luminous ($L_{IR} > 10^{13} L_{\odot} h_{65}^{-2}$) fraction of the extragalactic population characterised by predominant emission in the infrared (IR) wavelength range. These dusty objects are often thought to be the local analogues of the high-redshift sources being discovered in recent sub-mm surveys (Hughes et al. 1998, Ivison et al. 1998, Scott et al. 2002) and possibly the unresolved population that contributes to the IR background (Comastri et al. 1995, Fabian et al. 1998). The nature of the power source fueling their extreme luminosities therefore has implications for the origin of the IR/sub-mm backgrounds and galaxy evolution scenarios. Whether their powerful emission is due to thermal re-radiation by dust of UV/optical photons emanating from obscured compact starbursts or deeply dust enshrouded AGN remains a controversial issue as many luminous IR galaxies often display both starburst and AGN signatures. This is the so-called 'starburst-AGN controversy' that has been well studied, and to an extent elucidated, for ultraluminous IR galaxies (ULIGs) using the photometric and spectroscopic results of ISO (e.g. Genzel et al. 1998, Klaas et al. 2001).

For the faintest and most distant members of this population, investigating the underlying power source becomes even more difficult due to poorly sampled IR SEDs and the inability to obtain good quality spectroscopic measurements. Therefore, with the aim to ascertain the nature of the obscured power source, we obtained mid-far IR photometry of a sample of HyLIGs using the photometer (PHT) and camera (CAM) mounted on ISO. By combining these data with existing optical, IRAS and radio data we constructed SEDs which we interpreted by fitting state-of-the-art' radiative transfer models of obscured starbursts and dusty tori. The deconvolution of the SED into AGN and starburst components allowed us to determine likely fueling fractions to the total IR power.

2. SAMPLE & DATA REDUCTION

We present SEDs of four HyLIGs from an originally proposed sample of 15, limited only by observing constraints. Observations were carried out using PHOT at FIR wavelengths and imaged in the MIR with CAM.

CAM images at 6.75 and 15μm were taken in the photometric imaging CAM01 mode. Reduction was carried out using the CAM Interactive Analysis software[1] (CIA) with dark current, flat-fielding, deglitching and stabilisation corrections applied.

PHOT observations were taken using the observation modes PHT03 at 25μm and PHT22 at 60, 90 and 180μm. These filters were chosen to span the greatest wavelength range and complement the existing IRAS data. The data were reduced using PHOT Interactive Analysis (PIA) Software (version 9.1)[2] from the edited raw data products. PHT-P observations at 25μm were reduced using the standard procedure but in the absence of a complementary background measurement,

[1] The CAM data presented in this paper was analysed using 'CIA', a joint development by the ESA Astrophysics Division and the CAM Consortium. The CAM consortium is led by the CAM PI, C. Cesarsky.

[2] PIA is a joint development by the ESA Astrophysics division and the PHOT Consortium led by MPIA, Heidelberg. Contributing PHOT Consortium institutes are DIAS, RAL, AIP, MPIK and MPIA.

Proceedings of the Symposium *"Exploiting the ISO Data Archive - Infrared Astronomy in the Internet Age"*, 24–27 June 2002, Sigüenza, Spain (C. Gry, S. B. Peschke, J. Matagne et al. eds., ESA SP-511)

were used as an upper limit. The remaining long wavelength data was reduced using tools specifically developed for reducing chopped data. [See Verma et al. (2002) for details.] We assessed the reliability of the long wavelength detections by determining the level of cirrus confusion noise on each measurement.

3. ANALYSIS

3.1. SED FITTING

The resulting SEDs were compared to combinations of radiative transfer models of inclined dusty tori (Efstathiou, Hough & Young, 1995, EHY95) and state of the art starburst models (Efstathiou, Rowan-Robinson & Siebenmorgen 2000, ERS00). The contributions of both components were allowed to freely vary. Other parameters that were allowed to vary were orientation of the torus, starburst age and starburst optical depth. It is important to note that we were by no means sampling the full parameter space of starburst or AGN models since both are defined with discrete parameters. The number of free parameters we used was restricted by the sampling of the SED. This enabled the quality of the combined fit to be assessed using the reduced chi squared estimator. For the lowest chi-squared values we accepted all fits with the minimum chi-squared and one plus the minimum as reasonable fits. The degeneracy of combinations within this chi-squared range was investigated to determine the most likely starburst:torus contributions to the total power.

An accurate total luminosity was determined by integrating over the best fitting combined model. Thus errors incurred due to the approximations used to determine this quantity from IRAS fluxes were eliminated. In addition, the dust mass involved was directly obtained from the starburst models. The decoupling of the SED into starburst and AGN components, meant that SFRs were determined solely from the starburst luminosity.

3.2. FSC 00235+1024

The mean combination of the best fitting models to the SED of this source is 64%:36% starbursts:torus. Without a strong MIR constraint we cannot rule out the possibility of a stronger AGN component. However the current modelling shows that stronger torus components greatly over-predict the MIR emission measured by CAM. Both the dominance of the starburst contribution and the orientation of the dusty torus are consistent with soft X-ray upper limits and its narrow-line classification from optical spectra. This z=0.59 source has a total IR luminosity of $L_{IR} = 2.29 \times 10^{13} L_{\odot}$ with 65% originating from the starburst model giving a dust mass $M_D = 1.2 \times 10^9 M_{\odot}$.

3.3. TXS 0052+471

The SED of TXS0052+471 is best fit by a torus model alone. Within the range of best-fitting models, a low (<4%) starburst contribution was plausible but this combination passed through the sub-mm upper limits, and therefore a null starburst contribution was preferred. This source was discovered in a correlation of the IRAS Faint Source Reject Catalogue (FSR) with the TEXAS radio survey and is the only radio-loud object within our sample. The ISO detections provide evidence that the FSR source is real. At a redshift of 1.94, this quasar is one of the most luminous HyLIGs, with $L_{IR} = 1.1 \times 10^{14} L_{\odot}$.

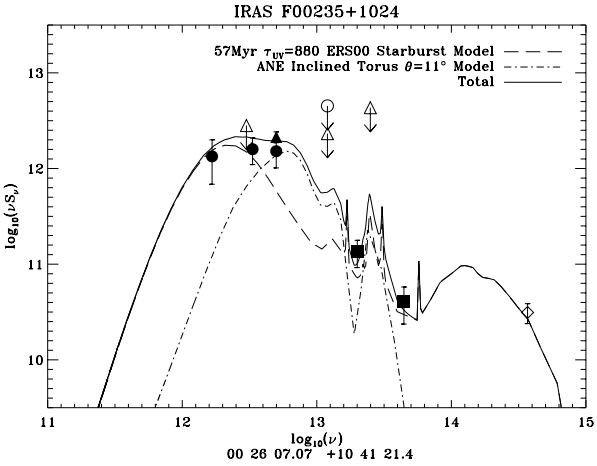

Figure 1. Best-fitting model for FSC00235. Detections are plotted as filled symbols and upper limits as open symbols with arrows plotted directly below: PHT - circles, CAM - squares and IRAS - traingles. Additional data obtained from literature are plotted on the SEDs as open diamonds (with arrows below if upper limits).

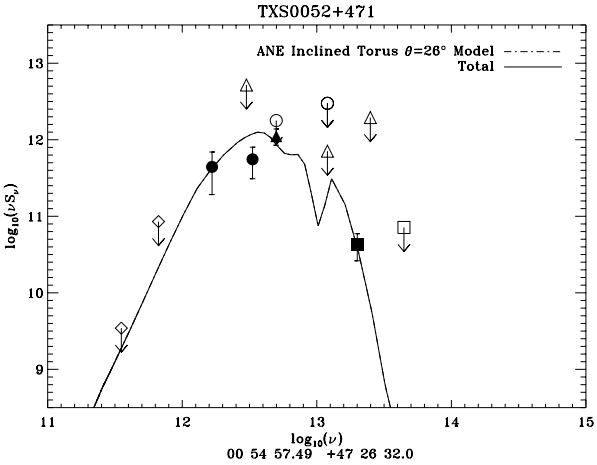

Figure 2. Best-fitting model for TXS0052+471. Key as Fig. 1.

3.4. FSC 14218+3845

The ISO photometry does not confirm the IRAS fluxes which are now believed to be contaminated by cirrus flux. By combining the PHOT and CAM data we were able to identify IR emission arising from the quasar previously associated with the IRAS source at z=1.21. Despite a drop in flux of over a factor of 10 this source remains a bona fide HyLIG with $L_{IR} =$

$2.27 \times 10^{13} L_{\odot}$. The fitting analysis showed a combined model at a level of 75-85%:15-25% starburst:torus was preferred to explain the SED over a range of torus only models or any other starburst AGN combination. The orientation of the torus ($59.5^{\rm deg}$) is consistent with the detection of broad lines in the optical spectrum.

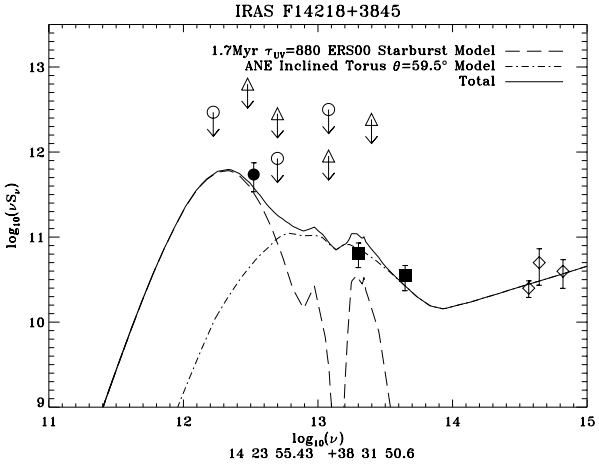

Figure 3. Best-fitting model for F14218+3845. Key as Fig. 1.

3.5. FSC 15307+3252

We combined our data with photometry from a CAM-CVF spectrum (Aussel et al. 1998) enabling the use of an extended set of starburst and torus models. The non-detection of PAH features in the MIR and the strong FIR detections dictate strong AGN and starburst components respectively. The majority of best-fitting combined models are predominantly torus fueled. The model shown represents one of the best fit models with 70%:30% torus to starburst contribution. The orientation of the torus model is consistent with 3 observational clues: Seyfert 2 classification, detection of a broad MgII line in the polarised spectrum and soft X-ray upper limits. The non-detection of CO(J = 4 → 3) by Yun & Scoville (1998) favours low gas mass and therefore a low starburst component. The dust mass estimated from the starburst model is consistent with limit on the gas mass.

4. THE FIR-RADIO CORRELATION

Here we demonstrate that the well known radio-IR correlation for starbursts and ULIGs extends to higher power for HyLIGs. Radio detections from the NVSS catalogue (Condon et al. 1998) were sought for all HyLIGs catalogued in Rowan-Robinson (2000, RR00). Excluding the TEXAS radio-loud quasars (those clustered around TXS 0052+471) we see that the HyLIGs follow the broad correlation seen in the Condon et al. (1991, C91) and Stanford et al. (2000, S00) data for LIGs and ULIGs. The mean q-value [used to parameterise the FIR-radio correlation $q = log_{10}(S_{60\mu m}/S_{1.41GHz})$] for the NVSS detected HyLIGs

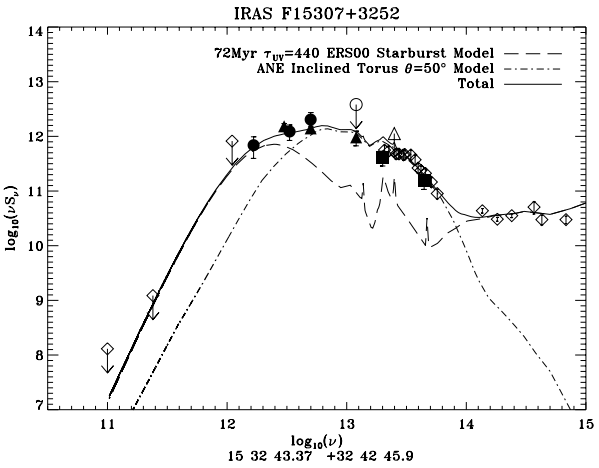

Figure 4. Best-fitting model for F15307+3252. Key as Fig. 1.

is 1.66. This is lower than the typical value determined for starburst galaxies and radio-quiet quasars (~ 2.3). However, if the sample is split we find that (a) the radio-loud TEXAS HyLIGs have $< q >= 0.89$ which is consistent with the value for radio-loud quasars ($0 < q < 1$) (b) for the remaining HyLIGs $< q >= 1.94$ which almost lies within the typical range for starburst and radio-quiet quasars (2-2.6) but is much lower than the mean derived for LIGs and ULIGs ($q = 2.34$ and $q = 2.28$ from C91 and S00, respectively). However, the NVSS undetected HyLIGs have radio fluxes *below* 2.7mJy (the completeness limits of the NVSS) and their inclusion will cause the value of $< q >$ to be higher.

5. SUMMARY

ISO measurements of HyLIGs have been performed to ascertain the nature of these extreme infrared objects.

a) Four objects, with faint IRAS detections, have been confirmed to be real infrared sources and constitute some of the most luminous sources in the Universe
($L_{IR} > 1 \times 10^{13.35} h_{50}^{-2} L_{\odot}$).

b) The broad-band SEDs of these objects have been compared to starburst and Seyfert models. The IR emission of FSC00235 and FSC14218 are predominantly starburst fueled whereas predominant AGN fueling is seen for TXS0052 and FSC15307.

c) The radio-IR luminosity correlation has been verified to continue to previously un-investigated radio and infrared luminosity powers. The mean q value for the radio-quiet sources (1.94) is lower than that previously determined for ULIGs (2.34) and indicates higher radio luminosities for HyLIGs.

With so few sources it is difficult to extrapolate our findings to the entire population. Nevertheless, we can state that **ALL of our sources require contributions from an AGN component to completely explain their IR SEDs**. This result in a sample of galaxies limited only by observing constraints suggests that obscured AGN and the hyperluminous phenomenon are linked. We therefore conclude from the results of this study, coupled with the multi-wavelength data available to date, that it

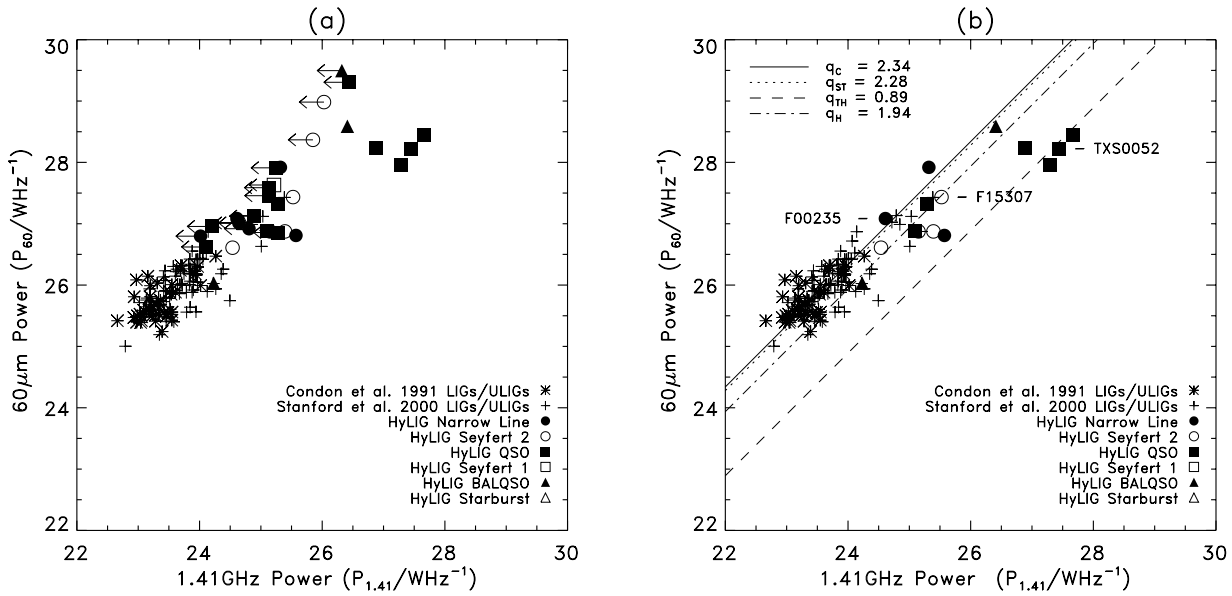

Figure 5. The figures above show the correlation between the calculated 60μm and 1.41GHz power. The plot includes LIGs and ULIGs from the samples of C91 and S00. It also contains data for the entire ISO-HyLIG sample and from the compilation of known HyLIGs from RR00. Plot (a) includes all detected sources and a radio upper limit of 2.7 mJy is shown for sources undetected within the NVSS survey. Plot (b) includes only those HyLIGs with confirmed NVSS counterparts. Overplotted are lines representing the median q *values for the C91 sample (q_C), the S00 sample (q_{ST}), the four radio-loud hyperluminous TEXAS sources (q_{TH}) and the remaining hyperluminous sources (q_H).*

is likely that HyLIGs contain AGN which contribute to the infrared emission. However, they are not energetically dominant in all HyLIGs.

In a complementary programme, we have performed similar analysis on three large and complete samples of ULIGs. We find that ∼70% of the samples require both AGN and starburst components to completely explain their NIR-FIR emission. In approximately one third of these cases, the torus model is the predominant contributor. Combining the results of the ULIG and HyLIG samples imply the following:

(i) Combined SED fits imply that a high fraction (∼70%) of U/HyLIGs present evidence of coeval AGN and starburst activity.

(ii) The fraction of bolometrically dominant AGN increases with luminosity (15-20% for ULIGs [Genzel et al. 1998, Verma et al. in prep] and 50% for HyLIGs [Verma et al. 2002]) which supports the findings of previous studies (e.g. Shier et al. 1996, RR00).

(iii) If HyLIGs are the local counterparts to the high-z sub-mm sources, we may find a substantial fraction to have significant power contributions from obscured AGN.

REFERENCES

Aussel H., Gerin M., Boulanger F., Desert F.X., Casoli F., Cutri R.M., Signore M., 1998, A&A, 334, L73

Comastri A., Setti G., Zamorani G., & Hasinger G., 1995, A&A, 296, 1

Condon J.J. Huang Z., Yin Q.F., & Thuan, T.X., 1991, ApJ, 378, 65, (*C91*)

Condon J.J., et al., 1998, AJ, 115, 1693

Cutri R.M., Huchra J.P., Low F.J., Brown R.L., vanden Bout P.A., 1994, ApJ, 424, L65

Efstathiou A., Hough J.H., & Young S., 1995, MNRAS, 277, 1134 (*EHY00*)

Efstathiou A., Rowan-Robinson M., Siebenmorgen R., 2000, MNRAS, 313,734 (*ERS00*)

Fabian A.C., Barcons X., Almaini O., & Iwasawa K., 1998, MNRAS, 297, L11

Genzel et al., 1998, ApJ, 514, L13

Hughes et al., 1998, Nature, 394, 291

Ivison et al., 1998, MNRAS, 298, 583

Klaas et al., 2001, A&A, 379, 823

Rowan-Robinson, 2000, MNRAS, 316, 885, (*RR00*)

Scott et al., 2002, MNRAS, 331, 817

Shier L.M., Rieke M.J., Rieke G.H., 1996, ApJ, 470, 222

Stanford S.A., Stern D., van Breugel W., & De Breuck C., 2000, ApJS, 131, 185, (*S00*)

Verma A., Rowan-Robinson M., McMahon R., Efstathiou A., 2002, MNRAS, 335, 574

Yun M.S., Scoville N.Z., 1998, ApJ, 507, 774